UNIVERSITY OF CALIFORNIA, SAN DIEGO

DISTAL FEMUR ARTICULAR CARTILAGE SURFACE TOPOLOGY: HEALTH, ACUTE INJURY, AND REPAIR

A dissertation submitted in partial satisfaction of the

requirements for the degree Doctor of Philosophy

in

Bioengineering

by

Bradley C Hansen

Committee in charge:

Robert L. Sah, Chair
Koichi Masuda
Jeffrey H. Omens
Michele M. Temple-Wong
Samuel R. Ward
Kun Zhang

2014

The dissertation of Bradley C Hansen is approved, and it is acceptable in quality and form for publication on microfilm and electronically:

_____

_____

_____

_____

_____

_____

Chair

University of California, San Diego

2014

TABLE OF CONTENTS

LIST OF FIGURES AND TABLES

EPIGRAPH

"Wisdom *is* the principal thing; *therefore* get wisdom:

and with all they getting get understanding."

KJV, Proverbs 4:7

ACKNOWLEDGMENTS

I would like to say thank you to everyone who has helped make this dissertation possible. First, I would like to acknowledge my advisor, Professor Robert Sah. Dr. Sah has constantly provided me with valuable scientific insight and direction throughout my studies. He has offered me opportunities to develop my skills and to associate with some of the greatest researchers in our field, to learn the scientific approach and skills I have needed to complete this work.

I would like to acknowledge my dissertation committee, Professor Koichi Masuda, Professor Jeff Omens, Dr. Michele Temple-Wong, Professor Sam Ward, and Professor Kun Zhang. Prof. Masuda advised me in the rabbit study of Chapter 2, providing his surgical expertise, direction, and support required to pull off such an endeavor. I was proud to work as Prof. Omens teaching assistant for three quarters, learning the methods that make him one of the most popular professors in the department. It was a pleasure to have Dr. Temple-Wong as my mentor in the Cartilage Tissue Engineering Lab, showing me the ropes and helping me learn the SOPs. In addition, I would like to acknowledge Dr. William Bugbee for advising me, providing clinical insight and research direction for Chapters 3 and 4.

Chapter 2, in full, is being prepared for submission to *Technology*. I would like to thank my co-authors, Jason Caffrey, Karli Gillette, Iliya Goldberg, Kirsten Cherry, Esther Cory, William McCarty, Tomonori Yamaguchi, Albert Chen, Michele Temple-Wong, Chris Raub, Koichi Masuda, and Robert Sah. In addition, I would like to thank Elaine Chan, for assistance with image processing and Won Bae, Van Wong, Johnny

Tam, Meena Siddiqui, Sahil Patel, Amran Asadi, and Roman Dittmar for assistance with the robot. This work was supported by research grants from the National Institutes of Health (R01 AR051565, P01 AG007996) and an award to the University of California–San Diego under the Howard Hughes Medical Institute Professors Program (for RLS).

Chapter 3 is being prepared for submission to the *Journal of Orthopaedic Research.* I would like to thank my co-authors, Esther Cory, William Bugbee, and Robert Sah. This work was supported by research grants from the Joint Restoration Foundation, the National Institutes of Health (R01 AR051565, P01 AG007996) and an award to the University of California–San Diego under the Howard Hughes Medical Institute Professors Program (for RLS).

Chapter 4 is also being prepared for submission to the *Journal of Orthopaedic Research.* I would like to thanks my co-authors, Esther Cory, Karen Samy, Andrea Pallante-Kichura, Albert Chen, William Bugbee, and Robert Sah. This work was supported by research grants from the National Institutes of Health (R01 AR051565, P01 AG007996) and an award to the University of California–San Diego under the Howard Hughes Medical Institute Professors Program (for RLS).

In addition to my co-authors, I would like to acknowledge members of the Cartilage Tissue Engineering Lab, with whom I have had the privilege of working on a variety of studiesI would like to thank Dr. Lucius Pomerantz, Will Oei, Murray Grissom, and Benjamin Hinton for their assistance with a variety of investigations of synovial fluid function and composition. It was a pleasure to share many late nights collecting synovial fluid and performing mechanical tests. I would again like to thank

the undergraduates I worked directly with on the studies presented in this dissertation, Karli Gillette, and Karen Samy, for their assistance with image analysis and intellectual curiosity. Thank you, Jason Caffrey, for your invaluable assistance with the robot; that project would not have been possible without your technical expertise. Thanks to the CTE Lab and Skeletal Translational Research Lab staff, past and present, especially Van Wong, Megan Bokar, Barb Schumacher, and Johnny Du, for their assistance with experiments and projects. I would like to thank my CTE PhD student predecessors, not already mentioned, Won Bae, Greg Williams, Megan Blewis, Ben Wong, Nancy Hseih-Bonaserra, Jennifer Chen, Jennifer Antonacci, EunHee Han, and Quynhhoa Nguyen for their influence and mentorship during my early graduate student years. I would like to again acknowledge William McCarty, Andrea Pallante-Kichura, and Elaine Chan for their guidance and assistance with my research, and allowing me to be a part of theirs at times. Thanks also to Jerome Hollenstein, Alex Hui, and Alvin Su for the time we shared as PhD students. I would like to wish current CTE PhD students, Neil Chang, Felix Shu, Jason Caffrey, Yang Sun, and Aimee Raleigh, a timely and fruitful completion of their PhD studies.

Lastly, I would like to thank my wife, Emmy, for her love, support, patience, and encouragement. She has been my source of inspiration for many wonderful years, and I look forward to an eternity of adventures together. I would like to thank my children, Gabe, Betsy, Luke, and Miriam for the gift that each of you are in my life. Also, I would like to thank my parents, George and Pat Hansen, for their support and encouragement. My only hope is to follow your example of hard work and dedication. I also thank my wife's parents, Drs. Charles and Clytee Gold, for their continual help.

Thanks also to my grandpa, Elmo Colton, and my siblings, nieces, and nephews for their love, support, and interest in my studies. Finally, a special thank you goes to my grandmas, Bessie Hansen and Miriam Colton, who passed away before they could see me graduate, but who I know were supporting me in spirit.

VITA

2007	B.S., Mechanical Engineering University of Utah, Salt Lake City, Utah
2007-2014	Graduate Student Researcher Cartilage Tissue Engineering Laboratory University of California, San Diego, La Jolla, California
2009	M.S., Bioengineering University of California, San Diego, La Jolla, California
2014	Ph.D., Bioengineering University of California, San Diego, La Jolla, California

Journal Articles

Hansen BC, Caffrey JP, Goldberg I, McCarty WJ, Cory E, Gillette KK, Cherry KE, Yamaguchi T, Temple-Wong M, Chen AC, Raub CB, Masuda K, Sah RL: Early, site-specific cartilage deterioration after anterior cruciate ligament transection in adult rabbit. *Technology J,* In Preparation, 2014.

Hansen BC, Cory E, Bugbee WM, Sah RL: Computational Topographic Match of Orthotopic vs. Non-orthotopic Lateral and Medial Femoral Condyle Osteochondral Allografts. *J Orthop Res*, In Preparation, 2014.

Hansen BC, Cory E, Samy K, Pallante-Kichura AL, Chen AC, Sah RL: Computational Topographic Match of Lateral Femoral Condyle Donor Osteochondral Allografts to Medial Femoral Condyle Recipient Sites in the Boer Goat. *J Orthop Res*, In Preparation, 2014.

Mologne TS, Cory E, Hansen BC, Naso AN, Chang N, Murphy MM, Provencher MT, Bugbee WD, Sah RL: Osteochondral Allograft Transplant to the Medial Femoral Condyle using a Medial or Lateral Femoral Condyle Allograft: Is there a Difference in Graft Sources? *Am J Sports Med*, Accepted, 2014.

McCarty WJ, Cheng JC, Hansen BC, Yamaguchi T, Firestein GS, Masuda K, Sah RL: The biophysical mechanisms of altered hyaluronan concentration in synovial fluid after anterior cruciate ligament transection. *Arthritis Rheum* 64(12)3993-4003, 2012.

McCarty WJ, Luan A, Siddiqui M, Hansen BC, Masuda K, Sah RL: The biomechanical properties of mixtures of blood and synovial fluid. *J Orthop Res* 29(2):240-6, 2011.

Selected Abstracts

Hansen BC, Cory E, Bugbee WM, Sah RL: Repair of Medial Femoral Condyle Defects by Lateral Femoral Condyle Allografts: A Virtual Allograft Study. *Trans Orthop Res Soc*, 40:1215, 2015.

Cory E*, Hansen BC*, Naso AN, Chang N, Murphy MM, Provencher MT, Bugbee WD, Mologne TS, Sah RL: Lateral femoral condyle allografts provide an acceptable articular contour when implanted into medial femoral condyle recipient sites. *Trans Orthop Res Soc* 39:343, 2014.

Hansen BC, Caffrey JP, Goldberg I, McCarty WJ, Cory E, Gillette KK, Cherry KE, Chan EF, Yamaguchi T, Bae WC, Temple-Wong M, Raub CB, Masuda K, Sah RL: Early, site-specific cartilage deterioration after anterior cruciate ligament transection in adult rabbit. *Trans Orthop Res Soc* 38:135, 2013.

Hansen BC, Hinton BJ, Caffrey JP, Pomerantz ML, Brinson DC, Szeto M, Hasegawa A, Temple-Wong MM, Lotz MK, Masuda K, Sah RL: Double lavage technique for determination of synovial fluid volume and constituent concentrations. *Trans Orthop Res Soc* 36:2046, 2011.

Hansen BC, Temple-Wong MM, Antonacci JM, Cai MZ, Grissom MJ, Love RE, Noori NB, Oei WF, Roberts JM, Schumacher BL, Lane JG, Sah RL: Internal derangement of the knee is associated with impaired synovial fluid lubricant function and composition. *Trans Orthop Res Soc* 35:1986, 2010.

ABSTRACT OF THE DISSERTATION

DISTAL FEMUR ARTICULAR CARTILAGE SURFACE TOPOLOGY:
HEALTH, ACUTE INJURY, AND REPAIR

by

Bradley C Hansen

Doctor of Philosophy in Bioengineering
University of California, San Diego, 2014
Professor Robert L. Sah, Chair

The properties of articular cartilage vary across the surface of the femur in the knee joint. These site-specific properties are affected by mechanical loading patterns, which are altered depending on the state of the joint. For instance, loading patterns are altered when the knee suffers an injury, and this may affect the articular surface in a site-specific manner to initiate or advance wear. *The overall motivation for this dissertation was to determine the sites susceptible to cartilage degeneration following*

joint injury, and the site-specificity required for cartilage repair by osteochondral allograft (OCA) transplantation.

To achieve this, a novel robotic mechanical test system (RMTS) and image processing software were developed to investigate the site-specific properties of articular cartilage following anterior cruciate ligament transection (ACLT) in the rabbit, and in OCA repair scenarios in humans and goats. The first objective was to identify sites where structural and functional properties of the cartilage are affected at an early stage in the rabbit ACLT model of joint injury. The RMTS mapped indentation stiffness across the ACLT and the unoperated, contralateral femora, finding the distal, weight-bearing region of the medial femoral condyle (MFC) to be less stiff 28 days following ACLT. The second objective was to investigate site-specificity in the orthotopic match that is the goal in OCA repair. Performing OCA repairs computationally with images of human condyles, the topographic match of non-orthotopic OCA from the lateral femoral condyle (LFC) to MFC recipient sites may be equivalent to that of orthotopic OCA from the MFC. The third objective was to perform the computational OCA repairs on Boer goat condyles. This identified OCA donor locations for testing orthotopic vs. non-orthotopic repair *in vivo* in an animal model.

This work has increased understanding of the topological variation of articular cartilage properties on the distal femur in health, injury, and repair. Knowing the sites susceptible to damage following joint injury, and being able to utilize non-orthotopic OCA for the repair of large cartilage defects have significant clinical implications. Additionally, this work presents technical achievements in producing the semi-automated RMTS and software that performs and evaluates OCA repairs.

CHAPTER 1

INTRODUCTION

1.1 Structure, Composition, and Function of Articular Cartilage

The knee joint is a complex system of tissues, which work together to transmit load and provide efficient movement of the lower limb. Articular cartilage covers the ends of the femur and tibia, and has a low-friction, wear-resistant surface and bears loads on the joint [22, 31]. The bones are connected by ligaments, which hold the joint together, stabilizing the joint during movement [13]. The joint is encapsulated by a synovial capsule, the lining of which provides transport of nutrients into the joint fluid, called synovial fluid. Besides the nutrient carrier role of the synovial fluid, it also acts as a lubricant, further reducing friction between cartilage-cartilage contacts [32].

Cartilage consists of a dense matrix of Type II Collagen (50% dry wt); Proteoglycans (PG) (30% dry wt) such as aggrecan, and water (80% wet wt) [6, 7]. The PG component of cartilage contributes to the compressive stiffness of the tissue, whereas the collagen matrix contributes to the tensile properties of the tissue.[20] Digestion of PG by trypsin has been shown to lower cartilage indentation stiffness.[29] However, compressive stiffness is also modulated by alterations to the collagen matrix.[5]

1.2 Injury Predisposes the Joint to Osteoarthritis

Injury to these tissues can disrupt the mechanical, mechanobiological, and metabolic balance of the joint, predisposing the joint to a degenerative arthropathy: post-traumatic osteoarthritis (PTOA). Like primary osteoarthritis (OA), PTOA involves degeneration of the articular cartilage, sclerosis of the subchondral bone, and the formation of osteophytes.[28] In PTOA, however, onset of these symptoms is typically much quicker; joints have been characterized as symptomatic between 15 and 20yrs following an injury.[17, 18, 42]

One of the most common injuries that lead to PTOA is the rupture or tear of the anterior cruciate ligament (ACL). The ACL is located between the condyles, originating at the posterior lateral femoral condyle and inserting at the anterior medial tibial plateau, crossing over the posterior cruciate ligament. Tearing of this ligament is one of the most common problems in orthopaedic sports medicine.[30, 41]

Due to this prognosis, identifying targets for early treatment of joint injury, especially ACL rupture, is imperative and remains the goal of many clinicians and investigators to prevent PTOA.[18] There is a need for broad analysis of tissue types in the knee joint, investigating the interactions that may be involved, using the sensitive measures to the alterations.[27]

1.3 Standard Knee Joint Coordinate Systems

Defining a standard coordinate system for the distal femur is important for research purposes (**Figure 1.1**), such as mapping properties of the tissues, and also for a variety of clinical purposes. Using standard reference frame allows comparison of tissue properties, such as cartilage thickness[9, 10, 15] or contact area[26]. Additionally, aligning the femur in a standard reference frame allows clinical analysis of tunnel placement for ACL repair [35, 36, 43] and the failure of total knee replacements. Indeed, misalignment of total knee replacements has been noted in 12% of revisions[44].

The femoral coordinate system has previously been defined using anatomic and mechanical landmarks. The shape of the femur lends itself to a standard direction along the axis of the femur. This is defined by either a mechanical axis or the anatomic axis[52]. The mechanical axis of the femur is the axis along which loads are transferred from the hip to the knee, and is typically defined from the center of the femoral head to the middle of the condyles[46, 52]. The anatomic axis, FAA, is defined by the shaft of the femur[9, 46], which is roughly 3° valgus to the mechanical axis.[52]

The distal femur, with the medial and lateral condyles, provides another anatomic and mechanical axis, although the formulation of this axis varies. The two most commonly used axes in cartilage research are denoted as the femoral transverse axis, FTA,[9, 26, 46, 48] which is formed by joining the centers of sphere fits of the condyles, and the posterior condylar line.[10, 46, 48] Other axes have been used, as well, including a mechanical axis defined from the contact region of the condyles[52], an axis joining the epicondyles[46, 48], and a cylinder fit of the condyles[15].

The third axis for the coordinate system is formulated using a cross product of the axes described above. The long axis is defined as normal to the transverse plane. Typically the axis running medial to lateral is used as a construction line[10], in order to find the axis perpendicular to the long axis of the femur, which is normal to the sagittal plane. This is done mathematically by finding the cross product of the long axis and the medial-lateral axis, and then finding the cross product of this intermediate axis and the long axis. This final axis is normal to the sagittal plane. The intermediate axis is used, too, to define the normal to the coronal plane.

The last part of the coordinate system, the origin, has been defined in various ways, as well. The most common choices for this are the distal end of the patellofemoral groove (the proximal end of the intercondylar notch)[46, 49, 52], the midpoint of the sphere fits to the condyles[9, 46, 49], or the point halfway between the anterior and posterior ends of the condyles[10].

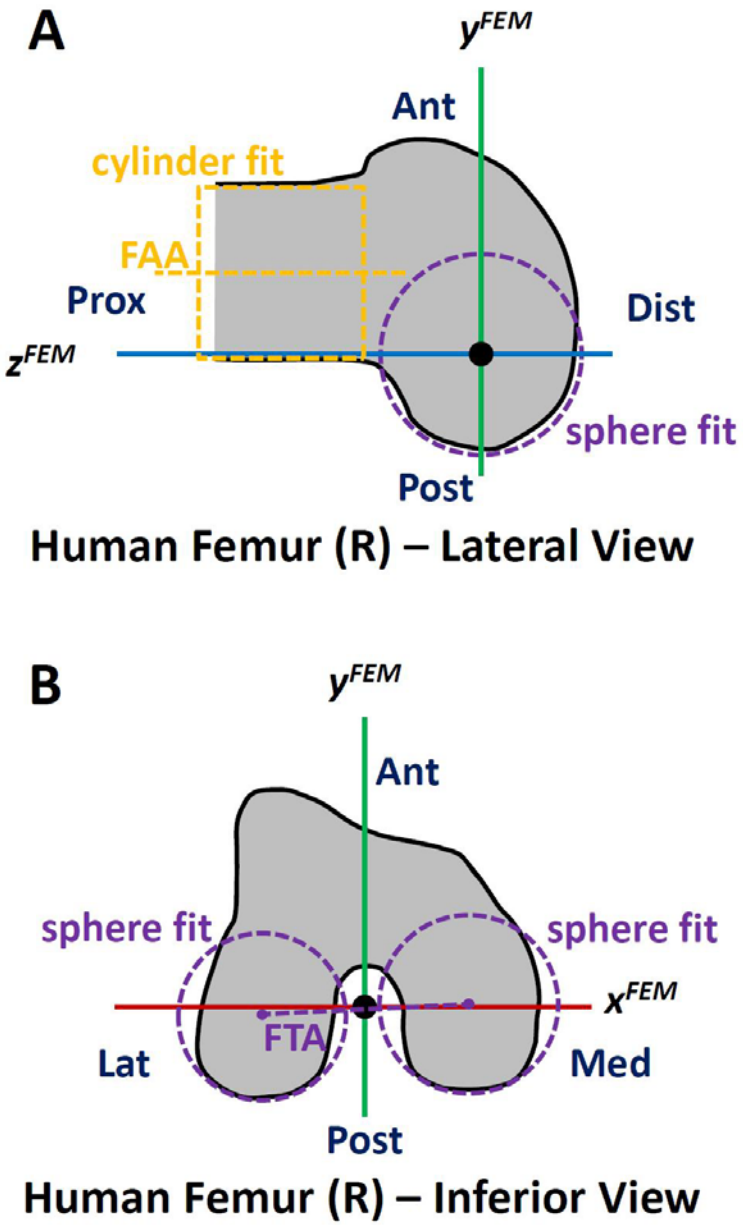

Figure 1.1. Anatomic Coordinate System of the Femur. Right (R) human femur shown in (A) lateral view and (B) inferior view. A cylinder is fit to the femoral diaphysis, generating an anatomic axis for the femur (FAA). Spheres are fit to the condyles, the centroids of which spheres are joined to create the femoral transverse axis (FTA). The origin (dark black circle) is the midpoint of the FTA. z^{FEM}, the z-axis of the femur coordinate system is parallel to the FAA, extending from the origin. y^{FEM}, the y-axis of the femur coordinate system, is defined by the cross product of the FAA and the FTA. x^{FEM} is then the cross product of y^{FEM} and z^{FEM}.

1.4 Topographic Variations in Cartilage Properties

The topographic and biomechanical properties of articular cartilage vary with location in the joint. Of particular interest are the thickness, curvature, and the mechanical stiffness of the cartilage. Thickness of cartilage has been measured at multiple locations in the knee of various species.[1, 2, 14, 16, 23-25, 38-40, 45] For example, there is a relationship for uncovered tibial plateau cartilage thickness to be anywhere from ~0.9 (canines[38]) to ~2 (rabbits[40]) times as thick as the opposing femoral condyle cartilage. For humans, the opposing tibial plateau cartilage is 1 to 1.2 times as thick as the femoral condyle cartilage.[2, 14, 24, 39, 45] The curvature of the articular surface has been investigated in particular due to the necessity to maintain contact mechanics during articular repair.[1] Mechanical stiffness varies across the surface of joints in humans and other species.[3, 40]

The susceptibility of the joint surfaces to cartilage degeneration also varies with location in the joint. Of note, there is a greater incidence of medial compartment degeneration, compared to the lateral compartment.[12, 21, 50] Topographic patterns of cartilage degeneration have been identified on the distal femur, which suggest progressive relationships.[4] Indeed, cartilage stiffness decreases with proximity to full thickness lesions in ACL-deficient knees, .[47]

1.5 Repair of Cartilage Defects by Osteochondral Allograft Transfer

Cartilage defects can be repaired using osteochondral dowel grafts from allogeneic donors. The procedure, known as osteochondral allograft (OCA) transfer, has a significant level of clinical success, improving patient knee scores.[8, 11, 19, 33, 51] When an OCA is placed, first the damaged region of the recipient's femur is reamed to create a cylindrical socket. A cylindrical OCA is then recovered from the condyle of the donor. The bottom bone surface of the OCA is trimmed based on the depth of the cylindrical socket reamed at the recipient site, then the OCA is gently tamped flush into place.[8] The target of this treatment is to restore the contour of the surface, restoring the contact mechanics of the joint.[8] To achieve this contour match, it is standard procedure to use of OCA from orthotopic locations on the donor condyles.

The practice of obtaining a site-matched OCA limits the number of repairs that can be performed. This is due in part to the higher incidence of damage on medial femoral condyles (MFC) than on lateral femoral condyles (LFC).[8, 12, 21, 50] The Joint Restoration Foundation has reported that MFC OCA constitute 97% of OCA requested; however, of the OCA suitable and available to surgeons, 75% are LFC OCA.[34] This presents an issue where MFC OCA may not be available for MFC repairs. To address this, an *ex vivo* OCA transplantation study [34] showed that LFC OCA, up to 20mm in diameter, can be implanted in MFC defects and fulfill the geometric surface match criteria of ±1.0mm [37] as well as MFC OCA. Although the process was successful *ex vivo*, it is unknown how specific the site match must be between donor and recipient sites to achieve a topographic match.

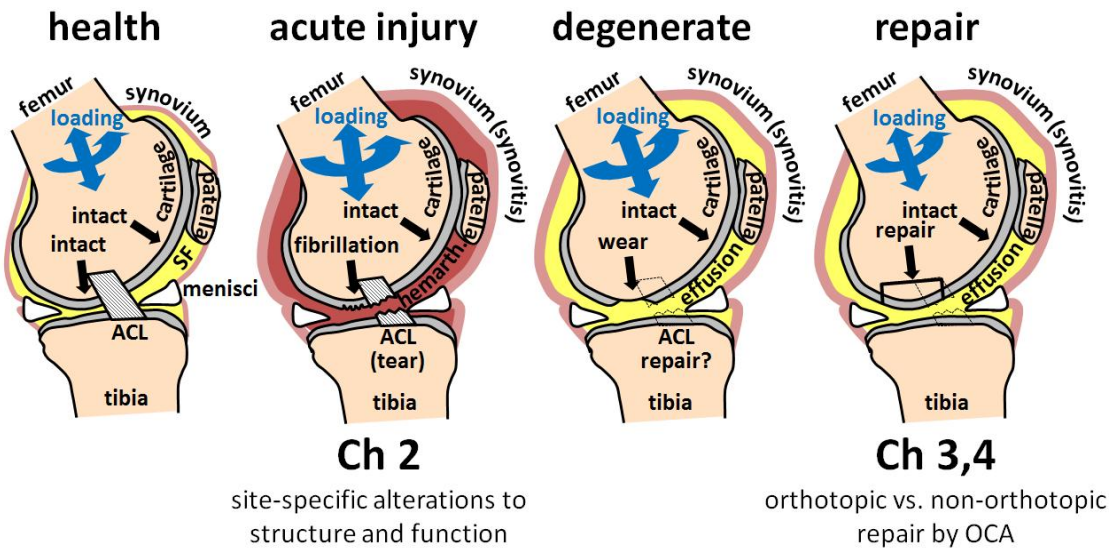

Figure 1.2:. Dissertation Overview. Chapter 2 considers the site-specific alterations to the structure and function of articular cartilage following joint injury. Chapters 3 and 4 investigates the possibility of non-orthotopic OCA repair.

1.6 Dissertation Objectives and Overview

The goal of this dissertation was to contribute to the understanding of site-specific properties of articular cartilage (**Figure 1.2**). Specifically, the site-specific alterations in cartilage properties were determined following joint injury, and the site-specificity required for cartilage repair by the osteochondral allografting technique. In order to achieve this, a novel robotic mechanical test system and novel image processing software were developed to investigate the site-specific properties of articular cartilage in a rabbit anterior cruciate ligament transection (ACLT) model and in *ex vivo* osteochondral allograft (OCA) studies in the human and goat. The first objective was to identify sites where structural and functional properties are affected at an early stage in the rabbit ACLT model of joint injury. The robotic mechanical test system mapped the indentation stiffness across the ACLT knee and the unoperated, contralateral knee, and found the distal medial femoral condyle (MFC), which is the weight-bearing region, to be less stiff. The second objective was to determine the site-specificity in the orthotopic match that is the goal in OCA repair. By performing the OCA repairs virtually on human hemi-condyles with custom software, the match to an MFC recipient site may be equivalent, whether the OCA is donated from another MFC or non-orthotopically from a lateral femoral condyle (LFC). The third objective was to perform the virtual OCA repairs on Boer goat hemi-condyles. This helped identify OCA harvest locations that can be used to test orthotopic vs. non-orthotopic repair *in vivo* in an animal model.

1.7 References

1. Ahmad CS, Cohen ZA, Levine WN, Ateshian GA, Mow VC: Biomechanical and topographic considerations for autologous osteochondral grafting in the knee. *Am J Sports Med* 29:201-6, 2001.

2. Ateshian G, Soslowsky L, Mow V: Quantitation of articular surface topography and cartilage thickness in knee joints using stereophotogrammetry. *J Biomech* 24:761-76, 1991.

3. Athanasiou KA, Rosenwasser MP, Buckwalter JA, Malinin TI, Mow VC: Interspecies comparisons of in situ intrinsic mechanical properties of distal femoral cartilage. *J Orthop Res* 9:330-40, 1991.

4. Bae WC, Payanal MM, Chen AC, Hsieh-Bonassera ND, Ballard BL, Lotz MK, Coutts RD, Bugbee WD, Sah RL: Topographic patterns of cartilage lesions in knee osteoarthritis. *Cartilage* 1:10-9, 2010.

5. Bae WC, Temple MM, Amiel D, Coutts RD, Niederauer GG, Sah RL: Indentation testing of human cartilage: sensitivity to articular surface degeneration. *Arthritis Rheum* 48:3382-94, 2003.

6. Buckwalter J, Hunziker E, Rosenberg L, Coutts R, Adams M, Eyre D: Articular cartilage: composition and structure. In: *Injury and Repair of the Musculoskeletal Soft Tissues,* ed. by SL-Y Woo, Buckwalter JA, American Academy of Orthopaedic Surgeons, Park Ridge, IL, 1988, 405-25.

7. Buckwalter JA, Mankin HJ: Articular cartilage. Part I: tissue design and chondrocyte-matrix interactions. *J Bone Joint Surg Am* 79-A:600-11, 1997.

8. Bugbee W, Cavallo M, Giannini S: Osteochondral allograft transplantation in the knee. *J Knee Surg* 25:109, 2012.

9. Cohen ZA, Mow VC, Henry JH, Levine WN, Ateshian GA: Templates of the cartilage layers of the patellofemoral joint and their use in the assessment of osteoarthritic cartilage damage. *Osteoarthritis Cartilage* 11:569-79, 2003.

10. Connolly A, FitzPatrick D, Moulton J, Lee J, Lerner A: Tibiofemoral cartilage thickness distribution and its correlation with anthropometric variables. *Proc Inst Mech Eng H* 222:29-39, 2008.

11. Convery FR, Meyers MH, Akeson WH: Fresh osteochondral allografting of the femoral condyle. *Clin Orthop Rel Res* 273:139-45, 1991.

12. Curl WW, Krome J, Gordon ES, Rushing J, Smith BP, Poehling GG: Cartilage injuries: a review of 31,516 knee arthroscopies. *Arthroscopy* 13:456-60, 1997.

13. Curwin S: Joint Structure and Function. In: *Joint Structure and Function: A Comprehensive Analysis,* ed. by PK Levangie, Norkin CC, FA Davis Co., Philadelphia, PA, 2005, 69-111.

14. Faber S, Eckstein F, Lukasz S, Mühlbauer R, Hohe J, Englmeier K-H, Reiser M: Gender differences in knee joint cartilage thickness, volume and articular surface areas: assessment with quantitative three-dimensional MR imaging. *Skeletal Radiol* 30:144-50, 2001.

15. Favre J, Scanlan SF, Erhart-Hledik JC, Blazek K, Andriacchi TP: Patterns of Femoral Cartilage Thickness are Different in Asymptomatic and Osteoarthritic Knees and Can be Used to Detect Disease-Related Differences Between Samples. *J Biomech Eng* 135:101002-10, 2013.

16. Frisbie D, Cross M, McIlwraith C: A comparative study of articular cartilage thickness in the stifle of animal species used in human pre-clinical studies compared to articular cartilage thickness in the human knee. *Vet Comp Orthop Traumatol* 19:142, 2006.

17. Gelber AC, Hochberg MC, Mead LA, Wang NY, Wigley FM, Klag MJ: Joint injury in young adults and risk for subsequent knee and hip osteoarthritis. *Ann Intern Med* 133:321-8, 2000.

18. Gillquist J, Messner K: Anterior cruciate ligament reconstruction and the long-term incidence of gonarthrosis. *Sports Med* 27:143-56, 1999.

19. Görtz S, Bugbee WD: Fresh osteochondral allografts: graft processing and clinical applications. *J Knee Surg* 19:231-40, 2006.

20. Han E, Chen SS, Klisch SM, Sah RL: Contribution of proteoglycan osmotic swelling pressure to the compressive properties of articular cartilage. *Biophys J* 101:916-24, 2011.

21. Hjelle K, Solheim E, Strand T, Muri R, Brittberg M: Articular cartilage defects in 1,000 knee arthroscopies. *Arthroscopy* 18:730-4, 2002.

22. Hunziker EB: Articular cartilage structure in humans and experimental animals. In: *Articular Cartilage and Osteoarthritis,* ed. by KE Kuettner, Schleyerbach R, Peyron JG, Hascall VC, Raven Press, New York, 1992, 183-99.

23. Kääb M, Ap Gwynn I, Nötzli H: Collagen fibre arrangement in the tibial plateau articular cartilage of man and other mammalian species. *J Anat* 193:23-34, 1998.

24. Karvonen R, Negendank W, Teitge R, Reed A, Miller P, Fernandez-Madrid F: Factors affecting articular cartilage thickness in osteoarthritis and aging. *J Rheumatol* 21:1310-8, 1994.

25. Kladny B, Bail H, Swoboda B, Schiwy-Bochat H, Beyer WF, Weseloh G: Cartilage thickness measurement in magnetic resonance imaging. *Osteoarthritis Cartilage* 4:181-6, 1996.

26. Kwak SD, Ahmad CS, Gardner TR, Grelsamer RP, Henry JH, Blankevoort L, Ateshian GA, Mow VC: Hamstrings and iliotibial band forces affect knee kinematics and contact pattern. *J Orthop Res* 18:101-8, 2000.

27. Laverty S, Girard CA, Williams JM, Hunziker EB, Pritzker KP: The OARSI histopathology initiative - recommendations for histological assessments of osteoarthritis in the rabbit. *Osteoarthritis Cartilage* 18 Suppl 3:S53-65, 2010.

28. Lohmander L, Englund P, Dahl L, Roos E: The long-term consequence of anterior cruciate ligament and meniscus injuries: osteoarthritis. *Am J Sports Med* 35:1756-69, 2007.

29. Lyyra T, Arokoski JP, Oksala N, Vihko A, Hyttinen M, Jurvelin JS, Kiviranta I: Experimental validation of arthroscopic cartilage stiffness measurement using enzymatically degraded cartilage samples. *Phys Med Biol* 44:525-35, 1999.

30. Magnussen RA, Granan LP, Dunn WR, Amendola A, Andrish JT, Brophy R, Carey JL, Flanigan D, Huston LJ, Jones M, Kaeding CC, McCarty EC, Marx RG, Matava MJ, Parker RD, Vidal A, Wolcott M, Wolf BR, Wright RW, Spindler KP, Engebretsen L: Cross-cultural comparison of patients undergoing ACL reconstruction in the United States and Norway. *Knee Surg Sports Traumatol Arthrosc* 18:98-105, 2010.

31. Mankin HJ, Mow VC, Buckwalter JA, Iannotti JP, Ratcliffe A: Form and function of articular cartilage. In: *Orthopaedic Basic Science,* ed. by SR Simon, American Academy of Orthopaedic Surgeons, Rosemont, IL, 1994, 1-44.

32. McCarty DJ: Synovial fluid. In: *Arthritis and Allied Conditions: A Textbook of Rheumatology,* ed. by WJ Koopman, Lippincott Williams & Wilkins, Philadelphia, 2001, 83-104.

33. Meyers MH, Akeson WH, Convery FR: Resurfacing of the knee with fresh osteochondral allograft. *J Bone Joint Surg Am* 71-A:704-13, 1989.

34. Mologne TS, Cory E, Hansen BC, Naso AN, Chang N, Murphy MM, Provencher MT, Bugbee WD, Sah RL: Osteochondral Allograft Transplant to the Medial Femoral Condyle Using a Medial or Lateral Femoral Condyle Allograft Is There a Difference in Graft Sources? *Am J Sports Med* 42:2205-13, 2014.

35. Musahl V, Burkart A, Debski RE, Van Scyoc A, Fu FH, Woo SL: Accuracy of anterior cruciate ligament tunnel placement with an active robotic system: a cadaveric study. *Arthroscopy* 18:968-73, 2002.

36. Musahl V, Burkart A, Debski RE, Van Scyoc A, Fu FH, Woo SL: Anterior cruciate ligament tunnel placement: Comparison of insertion site anatomy with the guidelines of a computer-assisted surgical system. *Arthroscopy* 19:154-60, 2003.

37. Nakagawa Y, Suzuki T, Kuroki H, Kobayashi M, Okamoto Y, Nakamura T: The effect of surface incongruity of grafted plugs in osteochondral grafting: a report of five cases. *Knee Surg Sports Traumatol Arthrosc* 15:591-6, 2007.

38. Panula HE, Hyttinen MM, Arokoski JP, Långsjö TK, Pelttari A, Kiviranta I, Helminen HJ: Articular cartilage superficial zone collagen birefringence reduced and cartilage thickness increased before surface fibrillation in experimental osteoarthritis. *Ann Rheum Dis* 57:237-45, 1998.

39. Pedersen DR, Goetz JE, Kurriger GL, Martin JA: Comparative digital cartilage histology for human and common osteoarthritis models. *Ortho Res Rev* 2013:13, 2013.

40. Räsänen T, Messner K: Regional variations of indentation stiffness and thickness of normal rabbit knee articular cartilage. *J Biomed Mater Res* 31:519-24, 1996.

41. Renstrom P, Ljungqvist A, Arendt E, Beynnon B, Fukubayashi T, Garrett W, Georgoulis T, Hewett TE, Johnson R, Krosshaug T, Mandelbaum B, Micheli L, Myklebust G, Roos E, Roos H, Schamasch P, Shultz S, Werner S, Wojtys E, Engebretsen L: Non-contact ACL injuries in female athletes: an International Olympic Committee current concepts statement. *Br J Sports Med* 42:394-412, 2008.

42. Roos H, Adalberth T, Dahlberg L, Lohmander L: Osteoarthritis of the knee after injury to the anterior cruciate ligament or meniscus: the influence of time and age. *Osteoarthritis Cartilage* 3:261-7, 1995.

43. Sadoghi P, Borbas P, Friesenbichler J, Scheipl S, Kastner N, Eberl R, Leithner A, Gruber G: Evaluating the tibial and femoral insertion site of the anterior cruciate ligament using an objective coordinate system: a cadaver study. *Injury* 43:1771-5, 2012.

44. Sharkey PF, Hozack WJ, Rothman RH, Shastri S, Jacoby SM: Insall Award paper. Why are total knee arthroplasties failing today? *Clin Orthop Rel Res*:7-13, 2002.

45. Shepherd D, Seedhom B: Thickness of human articular cartilage in joints of the lower limb. *Ann Rheum Dis* 58:27-34, 1999.

46. Tiefenbacher K, Ajami D, Rebek J: Self-Assembled Capsules of Unprecedented Shapes. *Angew Chem Int Ed* ePub, 2011.

47. Vasara AI, Jurvelin JS, Peterson L, Kiviranta I: Arthroscopic cartilage indentation and cartilage lesions of anterior cruciate ligament-deficient knees. *Am J Sports Med* 33:408-14, 2005.

48. Victor J, Van Doninck D, Labey L, Innocenti B, Parizel PM, Bellemans J: How precise can bony landmarks be determined on a CT scan of the knee? *Knee* 16:358-65, 2009.

49. Victor J, Van Doninck D, Labey L, Van Glabbeek F, Parizel P, Bellemans J: A common reference frame for describing rotation of the distal femur: a ct-based kinematic study using cadavers. *J Bone Joint Surg Br* 91:683-90, 2009.

50. Widuchowski W, Widuchowski J, Trzaska T: Articular cartilage defects: study of 25,124 knee arthroscopies. *Knee* 14:177-82, 2007.

51. Williams RJ, 3rd, Ranawat AS, Potter HG, Carter T, Warren RF: Fresh stored allografts for the treatment of osteochondral defects of the knee. *J Bone Joint Surg Am* 89:718-26, 2007.

52. Yoshioka Y, Siu D, Cooke TD: The anatomy and functional axes of the femur. *J Bone Joint Surg Am* 69:873-80, 1987.

CHAPTER 2

EARLY, SITE-SPECIFIC CARTILAGE DETERIORATION AFTER ANTERIOR CRUCIATE LIGAMENT TRANSECTION IN ADULT RABBITS

2.1 Abstract

INTRODUCTION: Focal cartilage lesions can develop rapidly following joint injuries, and are an attractive target for intervening in the development of osteoarthritis (OA), should the locations of the lesions be elucidated at the early stages of damage. OBJECTIVE: In this study, a novel robotic mechanical test system is utilized to determine site-specific stiffness of femoral condylar articular cartilage at 28 days post-operatively in the rabbit anterior cruciate ligament transection (ACLT) model of post-traumatic OA. METHODS: The robotic mechanical test system performed an indentation test at sites spaced evenly by arc-length along the antero-posterior direction of each condyle at 1.227±0.034mm, spanning the weight-bearing (WB) and non-weight-bearing (NWB) regions of the articular surfaces. RESULTS: Indentation structural stiffness (ISS) was lower (–37%) in the WB region of the medial femoral condyle (MFC) of ACLT knees compared to unoperated control (CTRL) knees (0.71

vs. 0.45 N/mm). Histological scores were greater (indicating more cartilage degeneration) in ACLT than CTRL knees, and were inversely correlated with ISS. CONCLUSION: These results provide a foundation for mechanistic and interventional studies.

2.2 Introduction

The structural and material biomechanical properties of articular cartilage vary with location in diarthrodial joints in health and disease.[2, 35] The biomechanical properties of articular cartilage vary topographically in normal joints.[2] Alterations in loading patterns, which occurs in an injury state, are a major risk factor in the initiation and progression of cartilage degeneration.[1] One major feature of cartilage degeneration and osteoarthritis (OA) is biomechanical softening of the surface layer of cartilage.[42, 43] Such abnormalities occur in distinct spatial patterns both in OA[4] and in animal models of OA, such as transection of the rabbit anterior cruciate ligament (ACL).[9] The softening of articular cartilage also varies with proximity to lesions.[44] The biomechanical softening of cartilage in OA is associated with surface abnormalities and decreased content of sulfated glycosaminoglycans (sGAG).[42]

ACL transection (ACLT) in the rabbit offers a model to investigate the initiation and development of OA after ACL injury in humans.[26] At 4 weeks post-ACLT, early signs of osteoarthritis appear macroscopically as a roughened surface[40, 50] and fibrillation[38, 40, 50, 52] and histologically as surface irregularities[40] and vertical clefts into the transitional zone[50] as well as decreased safranin-O staining in fibrillated areas.[50] These degenerative structural changes are often localized to the medial femoral condyle (MFC).[49, 50] At 9 weeks following ACLT in rabbits, full thickness erosion was observed to be localized to the anterolateral LFC and posteromedial MFC.[9] Such cartilage erosion may be due to progressive deterioration of cartilage, meniscus, and synovial fluid initiated soon after joint destabilization.[4]

Indentation test results reflect the complex tensile, shear, and compressive strain induced in articular cartilage under and near the indentation. While long-term creep or stress relaxation tests can be reduced to material properties, these properties vary markedly with depth and with strain. Indentation testing is sensitive to local variations in tissue degeneration.[5, 13, 23-25, 32, 37] An indentation structural stiffness parameter, *ISS*, can be defined by dividing the peak load by a small displacement, typically less than 10% of the tissue thickness, of a spherical indenter tip.[3, 18] *ISS* can be utilized to compute a material stiffness, and other material properties using constitutive models.[8, 18, 29, 31] The resultant indentation stiffness measure is influenced by both the sulfated glycosaminoclycan (sGAG) content and the state of the collagen matrix.[3] Indeed, *ISS* has been correlated to histological scores of cartilage[5] and sGAG content following trypsin digestion.[28] Microindentation testing, using automated atomic force microscopy on vertical sections of cartilage, shows that pericellular matrix stiffness varies with proximity to cells, and is lower in osteoarthritis.[12, 48]

An important consideration in indentation experiments is the perpendicular alignment of the indentation instrument to the cartilage surface. In the formulation of the models to mathematically analyze the indentation test, it is assumed that the indenter is perpendicular to the cartilage.[18, 31] Deviations from the correct alignment will distort the stress distribution within the cartilage.[41] To prevent misalignment between the indenter and cartilage surface, various techniques have been employed, including visualization tools and guides.[22, 28] Pierce et al describe an indentation setup that utilizes a 6 DoF robotic manipulator (RV-1A, Mitsubishi) to characterize the stiffness of cartilage from 10 x 10 x 8 mm^3 human osteochondral blocks.[33] Automating the

procedure of locating test sites and aligning the indenter perpendicular to the surface can improve the precision and accuracy of indentation stiffness testing.

The objective of this study was to determine the variation of indentation stiffness across the cartilage surface of femora from rabbits having undergone ACLT and correlate the mechanical measures to histopathological scores. In order to achieve this, the aims of this study were (1) to define test sites, relevant to the observed degeneration patterns, within a coordinate system defined by anatomic landmarks; (2) measure site-specific indentation stiffness using a semi-automated robotic indentation procedure; and (3) determine the relationship between indentation stiffness and histopathological indices of degeneration.

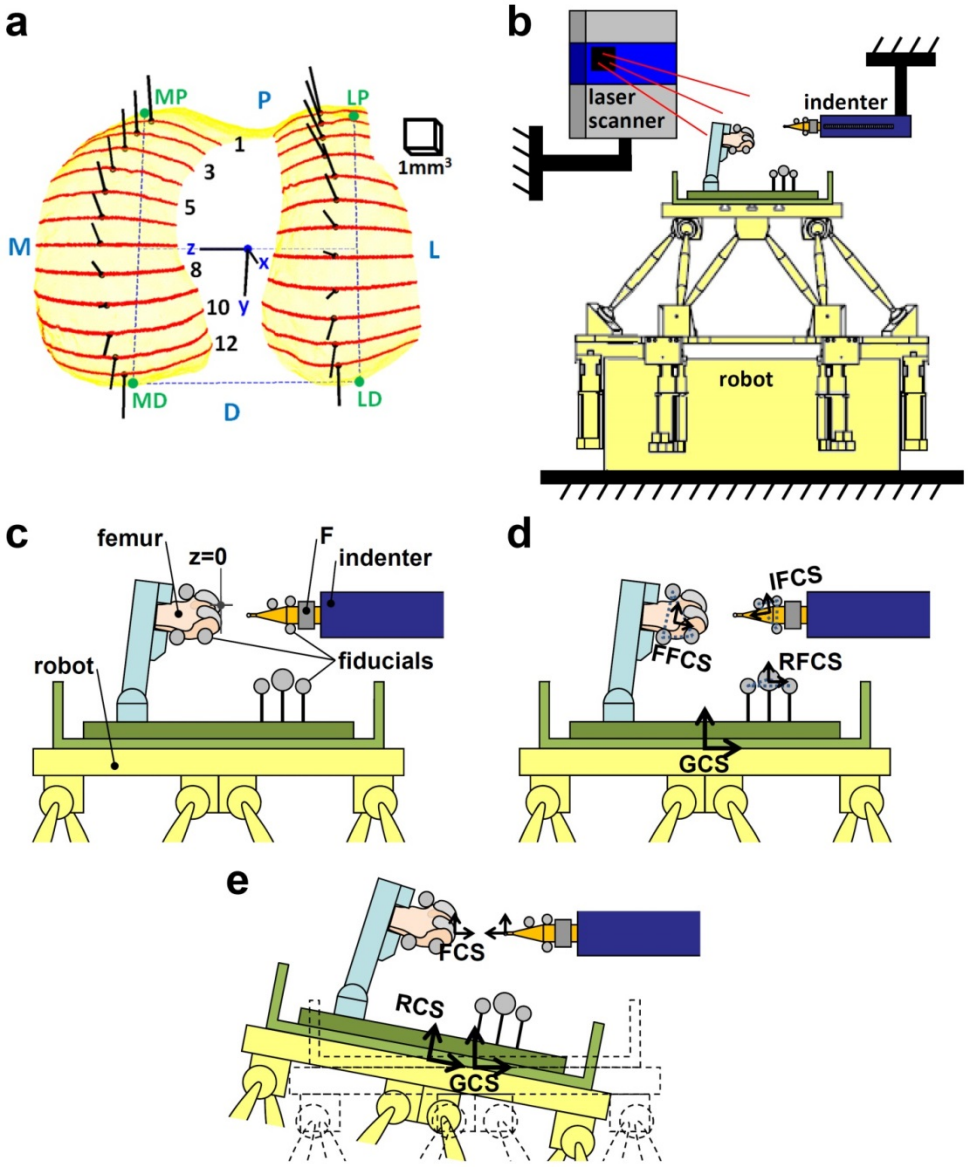

Figure 2.1: Robotic Indentation Test System. (**a**) Laser scan image of distal femur, showing the distal femur coordinate system (DFCS), the four alignment points (MP, LP, MD, and LD), and the 24 indentation test sites centered medially and laterally on gridlines spaced evenly proximally and distally. (**b**) Robotic indentation test system showing the important systems: laser scanner, robot (image courtesy PRSCO, Inc.), and indenter. (**c**) Diagram showing the femur, robot, and indenter in their relative positions with fiducial spheres attached that are used in registering the components. (**d**) The coordinate systems for computing the alignment parameters for the robot, including the global coordinate system (GCS), robot coordinate system (RCS), indenter coordinate system (ICS), and femoral test site coordinate system (FCS). (**e**) The robotic indentation test system with the surface point and the indenter aligned.

2.3 Methods

Study Design: The site-specific effects of unilateral ACLT in N=6 skeletally mature (age=12-14 months), female New Zealand white (NZW) rabbits on articular cartilage structure and function were investigated for the transected (ACLT) and the contralateral, unoperated control knee (CTRL) at an early time point of 28 days post-operatively. Structural and functional properties were assessed at 12 sites on each condyle, defined within a standard coordinate system, spanning both the weight bearing (WB, sites 8-12) and non-weight bearing (NWB, sites 1-7) regions of the MFC and LFC articular surfaces, and spaced to avoid overlap in testing areas, ensuring that each site had unique properties, and be greater than the estimated error in the test site definition.

Study 1: The first objective was to determine the precision of the test site locations due to observer inputs. 3-D laser scans of the distal end of ACLT and CTRL femora were acquired and landmarks were identified on the 3-D models. These landmarks were used to establish a standard distal femur coordinate system (DFCS), and guide the computation of the location of the test sites. After computing the sites for the individual samples, the precision was investigated by computing the mean location of each site, first by averaging the ACLT and CTRL from each animal, and then averaging across all animals. Interobserver and intraobserver variations were also assessed. For N=2 samples (2 ACLT and 2 CTRL), the landmarks were identified by 3

observers. For N=3 samples (3 ACLT and 3 CTRL), the landmarks were identified a second time by 1 observer.

Additionally, the precision in aligning test sites to the indenter, due to the registration of the femur to the robot, was determined. Test sites were defined on N=2 healthy rabbit femora, which were mounted on the robot and registered, determining the location of the femur and indenter in relation to the robot. Each test site was aligned to the indenter, which was fitted with a pin that was pushed into the tissue to the bone surface, making a small mark. Femora were removed from the apparatus, remounted and registered, and the pin marking procedure was repeated. India ink imaging and analysis were used to estimate the deviation of the pin marks. Additional studies were performed to confirm the rotational and translational accuracy and precision of the alignment.

Study 2: The early, site-specific effects of ACL transection on articular cartilage stiffness were determined by the robotic indentation system. After the 24 test sites were defined on ACLT and CTRL femora (N=6, both groups), the robotic test system aligned each test site to the indenter, which was used to yield indentation structural stiffness (*ISS*). Following the indentation test, femora were scanned by micro-computed tomography (μCT) to estimate cartilage thickness, *t*, at each of the 24 test sites. A regression between *ISS* and *t* was performed to compute a normalized, material stiffness (ISS_{NORM}).

Study 3: The relationships between stiffness and structural indices of deterioration, namely fixed charge density (FCD) and histological grade, were analyzed statistically. Imaging by μCT was repeated with contrast-enhancement that allows the visualization of fixed charge, the density of which was quantified for each test site. Sagittal sections were cut from each condyle and histochemically processed. Histological scores were given to the NWB (sites 1-7) and WB (sites 8-12) regions, rather than individual sites due to limitations in the grading process. Mean *ISS* and mean ISS_{NORM} were computed for these regions, and ranked histological scores were correlated with *ISS* and ISS_{NORM}, computing a Spearman's correlation coefficient.

Animal Surgery and Sample Preparation: Unilateral ACLT was performed on skeletally mature NZW rabbits using a protocol approved by the Institutional Animal Care and Use Committee at the University of California–San Diego. 28 days post-operatively, animals were sacrificed, and right (ACLT) and left (CTRL) hindlimbs were harvested and frozen intact to -80°C. Before testing, the intact hindlimbs were thawed at 4°C, and the femora were dissected, leaving the cartilage layer intact. Throughout dissection the cartilage surfaces were hydrated with phosphate-buffered saline with protease inhibitors (PBS+PI) (PI: 2 mM Na-EDTA, 1 mM PMSF, 5 mM Benz-HCL, and 10 mM NEM). Fiducial spheres, 3/8” in diameter, on threaded rods, were attached to the femora, two on the shaft roughly 2cm proximally from the condyles and one at an epicondyle. An India ink imaging procedure[9] was utilized to investigate the articular cartilage for the presence or absence of fibrillation, full

thickness erosion, or iatrogenic injury, to determine whether any samples or locations should be excluded from the study.

Laser Scanning of Cartilage Surfaces: The distal ends of the femora were imaged by a laser scanner to acquire 3-D models of the cartilage surface, fiducial spheres, and certain anatomic landmarks. After the fiducial spheres were attached, femora were imaged using a laser scanner with an in-plane resolution of ~250 points per mm^2 (NextEngine HD Pro, NextEngine, Inc., Santa Monica, CA). After processing the scans, the cartilage surface was manually segmented from the scan data, to ~100,000 3-D data points. Also segmented from the scan were the fiducial spheres, to ~100,000 data points, for registration, and four anatomical locations, to ~500 points, for defining the DFCS.

Distal Femur Coordinate System: The DFCS was defined in order to reproducibly register the femora. In the present study, it was necessary to localize a standard coordinate system using features of the distal femur, since the diaphysis was not imaged, similar to previous 2D and 3D studies that investigated regional properties of femoral articular cartilage.[10, 11, 14, 35] Four alignment points established the DCFS. The first two were the points that define the posterior condylar line, noted as LD and MD. The other two were the anatomic depressions at the proximal end of the MFC and LFC, noted as LP & MP (**Figure 2.1.b**). To construct the DCFS, first, the proximal points, LP & MP, were connected to distal points, LD & MD, respectively, making proximal-distal lines along the medial and lateral sides of the femur. The

midpoints of these medial and lateral lines were connected by a third line, which served as the z-axis of the DFCS. The origin of the DFCS was the centroid of the four alignment points. The y-axis was defined as the line extending from the DFCS origin, perpendicular to the z-axis, intersecting the posterior condylar line. The x-axis was defined by the cross product of the y- and z-axes (**Figure 2.1.a**).

Indentation Test Site Locations: The locations and normal vectors for the test sites were calculated along the center of each condyle. Custom MATLAB (MathWorks, Inc., Natick, MA) algorithms locate 12 test sites on each condyle by (1) spacing 12 medial-lateral gridlines along the proximal-distal direction equally by arc length of a spline fit to the articular surface in a plane bisecting the condyle and then (2) placing the test sites at the midpoint of each gridline covering the condyle width (**Figure 2.1.a**). Sites on each condyle are named MFC 1 through 12 and LFC 1 through 12, where 1 is the most proximal point on each condyle. Surface data within 1mm of the test site were used to compute the surface normal to use in the alignment (**Figure 2.1.a**). Once the test sites were calculated, the femora were attached to the robotic indentation test system (**Figure 2.1.b**). The average test site locations were computed, first by averaging the ACLT and CTRL from each animal, and then averaging across all animals.

Inter- and intra-observer precision in calculating the test sites was computed, to determine the repeatability of the manual process of segmenting the anatomic landmarks and condyles. For N=2 samples (2 ACLT and 2 CTRL), the landmarks and condyle boundaries were identified by 3 observers. For N=3 samples (3 ACLT and 3

CTRL), the landmarks and condyle boundaries were identified a second time by 1 observer. The precision of the test site computations was investigated by computing the mean and standard deviation of each site, first by averaging the ACLT and CTRL sites from the N=2 for inter-observer and N=3 for intra-observer, and then averaging across all N=2 or N=3 animals.

Registration of Femur, Robot, and Indenter: The femur samples, robot, and indentation system were registered to a global coordinate system (GCS) by tracking fiducial spheres with a laser scanner (NextEngine HD, NextEngine, Inc., Santa Monica, CA, resolution ~62 points per mm^2, **Figure 2.1.b,c**). The origin of the GCS was established by tracking 3 fiducial spheres with the laser scanner as the robot was rotated through 50 angular positions (combinations of angles about the x- and y-axes, no translation). The orientation of the GCS was established by tracking the same spheres through 5 translational positions (center position and 2 points along both the x-axis and the y-axis, no rotation). The robot coordinate system (RCS) was defined by the position of the robot, relative to the GCS, and aligned with the GCS when the robot was at its initial position. The origin of the indenter coordinate system (ICS) was determined as the position of the indenter tip in the laser scan data, defined relative to the fiducial spheres on the robot. The indenter tip also had fiducial spheres attached to it, and the orientation of the ICS was determined by tracking 3 positions of these fiducial spheres along the indenters motion axis. The test sites on the femora were defined relative to the GCS using the fiducial spheres attached to the femur (**Figure 2.1.c**).

Robotic Alignment of Indentation Test Sites: The robot achieved alignment of the test sites perpendicular to the indenter tip. Once the coordinate systems were defined, the robot motion parameters that provided alignment of the test sites to the indenter tip, with the indenter perpendicular to the cartilage surface, were computed. Then, each test site was aligned sequentially to the indenter using the robot in an automated procedure.

The precision in the alignment of rabbit femora to the indenter by the robot was determined, relative to the method of registering the femur to the robotic system, using a pin marking procedure and India ink imaging methods. N=2 normal, skeletally mature (age=10 months) NZW rabbit femora were imaged with the laser scanner, processed and registered, as described above. Replacing the indenter tip with a pin, each test site was aligned perpendicular to the pin, which was then pushed into the cartilage up to a load of 100g, creating small marks. The femora were removed from the robot, then replaced and registered once again. Then, the pin marking procedure was repeated. Femora were then imaged using the India ink method.[9] The distance between corresponding needle marks was estimated using digital imaging techniques in ImageJ (U. S. National Institutes of Health, Bethesda, Maryland, USA). The 2-D deviation from the mean location of pin marks was computed as a measure of precision in alignment.

The accuracy of this alignment strategy was determined with a target with known dimensions mounted on a flat surface. Registered in the same fashion as the indentation test sites, the robot aligned the target with the indenter. Photographs were

taken of the aligned target, and measurement tools in ImageJ were used to estimate the angular and translational offsets.

Indentation Testing: Indentation structural stiffness was determined at each test site on the femoral condyles using the custom indentation system (**Figure 2.1.c**). At each test site the robot aligned perpendicular to the indenter, in sequence using the automated procedure, the indentation protocol was as follows: a 0.4mm spherical-ended indenter was depressed into the tissue to a 0.16g preload, followed by indentation to a depth of d = 25μm to 100μm/s, held for 1s, then released. Hydration of the tissue was maintained during the test with PBS+PI. The repeatability of the indentation stiffness measures, relative to the alignment by the robot, was assessed by realigning the test sites to the indenter and repeating the indentations on N=8 femora. The repeatability of the indentation stiffness measures, relative to the registration procedure, was assessed by repeating the registration and alignment of test sites to the indenter, as performed previously during the pin marking procedure, and repeating the indentations on N=3 femora. After indentation testing, femora were fixed for 4 days in 4% paraformaldehyde in PBS.

μCT for Cartilage Thickness and FCD: The nearest-neighbor thickness of articular cartilage at the test sites was estimated from μCT images. Femora were scanned at $(9\mu m)^3$ resolution in a μCT scanner (Skyscan 1076, Skyscan, Kontich, BE), with an applied potential of 100kVp and current 100μA, utilizing a 1.0mm Al filter. 3D models of the cartilage and bone were created using Mimics (Materialise, Inc.) at a

$(36\mu m)^3$ resolution. The cartilage models were registered to the corresponding laser scan surfaces using surface registration functions in Mimics. Matching the test sites computed on the laser scan surface to the μCT cartilage surface, thickness was estimated in MATLAB using a nearest-neighbor approach between each test point, as well as four surrounding points, one at 200μm in each direction proximally, distally, medially, and laterally from the test point, and the μCT bone surface.

Femora were rescanned following equilibration in Hexabrix (HEX) solution for determination of site-specific fixed-charge density. Femora were placed in 20% HEX in PBS+PI for 48 hours. Scans were made at $(9\mu m)^3$ resolution as before. The image data was imported into MATLAB for site-specific analysis of the fixed-charge density. After matching the surfaces from the laser scan and the μCT images, a 100x100x200 μm^3 region-of-interest (ROI) was obtained of each test site. From the ROI, the average grayscale intensity of the cartilage from 3 sections in the coronal plane and 3 sections in the sagittal plane was used to quantify HEX uptake, relative to HEX standards (0%, 5%, 10%, 15%, and 20% HEX in PBS) scanned at the same resolution.

Histochemical Analysis. Femoral condyles were bisected with an IsoMet low-speed saw (Buehler, Lake Bluff, IL) and three 10 μm thick, serial cryosections were obtained in the approximate plane and location of the indentation testing. This plane was determined by aligning the cutting plane parallel to and 0.5 mm laterally displaced from the plane bisecting the condyles. Sections were stained with fast green-Safranin-O, and Hematoxylin and Eosin, then graded using the OARSI[26] and

Shapiro-modified Mankin[39] scoring systems for non-weight bearing (NWB, sites 2-7) and weight-bearing (WB, sites 8-11). Scoring is reported as the average of 3 observers (ICC=0.6-0.8). For a representative sample, the surface of the articular cartilage was determined from the SafraninO-stained sections, and matched to the indentation test sites so that views of a test site in the WB region and a test site in the NWB region could be obtained.

Data Analysis and Statistics: India ink and μCT images were used to determine inclusion of individual sites in the results. The articular surfaces were screened for iatrogenic cuts, extensive or full-thickness erosion, or other abnormalities. Sites with these abnormalities were excluded from the analysis. One site on one CTRL sample (ACL-01 L, site MFC 3) was not included in the results because of an iatrogenic cut on the surface that passed through the test site. One site on one ACLT sample (ACL-21 R, site LFC 12) was not included in the results because of extensive erosion observed in the India ink and μCT images.

The peak loads, P, for the indentations were used to calculate indentation structural stiffness, by: $ISS = P/d$. Thickness, h, is given as the average of the 5 measures taken. A regression between ISS and h provides an equation for ISS_F, defined that was used to normalize ISS as: $ISS_{NORM} = ISS/ISS_F$.[8] Data are expressed as mean±SD for n=6 samples. An unpaired t-test between ACLT and CTRL was performed using SYSTAT (Systat Software, Inc., San Jose, CA) for ISS, ISS_{NORM}, and t at each site to test the effects of ACLT.

Ranked histological scores were correlated with *ISS* and ISS_{NORM}, computing a Spearman's correlation coefficient, using SYSTAT, to compare against a critical value to determine significance at $p<0.05$.

2.4 Results

(1) Test Site Precision: The test site locations, computed within the DFCS to span the WB and NWB regions, varied little between samples, and the space between adjacent test sites was more than twice the variability in defining the sites. The 12 sites were placed along each condyle at an average distance between sites of 1227±34μm, with sites spaced on the MFC at 1237±27μm and on the LFC at 1218±50μm (**Figure 2.2**). The distance from the mean of corresponding ACLT and CTRL sites was 287±161μm for N=6 samples (**Table 2.1, Figure 2.2**). The absolute XYZ locations of these test points, relative to the defined coordinate system, are given in **Table 2.1**.

The computations of the test sites were not affected by the manual segmentation of the cartilage surface and anatomic landmarks. The average distance from the mean location to sites defined by repeated segmentation of N=3 femora samples by a single observer was 204±86μm. Comparing the segmentation performed by 3 observers on N=2 samples, the average distance from the mean location of the test sites was slightly greater at 288±155μm (**Figure 2.2**).

Alignment of test sites to the indenter by the robot was within acceptable limits for accuracy and precision. The robot aligned the indenter perpendicular to the flat target with an angular error of 1.20±0.42° and an in-plane offset of 151±48μm. Repeating the registration and alignment steps between marking the surface of normal rabbit knees using a pin resulted in a distance of 101±36μm from the mean test site to the pin marks (**Figure 2.3**).

Table 2.1: Test Site Locations. Mean (*SD*) location of test sites relative to the DFCS for N=6 samples and the variability between corresponding sites on ACLT and CTRL femora. All units in mm.

Side	Site	L (CTRL)			R (ACLT)			D_i
	P							
LFC	1	3.32	4.77	-3.33	3.41	4.83	3.37	0.227 ± 0.088
		(*0.12*	*0.13*	*0.14*)	(*0.1*	*0.15*	*0.47*)	
	2	4.21	4.02	-3.77	4.35	4.06	3.75	0.284 ± 0.135
		(*0.17*	*0.13*	*0.18*)	(*0.1*	*0.14*	*0.27*)	
	3	4.97	3.11	-4.03	5.14	3.12	3.85	0.342 ± 0.168
		(*0.17*	*0.15*	*0.17*)	(*0.1*	*0.12*	*0.26*)	
	4	5.59	2.14	-4.25	5.77	2.1	4	0.363 ± 0.185
		(*0.22*	*0.12*	*0.14*)	(*0.16*	*0.11*	*0.17*)	
	5	6.13	1.06	-4.6	6.28	1.01	4.25	0.38 ± 0.213
		(*0.24*	*0.12*	*0.14*)	(*0.14*	*0.12*	*0.25*)	
	6	6.52	-0.08	-4.85	6.64	-0.12	4.46	0.395 ± 0.187
		(*0.22*	*0.09*	*0.25*)	(*0.14*	*0.09*	*0.27*)	
	7	6.7	-1.29	-5	6.86	-1.38	4.64	0.425 ± 0.193
		(*0.22*	*0.1*	*0.27*)	(*0.12*	*0.07*	*0.26*)	
	8	6.59	-2.53	-5.07	6.76	-2.59	4.77	0.454 ± 0.181
		(*0.23*	*0.13*	*0.29*)	(*0.12*	*0.06*	*0.28*)	
	9	6.2	-3.69	-5.07	6.29	-3.75	4.77	0.429 ± 0.184
		(*0.2*	*0.08*	*0.22*)	(*0.12*	*0.06*	*0.27*)	
	10	5.47	-4.7	-4.99	5.55	-4.72	4.73	0.399 ± 0.185
		(*0.15*	*0.08*	*0.19*)	(*0.1*	*0.04*	*0.31*)	
	11	4.52	-5.47	-4.92	4.56	-5.51	4.69	0.368 ± 0.224
		(*0.11*	*0.11*	*0.2*)	(*0.06*	*0.09*	*0.35*)	
	12	3.43	-6.01	-4.92	3.45	-6.04	4.59	0.293 ± 0.224
		(*0.08*	*0.11*	*0.19*)	(*0.03*	*0.05*	*0.37*)	
	D							
	P							
MFC	1	3.1	4.41	3.62	3.15	4.43	-4.11	0.221 ± 0.117
		(*0.17*	*0.2*	*0.63*)	(*0.1*	*0.15*	*0.39*)	
	2	3.94	3.62	4.06	3.97	3.6	-4.64	0.207 ± 0.069
		(*0.27*	*0.27*	*0.59*)	(*0.14*	*0.15*	*0.31*)	
	3	4.7	2.72	4.4	4.68	2.64	-5.03	0.202 ± 0.04
		(*0.35*	*0.23*	*0.49*)	(*0.22*	*0.1*	*0.26*)	
	4	5.35	1.68	4.59	5.3	1.58	-5.27	0.212 ± 0.068
		(*0.43*	*0.21*	*0.4*)	(*0.26*	*0.07*	*0.22*)	
	5	5.81	0.59	4.66	5.77	0.44	-5.37	0.234 ± 0.089
		(*0.48*	*0.19*	*0.34*)	(*0.32*	*0.05*	*0.24*)	
	6	6.15	-0.57	4.67	6.11	-0.76	-5.28	0.24 ± 0.123
		(*0.49*	*0.15*	*0.33*)	(*0.33*	*0.08*	*0.18*)	
	7	6.36	-1.78	4.59	6.37	-2.04	-5.03	0.246 ± 0.124
		(*0.49*	*0.11*	*0.31*)	(*0.37*	*0.17*	*0.15*)	
	8	6.45	-3.04	4.4	6.44	-3.26	-4.77	0.231 ± 0.127
		(*0.46*	*0.14*	*0.31*)	(*0.43*	*0.24*	*0.14*)	
	9	6.19	-4.26	4.21	6.17	-4.46	-4.55	0.201 ± 0.067
		(*0.4*	*0.23*	*0.27*)	(*0.38*	*0.28*	*0.13*)	
	10	5.58	-5.24	4.1	5.56	-5.43	-4.41	0.187 ± 0.061
		(*0.35*	*0.27*	*0.22*)	(*0.33*	*0.32*	*0.16*)	
	11	4.71	-6.02	4.03	4.76	-6.15	-4.28	0.143 ± 0.076
		(*0.21*	*0.29*	*0.14*)	(*0.23*	*0.34*	*0.21*)	
	12	3.67	-6.43	3.97	3.77	-6.6	-4.16	0.211 ± 0.079
		(*0.11*	*0.22*	*0.1*)	(*0.18*	*0.29*	*0.22*)	
	D							
LFC								0.363 ± 0.181
MFC								0.211 ± 0.088
All Sites								0.287 ± 0.161

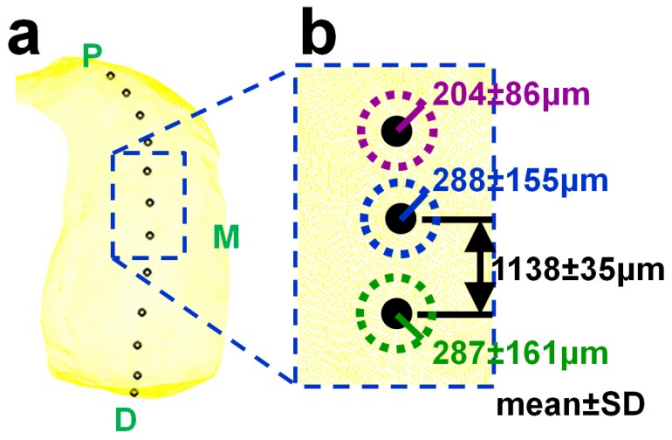

Figure 2.2: Varibility in Test Site Calculations. Average distances from mean locations for intraobserver variability (purple circle), interobserver (blue circle) variability, and right (ACLT) versus left (CTRL), or within sample, variability (green circle). Also, the distance between neighboring sites.

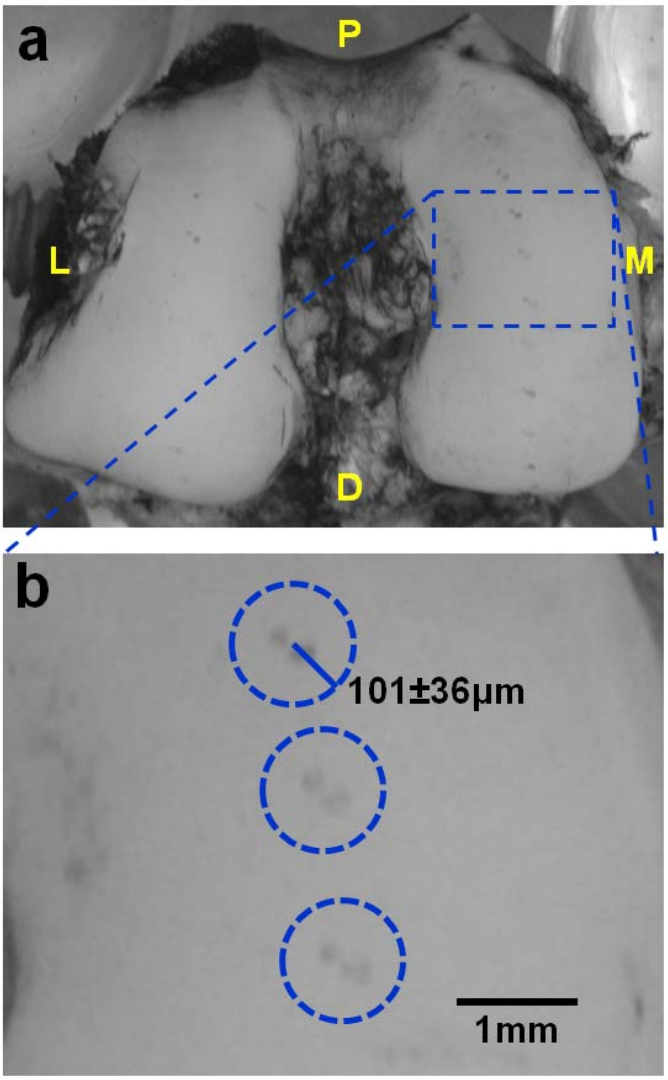

Figure 2.3: Variability in Robotic Alignment. Pin-marked femur showing alignment variability, with average distance from mean locations indicated.

(2) Site-specific Indentation Stiffness in ACLT: Despite the femoral articular cartilage surfaces being generally intact, with some minor fibrillation in ACLT, indentation testing revealed that the cartilage of ACLT knees was softer than that of CTRL knees at specific test sites. *ISS* was lower in ACLT than CTRL at MFC site 7 (–36%, 0.71±0.11 vs. 0.45±0.10 N/mm, $p<0.01$) and MFC site 8 (–31%, 0.63±0.13 vs. 0.43±0.11 N/mm, $p<0.05$) (**Figure 2.5.a&b**). There was a trend for *ISS* to be lower at MFC site 9 (–33%, 0.51±0.17 vs. 0.35±0.14 N/mm, $p=0.095$).

Site-specific cartilage thickness was similar between ACLT and CTRL knees (**Figure 2.5.c&d**). Cartilage in the distal regions of both the MFC and LFC were thicker than the proximal regions. MFC site 9 was the thickest, at 0.506±0.129mm, and MFC site 6 was the thinnest, at 0.242±0.037mm. Also, the cartilage was thicker on the MFC than the LFC (0.355±0.084mm vs. 0.253±0.067mm).

ISS_{NORM} followed the same trends as *ISS*. In normalizing the stiffness measures, the curve fit between *ISS* and *h* had $R^2=0.34$ (**Figure 2.4**). The parameters in the ISS_F equation, in the form of $ISS_F(h) = b + \frac{\left[Ae^{-\tau(h-h_O)}\right]}{\left[h-h_O\right]^c}$, were h_o = 0.0920mm, b = 0.4223N/mm, A = 0.1345, τ = -3.8131mm^{-1}, and c = 0.6452. ISS_{NORM}, the indentation structural stiffness normalized by ISS_F, was lower in ACLT than CTRL at MFC site 7 (-37%, 1.14±0.16 vs. 0.72±0.17, $p<0.01$) and MFC site 8 (-31%, 1.20±0.23 vs. 0.82±0.20, $p<0.05$). The trend of softening in ACLT at MFC site 9 was also observed with ISS_{NORM} (-33%, 1.07±0.36 vs. 0.72±0.30, $p=0.097$, **Figure 2.5.e&f**).

The repeated indentation measures were in agreement with the initial indentation measures. The overall average CV between indentation measures with repeated alignment, without repeating the registration, was 10.2%. Repeating both the registration and alignment resulted in an overall average CV of 10.3% between the initial indentation stiffness measures and the repeated measures.

(3) Correlation of Stiffness with Structural Parameters: Contrast-enhanced μCT imaging did not show any differences between ACLT and CTRL at any of the test sites. HEX uptake for all sites on both the MFC and LFC for both groups was ~12% (**Figure 2.5.g&h**). This can be observed in the ACLT and CTRL of a representative sample at sites 8, in the WB region, and 4, in the NWB region (**Figure 2.8**).

Site-specific softening was consistent with mild and localized histological and imaging indices of deterioration (**Figure 2.6**). Deterioration was observed in the ACLT, compared to the CTRL in a representative sample at sites 8, in the WB region, and 4, in the NWB region (**Figure 2.6**). Both Mankin-Shapiro and OARSI scores were greater in ACLT than CTRL for NWB and WB regions (5.6 vs. 3, $p<0.001$, and 7.3 vs. 4.2, $p<0.001$, respectively). ACLT also had an effect on Safranin-O subscores, where ACLT ($p<0.05$) was more degenerate than CTRL ($p=0.07$). In the WB region, the total Shapiro-Mankin score correlated negatively with *ISS* and ISS_{NORM} ($\rho=-0.61$, $p<0.05$, one-tailed $\rho_{critical} = -0.59$), while combined (WB+NWB) *ISS* correlated negatively with combined OARSI score ($\rho=-0.61$, $p<0.05$) (**Figure 2.7**).

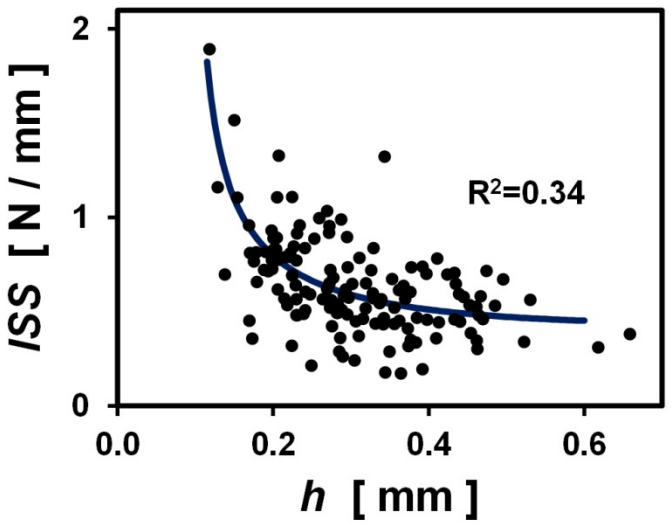

Figure 2.4: Curve Fit between Stiffness and Thickness. Fit of CTRL stiffness and thickness data from all locations on both condyles. $R^2 = 0.34$.

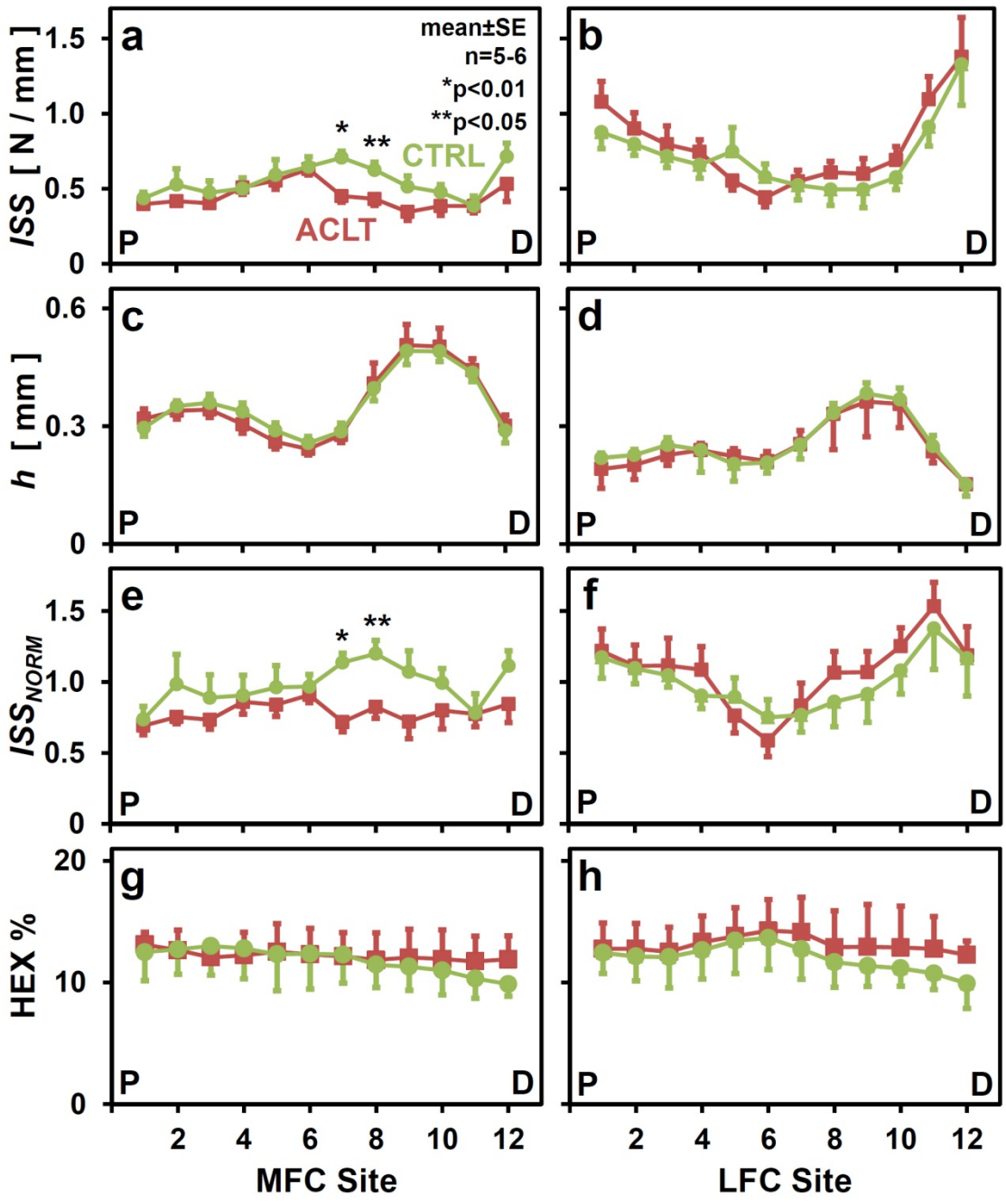

Figure 2.5: Site-Specific Properties of ACLT vs. CTRL. Indentation stiffness (**a**, **b**), cartilage thickness (**c**, **d**), and normalized indentation stiffness (**e**, **f**) on the (**a**, **c**, **e**) MFC and (**b**, **d**, **f**) LFC of ACLT and CTRL femora (mean±SD, N=5-6). * = $p<0.01$, ** = $p<0.05$.

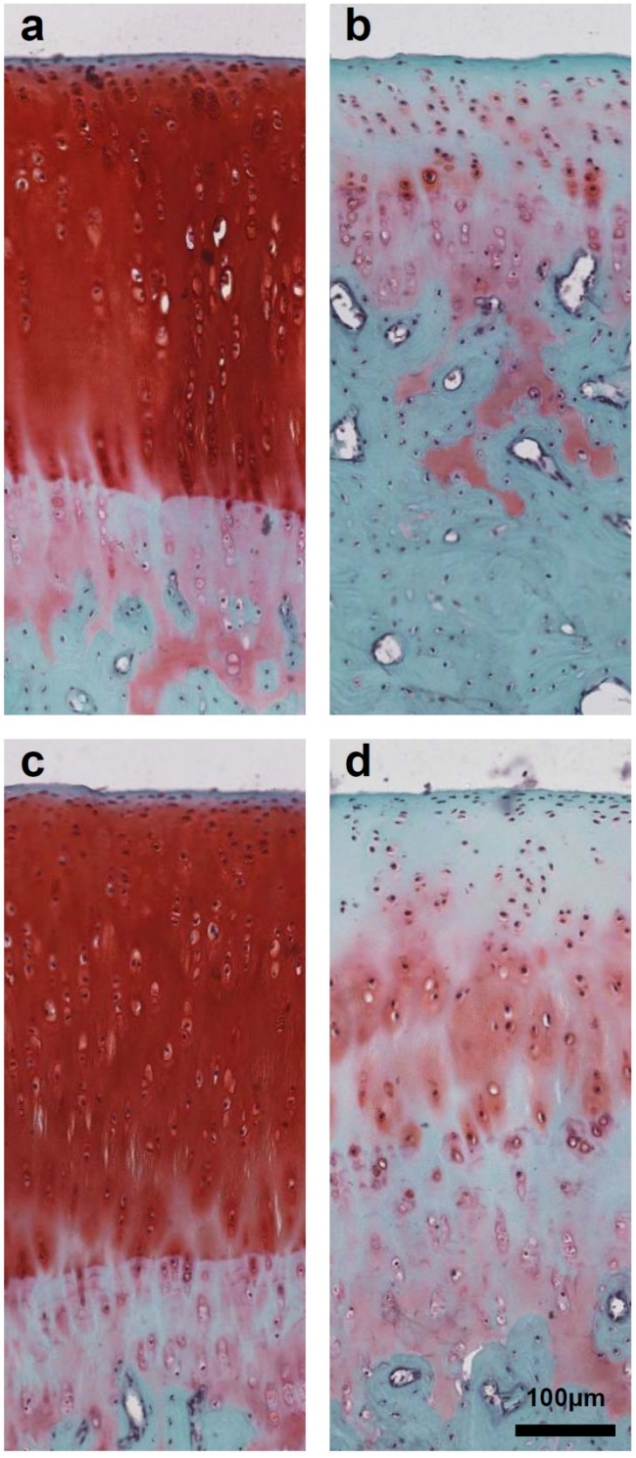

Figure 2.6: Representative Site-Specific Histology. Typical section, stained with SafraninO, of weight bearing site (MFC site 8, **a&b**) and a non-weight bearing site (MFC site 4, **c&d**) from both (**a&c**) CTRL and (**b&d**) ACLT.

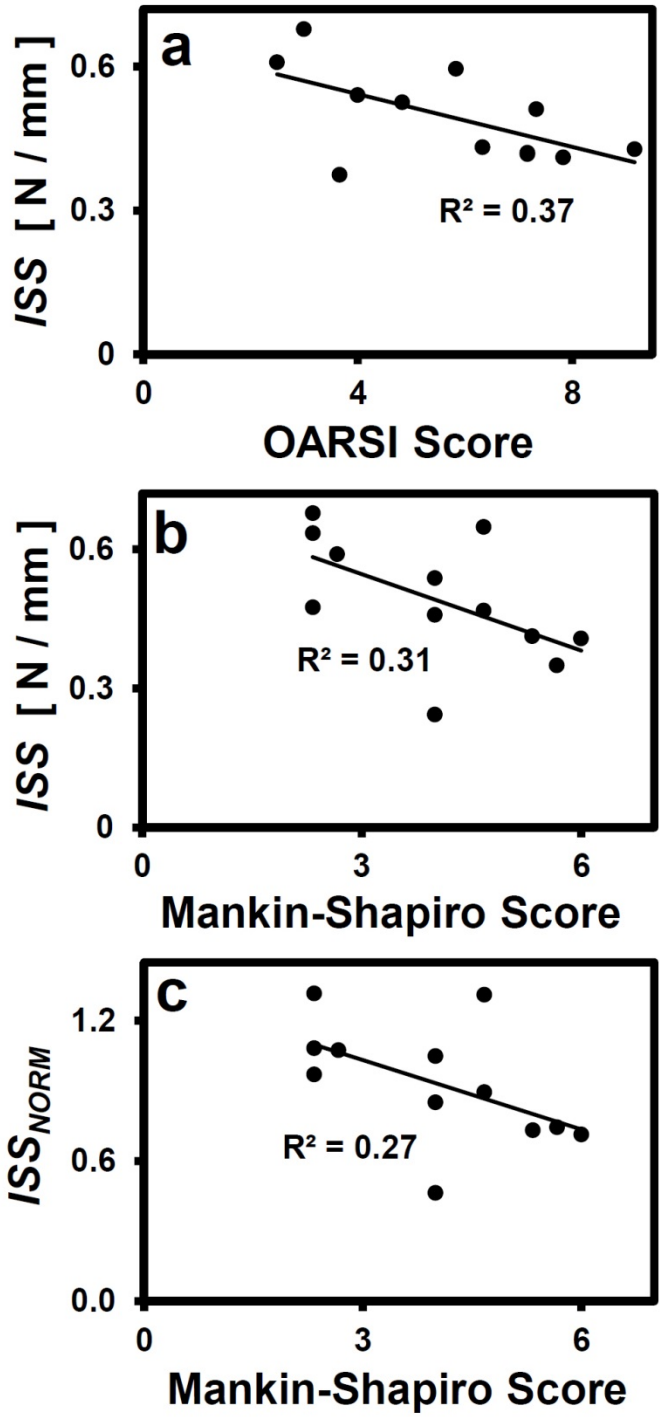

Figure 2.7: Correlation between Stiffness and Histological Scores. Correlation is for data in the weight-bearing region.

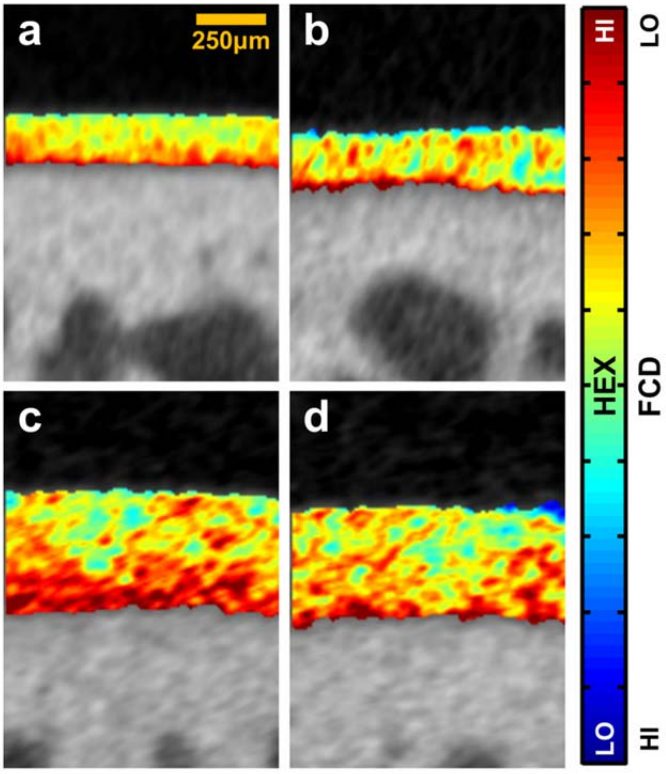

Figure 2.8: Representative Site-Specific μCT Images. Typical μCT image of a non-weight-bearing site (MFC site 4, **a**&**b**) and a weight-bearing site (MFC site 8, **c**&**d**) from both (**a**&**c**) CTRL and (**b**&**d**) ACLT.

2.5 Discussion

These results suggest that ACLT causes a functional impairment of articular cartilage, in the WB region of the MFC, by 28 days following the insult. This impairment is related to structural changes in the collagen matrix. In this study, the process of computing the location of test sites and achieving alignment with reasonable precision using the robotic test system was verified. Mechanical softening in ACLT relative to CTRL was observed at select test sites on the MFC. Furthermore, the association of softening and histological score in the WB region of ACLT suggests changes in the collagen matrix are responsible for the loss in stiffness. These observations help explain where degradation of cartilage occurs during the initial stages following ACLT and the changes in the structure associated with the functional impairment.

In defining the test sites, several assumptions were made and certain limitations of the robotic testing procedure were considered. The test sites were computed based on the articular surface geometry and a coordinate system defined by anatomic landmarks. The landmarks were readily identifiable on all samples, and selection of these landmarks was assumedly consistent. Previous studies of selecting anatomic landmarks on the human femur in 3-D image data have shown low inter- and intra-observer variability.[45, 46] Due to possible interference between the femur, mounted in the vise, and the indenter, it was determined that the most distal region of the femur would be untestable. Despite these limitations, both the weight-bearing and non-weight-bearing regions of the rabbit knee[14] were able to be tested. The

histochemical analysis presented an additional limitation, in that planar histological slices were compared to test sites that deviate in medial-lateral direction. However the medial-lateral deviation was only ~0.5mm, which was less than the distance that properties would have changed significantly.

Cartilage degeneration following ACLT occurs regionally[9] and, as shown in this study, these regions may be elucidated at earlier time points by mechanical measurement. Mechanistically, this study demonstrates a functional softening of cartilage tissue at an early time point following ACLT that may lead to the later fibrillation and wear characteristic of this model of OA. Additionally, cartilage degeneration may be the result of wear due to increased sliding distances and forces combined with inflammation-mediated chemical degradation of the matrix.

At 28 days following ACL transection, the site-specific softening observed in this study is consistent with previous studies. Softening of cartilage at sites MFC 7 and MFC 8 showed slight to moderate surface disruption[7, 17] and some loss of proteoglycan, without full thickness ulceration or significant changes in thickness.[50] The locations where softening was observed in this study correspond to the largest location of degeneration at 9 weeks following ACL transection.[9] That the softening correlated with the histochemical scores, but not FCD, indicates the softening at 28 days following ACL transection may be due to fibrillation of the superficial matrix alone, or in combination with PG depletion that was not detected in this study.

Using laser scan data, test sites were reproducibly located on the rabbit femur, with ACLT and CTRL being reasonably similar, covering a large enough test area to detect site-specific changes in stiffness following ACLT. The main source of error is

likely in the imaging technique; the highly reflective cartilage surface produces significant noise in the laser scan images and data undergoes two smoothing steps in order to achieve a sufficiently flat surface. This noise is likely due to the inherent shiny appearance the tissue, as the NextEngine laser scanner is known to be sensitive to the reflectivity and color of the surface being scanned, as well as the ambient light.[27, 34, 51]

The parallel design of the 6 DoF robot used in this test is well suited for biomechanical test applications. Parallel robots, such as the rotopod used in this study, are known for their exceptional rigidity and accuracy, and low compliance.[30] However, the range of motion in certain directions is typically limited. Despite this limitation, parallel robots have been used to replicate gait patterns of the human foot and ankle in order to investigate ground reaction forces[20, 47], investigate spine biomechanics[16, 21], and reproduce gait patterns of the ovine knee.[19] Robotic technology has many applications in orthopaedic research, to evaluate kinematics of ligaments, menisci, and other tissues, as well as methods for reconstruction of these structures in situ.[15, 36]

The ramp indentation procedure utilized in this study is suitable for both the multiple-site testing scheme and determining softening of cartilage. Since multiple test sites were being investigated, it is important that the test is rapid in order to maintain the quality of the tissue. Indentation can be used to characterize material properties of articular cartilage, with models of the test established to obtain Young's modulus, shear modulus, Poisson's ratio, bulk modulus, aggregate modulus, or dynamic modulus, depending on the indentation testing parameters.[18, 29] There are some

important caveats and assumptions that must be considered when performing an indentation test,[6] most importantly the thickness of the tissue, which affects both the required indenter tip contact area and the depth of testing.[18] The protocol used in this study included a 0.4mm spherical-ended tip depressed 25μm, less than 10% of the tissue thickness for most test sites, into the tissue, satisfying these test requirements.

The robotic indentation method and the results obtained offer a variety of possible directions for future studies. The identification of early, site-specific changes in articular cartilage in the rabbit ACLT model of PTOA provides a foundation for mechanistic and interventional studies. For instance, the site-specific degeneration of cartilage in the rabbit ACLT model at earlier and later time points can be investigated, to determine temporal patterns of disease progression. These data will aid in designing interventions to be given at specific time points, optimizing the effect in preventing degeneration and restoring function. Furthermore, the robotic indentation method can be used to evaluate such interventions. The robot indentation method can also be adapted to evaluate cartilage degeneration or repair in a variety of animal models or human tissue retrieval studies.

2.6 Glossary

OA – Osteoarthritis

PTOA – Post-traumatic osteoarthritis

ACL – Anterior Cruciate Ligament

ACLT – Anterior Cruciate Ligament Transection; also used as the name of the experimental group in the ACLT studies

CTRL – Control group; in the ACLT study, this was the unoperated, contralateral knee

LFC – Lateral Femoral Condyle

MFC – Medial Femoral Condyle

DoF – Degrees of Freedom

PBS, PBS+PI – Phosphate buffered saline, phosphate buffered saline with protease inhibitors

ISS – Indentation structural stiffness, defined by dividing the measured force by the input displacement

ISS_{NORM} – Normalized indentation structural stiffness, defined by dividing ISS by the theoretical value at the thickness of the site

t – Cartilage thickness

FCD – Fixed charge density

2.7 Acknowledgments

This chapter, in full, will be submitted to *Technology.* The dissertation author is the primary investigator and thanks co-authors, Jason P. Caffrey, M.S., Karli K. Gillette, Iliya Goldberg, M.S., Kirsten E. Cherry, Esther Cory, M.S., William J. McCarty, Ph.D., Tomonori Yamaguchi, M.S., Albert C. Chen, Ph.D., Michele M. Temple-Wong, Ph.D., Chris B. Raub, Ph.D., Koichi Masuda, M.D., Robert L. Sah, M.D., Sc.D. The authors thank Elaine F. Chan, Ph.D., for assistance with image processing and Won C. Bae, Ph.D., Van Wong, Johnny Tam, Meena Siddiqui, Sahil Patel, Amran Asadi, and Roman Dittmar for assistance with the robot.

This work was supported by research grants from the National Institutes of Health (R01 AR051565, P01 AG007996) and an award to the University of California–San Diego under the Howard Hughes Medical Institute Professors Program (RLS).

2.8 References

1. Andriacchi TP, Mundermann A: The role of ambulatory mechanics in the initiation and progression of knee osteoarthritis. *Curr Opin Rheumatol* 18:514-8, 2006.

2. Athanasiou KA, Rosenwasser MP, Buckwalter JA, Malinin TI, Mow VC: Interspecies comparisons of in situ intrinsic mechanical properties of distal femoral cartilage. *J Orthop Res* 9:330-40, 1991.

3. Bae WC, Lewis CW, Levenston ME, Sah RL: Indentation testing of human articular cartilage: effects of probe tip geometry and indentation depth on intra-tissue strain. *J Biomech* 39:1039-47, 2006.

4. Bae WC, Payanal MM, Chen AC, Hsieh-Bonassera ND, Ballard BL, Lotz MK, Coutts RD, Bugbee WD, Sah RL: Topographic patterns of cartilage lesions in knee osteoarthritis. *Cartilage* 1:10-9, 2010.

5. Bae WC, Temple MM, Amiel D, Coutts RD, Niederauer GG, Sah RL: Indentation testing of human cartilage: sensitivity to articular surface degeneration. *Arthritis Rheum* 48:3382-94, 2003.

6. Bae WC, Temple MM, Rivard KL, Bowden K, Healey RM, Amiel D, Coutts RD, Niederauer GG, Sah RL: Sensitivity of indentation testing of human articular cartilage to probe and tissue characteristics. *Int Cart Repair Soc* 4, 2002.

7. Batiste DL, Kirkley A, Laverty S, Thain LM, Spouge AR, Gati JS, Foster PJ, Holdsworth DW: High-resolution MRI and micro-CT in an ex vivo rabbit anterior cruciate ligament transection model of osteoarthritis. *Osteoarthritis Cartilage* 12:614-26, 2004.

8. Chan EF, Liu I-L, Semler EJ, Aberman HM, Simon TM, Chen AC, Truncale KG, Sah RL: Association of 3-dimensional cartilage and bone structure with articular cartilage properties in and adjacent to autologous osteochondral grafts after 6 and 12 months in a goat model. *Cartilage* 3:255-66, 2012.

9. Chang DG, Iverson EP, Schinagl RM, Sonoda M, Amiel D, Coutts RD, Sah RL: Quantitation and localization of cartilage degeneration following the induction of osteoarthritis in the rabbit knee. *Osteoarthritis Cartilage* 5:357-72, 1997.

10. Chang N, Cory E, Chen AC, Raub CB, Chan EF, Urbina AM, Otsuki S, Hasegawa A, Lotz MK, Sah RL: Spatial variation in indentation properties of human femoral articular cartilage. *Trans Orthop Res Soc,* Long Beach, CA, 36:2137, 2011.

11. Connolly A, FitzPatrick D, Moulton J, Lee J, Lerner A: Tibiofemoral cartilage thickness distribution and its correlation with anthropometric variables. *Proc Inst Mech Eng H* 222:29-39, 2008.

12. Darling EM, Wilusz RE, Bolognesi MP, Zauscher S, Guilak F: Spatial mapping of the biomechanical properties of the pericellular matrix of articular cartilage measured in situ via atomic force microscopy. *Biophys J* 98:2848-56, 2010.

13. Desrochers J, Amrein MW, Matyas JR: Viscoelasticity of the articular cartilage surface in early osteoarthritis. *Osteoarthritis Cartilage* 20:413-21, 2012.

14. Eggli PS, Hunziker EB, Schenk RK: Quantitation of structural features characterizing weight- and less-weight-bearing regions in articular cartilage: a stereological analysis of medial femoral condyles in young adult rabbits. *Anat Rec* 222:217-27, 1988.

15. Fujie H, Mabuchi K, Woo SL, Livesay GA, Arai S, Tsukamoto Y: The use of robotics technology to study human joint kinematics: a new methodology. *J Biomech Eng* 115:211-7, 1993.

16. Goertzen DJ, Kawchuk GN: A novel application of velocity-based force control for use in robotic biomechanical testing. *J Biomech* 42:366-9, 2009.

17. Hashimoto S, Ochs RL, Komiya S, Lotz M: Linkage of chondrocyte apoptosis and cartilage degradation in human osteoarthritis. *Arthritis Rheum* 41:1632-8, 1998.

18. Hayes WC, Keer LM, Herrmann G, Mockros LF: A mathematical analysis for indentation tests of articular cartilage. *J Biomech* 5:541-51, 1972.

19. Howard RA, Rosvold JM, Darcy SP, Corr DT, Shrive NG, Tapper JE, Ronsky JL, Beveridge JE, Marchuk LL, Frank CB: Reproduction of in vivo motion using a parallel robot. *J Biomech Eng* 129:743-9, 2007.

20. Jackson LT, Aubin PM, Cowley MS, Sangeorzan BJ, Ledoux WR: A robotic cadaveric flatfoot analysis of stance phase. *J Biomech Eng* 133:051005, 2011.

21. Kawchuk GN, Carrasco A, Beecher G, Goertzen D, Prasad N: Identification of spinal tissues loaded by manual therapy: a robot-based serial dissection technique applied in porcine motion segments. *Spine* 35:1983-90, 2010.

22. Kempson GE, Freeman MA, Swanson SA: The determination of a creep modulus for articular cartilage from indentation tests of the human femoral head. *J Biomech* 4:239-50, 1971.

23. Kempson GE, Muir H, Swanson SA, Freeman MA: Correlations between stiffness and the chemical constituents of cartilage on the human femoral head. *Biochim Biophys Acta* 215:70-7, 1970.

24. Kiviranta P, Lammentausta E, Toyras J, Kiviranta I, Jurvelin JS: Indentation diagnostics of cartilage degeneration. *Osteoarthritis Cartilage* 16:796-804, 2008.

25. Laasanen MS, Toyras J, Hirvonen J, Saarakkala S, Korhonen RK, Nieminen MT, Kiviranta I, Jurvelin JS: Novel mechano-acoustic technique and instrument for diagnosis of cartilage degeneration. *Physiol Meas* 23:491-503, 2002.

26. Laverty S, Girard CA, Williams JM, Hunziker EB, Pritzker KP: The OARSI histopathology initiative - recommendations for histological assessments of osteoarthritis in the rabbit. *Osteoarthritis Cartilage* 18 Suppl 3:S53-65, 2010.

27. Lemeš S, Zaimović-Uzunović N: Study of ambient light influence on laser 3D scanning. *ICIT & MPT,* 7:327-30, 2009.

28. Lyyra T, Arokoski JP, Oksala N, Vihko A, Hyttinen M, Jurvelin JS, Kiviranta I: Experimental validation of arthroscopic cartilage stiffness measurement using enzymatically degraded cartilage samples. *Phys Med Biol* 44:525-35, 1999.

29. Mak AF, Lai WM, Mow VC: Biphasic indentation of articular cartilage--I. Theoretical analysis. *J Biomech* 20:703-14, 1987.

30. Merlet JP. Parallel robots. 2nd ed. Dordrecht ; Boston, MA: Kluwer Academic Publishers; 2006.

31. Mow VC, Gibbs MC, Lai WM, Zhu WB, Athanasiou KA: Biphasic indentation of articular cartilage--II. A numerical algorithm and an experimental study. *J Biomech* 22:853-61, 1989.

32. Niederauer GG, Niederauer GM, Cullen LC, Jr., Athanasiou KA, Thomas JB, Niederauer MQ: Correlation of cartilage stiffness to thickness and level of degeneration using a handheld indentation probe. *Ann Biomed Eng* 32:352-9, 2004.

33. Pierce DM, Trobin W, Trattnig S, Bischof H, Holzapfel GA: A phenomenological approach toward patient-specific computational modeling of articular cartilage including collagen fiber tracking. *J Biomech Eng* 131:091006, 2009.

34. Polo M-E, Felicísimo ÁM: Analysis of uncertainty and repeatability of a low-cost 3D laser scanner. *Sensors* 12:9046-54, 2012.

35. Räsänen T, Messner K: Regional variations of indentation stiffness and thickness of normal rabbit knee articular cartilage. *J Biomed Mater Res* 31:519-24, 1996.

36. Rudy TW, Livesay GA, Woo SL, Fu FH: A combined robotic/universal force sensor approach to determine in situ forces of knee ligaments. *J Biomech* 29:1357-60, 1996.

37. Saarakkala S, Laasanen MS, Jurvelin JS, Torronen K, Lammi MJ, Lappalainen R, Toyras J: Ultrasound indentation of normal and spontaneously degenerated bovine articular cartilage. *Osteoarthritis Cartilage* 11:697-705, 2003.

38. Saito M, Sasho T, Yamaguchi S, Ikegawa N, Akagi R, Muramatsu Y, Mukoyama S, Ochiai N, Nakamura J, Nakagawa K, Nakajima A, Takahashi K: Angiogenic activity of subchondral bone during the progression of osteoarthritis in a rabbit anterior cruciate ligament transection model. *Osteoarthritis Cartilage* 20:1574-82, 2012.

39. Shapiro F, Glimcher MJ: Induction of osteoarthrosis in the rabbit knee joint: histologic changes following meniscectomy and meniscal lesions. *Clin Orthop Rel Res* 147:287-95, 1980.

40. Shirai T, Kobayashi M, Nishitani K, Satake T, Kuroki H, Nakagawa Y, Nakamura T: Chondroprotective effect of alendronate in a rabbit model of osteoarthritis. *J Orthop Res* 29:1572-7, 2011.

41. Swann AC, Seedhom BB: Improved techniques for measuring the indentation and thickness of articular cartilage. *Proc Inst Mech Eng H* 203:143-50, 1989.

42. Temple-Wong MM, Bae WC, Chen MQ, Bugbee WD, Amiel D, Coutts RD, Lotz M, Sah RL: Biomechanical, structural, and biochemical indices of degenerative and osteoarthritic deterioration of adult human articular cartilage of the femoral condyle. *Osteoarthritis Cartilage* 17:1469-76, 2009.

43. Temple MM, Bae WC, Chen MQ, Lotz M, Amiel D, Coutts RD, Sah RL: Age- and site-associated biomechanical weakening of human articular cartilage of the femoral condyle. *Osteoarthritis Cartilage* 15:1042-52, 2007.

44. Vasara AI, Jurvelin JS, Peterson L, Kiviranta I: Arthroscopic cartilage indentation and cartilage lesions of anterior cruciate ligament-deficient knees. *Am J Sports Med* 33:408-14, 2005.

45. Victor J, Van Doninck D, Labey L, Innocenti B, Parizel PM, Bellemans J: How precise can bony landmarks be determined on a CT scan of the knee? *Knee* 16:358-65, 2009.

46. Victor J, Van Doninck D, Labey L, Van Glabbeek F, Parizel P, Bellemans J: A common reference frame for describing rotation of the distal femur: a ct-based kinematic study using cadavers. *J Bone Joint Surg Br* 91:683-90, 2009.

47. Whittaker EC, Aubin PM, Ledoux WR: Foot bone kinematics as measured in a cadaveric robotic gait simulator. *Gait Posture* 33:645-50, 2011.

48. Wilusz RE, Zauscher S, Guilak F: Micromechanical mapping of early osteoarthritic changes in the pericellular matrix of human articular cartilage. *Osteoarthritis Cartilage*, 2013.

49. Wu H, Du J, Zheng Q: Expression of MMP-1 in cartilage and synovium of experimentally induced rabbit ACLT traumatic osteoarthritis: immunohistochemical study. *Rheumatol Int* 29:31-6, 2008.

50. Yoshioka M, Coutts RD, Amiel D, Hacker SA: Characterization of a model of osteoarthritis in the rabbit knee. *Osteoarthritis Cartilage* 4:87-98, 1996.

51. Zaimovic-Uzunovic N, Lemes S: Influences of surface parameters on laser 3D scanning. *IMEKO CONFERENCE PROCEEDINGS: INTERNATIONAL SYMPOSIUM ON MEASUREMENT AND QUALITY CONTROL*, 2010.

52. Zhao Z, Ji H, Jing R, Wang M, Liu C, Zhai L, Bai X, Xing G: Extracorporeal shock-wave therapy reduces progression of knee osteoarthritis in rabbits by reducing nitric oxide level and chondrocyte apoptosis. *Arch Orthop Trauma Surg* 132:1547-53, 2012.

CHAPTER 3

COMPUTATIONAL TOPOGRAPHIC MATCH OF ORTHOTOPIC VS. NON-ORTHOTOPIC LATERAL AND MEDIAL FEMORAL CONDYLE OSTEOCHONDRAL ALLOGRAFTS

3.1 Abstract

INTRODUCTION: Fresh osteochondral allograft (OCA) transplantation is effective for repairing large articular lesions on the medial femoral condyle (MFC); however, the practice of obtaining an orthotopic OCA limits the number of repairs performed. Recent studies show that lateral femoral condyle (LFC) OCA, up to 20mm in diameter, can be implanted in MFC defects and create a geometric surface match. HYPOTHESIS: Non-orthotopic LFC and MFC OCA can restore the topographic properties of MFC recipient sites as well as orthotopic MFC OCA. OBJECTIVE: Investigate the computational fit of OCA, recovered from three defined sites on LFCs and MFCs, placed in three defined MFC recipient sites. METHODS: Eight LFCs and 16 MFCs were imaged by micro computed tomography (μCT), and divided into three groups: MFC recipients (MFCr, N=8), MFC donors (MFCd, N=8), and LFC donors

(LFCd, N=8). Three 20mm sites (0, 1, and 2) were defined on MFCr and MFCd, and on the LFCd in contralateral locations, within a standard coordinate system. OCA from these MFCd and LFCd locations were placed in the MFCr locations computationally in 3-D by minimizing RMS vertical deviation between the edges of the graft and recipient. RMS vertical deviation of OCA, s_{RMS}, and step-off at the edges, $h_{step,RMS}$, were determined, and the percent of the graft surface area and circumference that was proud, A_{proud} and C_{proud}, and within the acceptable distance (±1mm), A_{acc} and C_{acc}, was determined. RESULTS: There was no significant difference in s_{RMS}, $h_{step,RMS}$, A_{acc}, A_{proud}, C_{acc}, or C_{proud} for any combination of MFCd or LFCd site and MFCr site, although variations in the deviation and step-off patterns did exist. MFCd OCA repaired MFCr with $A_{acc}\geq 99\%$, whereas LFCd OCA repaired MFCr defects with $A_{acc}\geq 98\%$. All OCA repaired MFCr defects with $C_{acc}=100\%$, except MFCd and LFCd site 0 repaired the three MFCr defects with $C_{acc}\geq 99\%$ and $\geq 95\%$, respectively. CONCLUSION: These results indicate that LFCd OCA and non-orthotopic MFCd OCA provide a match to the MFCr surface topology at least as good as orthotopic OCA from MFCd.

3.2 Introduction

Fresh osteochondral allograft (OCA) transplantation is a successful method for the repair of large articular lesions on the femoral condyles.[7, 21, 34] In this procedure, the damaged region of the condyle is replaced with a cylindrical osteochondral core, from an orthotopic donor.[9, 22] The ultimate goal is that the OCA will integrate with the host subchondral bone and articular cartilage, to become a biologically active, functional replacement. The success in this goal is dependent on the topographic match to the articular surface.

There are both mechanical and biological factors that lead to successful OCA integration when there is a topographical match between the OCA and host articular surface. A flush topographical match restores the mechanics of the joint,[15, 31] and deviations from this can negatively affect the repair.[15] Obtaining OCA from the matching locations and similar tissue sources is thought to improve the chances of successful repair.[16] The success of the repair is also correlated to the long-term viability of the cells[28], which is affected by the duration and temperature of storage prior to implantation.[29] The subchondral bone integration, while typically good in OCA repairs, can be affected by excessive subchondral disruption at implantation.[26]

The practice of obtaining a site-matched OCA limits the number of repairs that can be performed. This is due in part to the higher incidence of damage on medial femoral condyles (MFC) than on lateral femoral condyles (LFC).[7, 11, 14, 33] The Joint Restoration Foundation has reported that MFC OCA constitute 97% of OCA requested; however, of the OCA suitable and available to surgeons, 75% are LFC

OCA.[23] This presents an issue where MFC OCA may not be available for MFC repairs. To address this, an *ex vivo* OCA transplantation study [23] showed that LFC OCA, up to 20mm in diameter, can be implanted in MFC defects and fulfill the geometric surface match criteria of ±1.0mm [24] as well as MFC OCA.

Although the process was successful *ex vivo*, it is unknown how specific the site match must be between donor and recipient sites to achieve a topographic match. We hypothesize that OCA harvested from multiple sites of LFC and MFC donor hemi-condyles can restore the topographic properties of a variety of MFC recipient sites. This study aims to answer this hypothesis by performing OCA transfer computationally with micro computed tomography (μCT) images, placing OCA from three defined donor sites on the MFC, and three contralateral sites on the LFC, into three defined recipient sites on the MFC, and testing the geometric match of orthotopic and non-orthotopic OCA.

3.3 Methods

Study Design. OCA from N=8 LFC donors (LFCd) and N=8 MFC donors (MFCd) were placed in N=8 MFC recipients (MFCr) with a custom, μCT image-based MATLAB (Mathworks, Natick, MA) program that places OCA computationally in 3-D. Computational OCA from three defined sites on LFCd and MFCd were placed in three defined sites on MFCr, testing whether non-orthotopic OCA from LFCd and MFCd provide a match comparable to orthotopic OCA from MFCd, when placed into an MFC defect. The match of the OCA was characterized by vertical deviation and step-off at the edges of the graft. The results were tested using a 2-way ANOVA with repeated factors of condyle (MFCd vs. LFCd) and site (0, 1, or 2).

Twenty-four human knee condyles (16 MFCs and 8 LFCs) were provided by the Joint Restoration Foundation and scanned by μCT. The specimens, provided frozen, were visually inspected for defects in the articular surface. Eight MFC were assigned to be recipients (MFCr), and eight MFC were assigned to be donors (MFCd), as were the eight LFC (LFCd). The MFCd and LFCd were matched to MFCr as described previously,[23] by size and side, matching MFCd ipsilateral and LFCd contralateral to MFCr (right MFCd and left LFCd matched to right MFCd, and vice versa). Condyles were scanned by μCT (Skyscan 1076, Skyscan, Kontich, BE), at 18-mm isotropic voxel size by applying an electrical potential of 100 kVp and a current of 100 mA, using a 0.038-mm copper and 0.5-mm aluminum filter.

Condyle Registration. In order to define 3 standard sites on the condyles, the μCT images were registered to a standard, anatomic coordinate system. This registration was facilitated by use of an atlas – a template onto which the MFCs and LFCs could be registered – created from a computed tomography (CT) scan of a normal human cadaveric knee. The cadaver knee was scanned in a GE Discovery CT scanner (CT 750HD, GE Healthcare, Little Chalfont, UK), with a slice thickness of 0.625mm and in-plane resolution of 0.31mm. The femur was reconstructed in 3-D in Mimics (Materialise, Leuven, BE), and the subchondral bone surfaces of the MFC and LFC, and the surface of the femoral diaphysis, were obtained from the reconstruction. Importing these surfaces into MATLAB, the femur was aligned to an anatomic coordinate system, based on sphere fits to the condyles and a cylinder fit to the diaphysis.[32] In this formulation, the femoral diaphysis was fit to a cylinder, creating an anatomic axis, which was denoted as the *z* axis. Next, the bone surfaces of the MFC and LFC were each fit to a sphere, and the centroids of these spheres were connected to create a construction line, known as the femoral transverse axis (FTA).[32] Then, the cross product of the *z* axis and the construction line was computed to give the *y* axis. The final step was to perform the cross product of the *y* axis and *z* axis, to give the *x* axis, which was almost parallel with the FTA.

The μCT images of the MFCd, MFCr, and LFCd were then registered to the LFC and MFC of the atlas, aligning them to the anatomic coordinate system (**Figure 3.1.A**). The μCT images were imported into MATLAB, and the subchondral bone surface of MFCd, MFCr, and LFCd was determined by thresholding. The medial or lateral sulci, as well as the posterior boundary of the condyles, were identified on the

subchondral bone of the atlas and the MFCd, MFCr, and LFCd. The condyles were registered to the atlas with these anatomic markers, and thereby registered to the anatomic coordinate system.

Standard Recipient and Donor Sites. Three 20mm donor and recipient sites of the MFC were chosen to lie within an area typically afflicted by cartilage erosion,[5] and three 20mm donor sites of the LFC were chosen to be in a contralateral location. The anterior margin of these regions was 9.5° from the *z*-axis of the femur, in the sagittal plane. From there, two 20mm diameter sites on each condyle were spaced 10mm and 20mm posteriorly by arc length (**Figure 3.1.A**). A normal vector was computed from the articular surface of the 20mm diameter areas, defining the *z*-axis for the OCA and defects.

The 20mm donor and recipient regions were characterized by nearest-neighbor thickness, h^{AC}, and fit to a sphere. After aligning the images with the normal vectors of the 20mm regions, maintaining the medial-lateral orientation in the transverse plane, the articular cartilage surface was determined by thresholding, creating a $(72\mu m)^2$ grid in the medial-lateral and anterior-posterior directions. The nearest-neighbor distance from each point in this grid to the subchondral bone surface was then computed. The articular cartilage surface was then fit to a sphere, and the deviation from this sphere vertically, along the *z*-axis of the 20mm OCA region, was computed.

Computational Placement of OCA. OCA from the three MFCd sites and three LFCd sites were placed in three MFCr sites, creating 3x3x2=18 repair situations

(**Figure 3.1.B**), computationally in 3-D, by minimizing the RMS deviation, s_{RMS}, between the edges of the OCA and recipient articular surfaces (**Figure 3.1.C**). First, the OCA surface was rotated about the medial-lateral and anterior-posterior axes, by α and β, respectively (each, -5° to 5°). At each α-β combination, the translation along the vertical axis of the OCA, z, was found by minimizing the s_{RMS} between 1mm-wide edges of the OCA and recipient. The α-β-z combination with the lowest s_{RMS} was selected as the optimal graft placement position, and the μCT image of the OCA was rotated, translated, and cropped in 3-D to place it in the μCT image of the recipient.

Quantification of Repairs and Statistics. To describe the fit of each donor OCA to each recipient site, the vertical deviation, s, and step-off height, h_{step}, were mapped, and s_{RMS} and $h_{step,RMS}$, respectively, were computed for each of the 18 repair situations. Additionally, the percent of the graft surface area that was acceptable (within ±1mm, $A_{acceptable}$) or proud (>0mm, A_{proud}) in deviation, and the percent of the graft circumference that was acceptable (within ±1mm, $C_{acceptable}$) or proud (>0mm, C_{proud}) in step-off height, were computed.

The mean±SD for s_{RMS}, $h_{step,RMS}$, A_{proud}, A_{acc}, C_{proud}, and C_{acc} measures were computed. The effects of condyle and donor site on these measures were tested for each of the 18 repair situations by 2-way ANOVA.

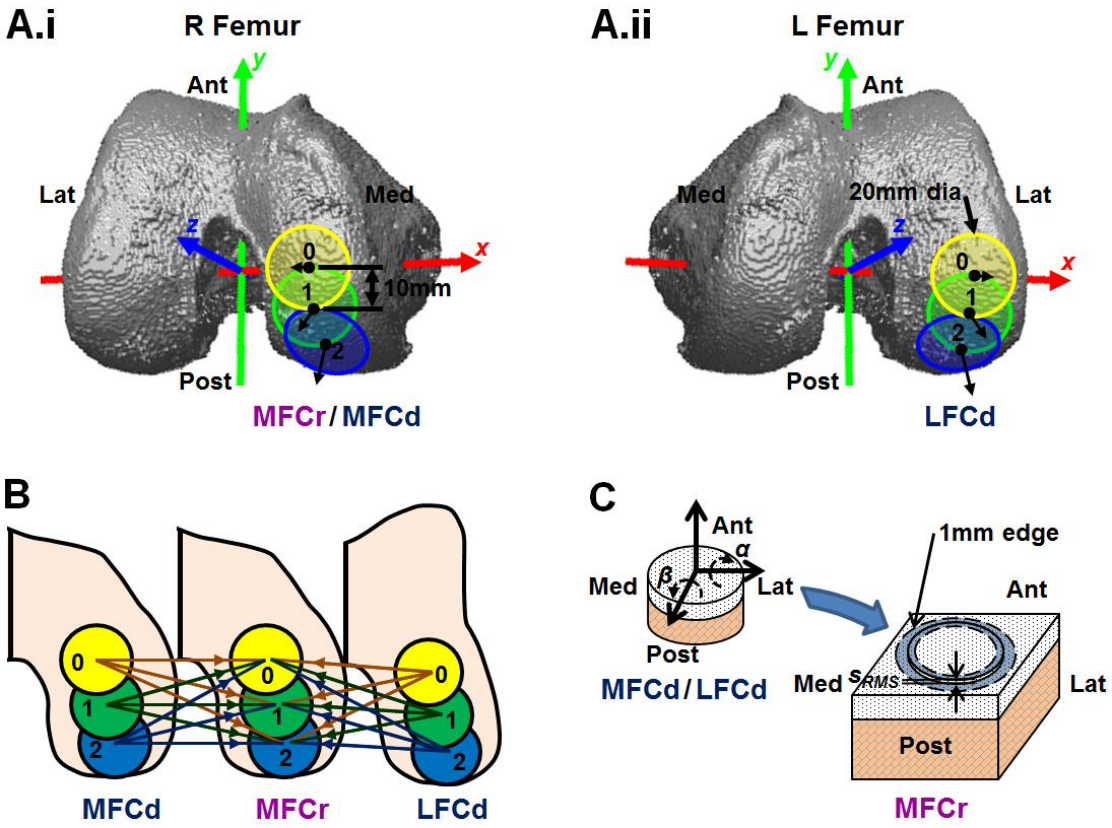

Figure 3.1: Computational OCA Study Design. Three 20mm-diameter sites defined 10mm apart, by arc length, on (**A.i**) MFCr and MFCd and in (**A.ii**) contralateral locations on LFCd, within a standard, anatomic coordinate system. (**B**) 18 repair situations were created, computationally implanting OCA from each MFCd and LFCd site was into each MFCr site. (**C**) Computational implantation performed by rotating donor surfaces by α and β, and translating along the OCA vertical axis, to minimize the RMS deviation of the 1mm-wide edge of the repair.

3.4 Results

Cartilage Thickness and Sphere Fit. The thickness and fit to a sphere of the donor and recipient sites varied regionally (**Figure 3.2**). Thickness tended to increase on the LFC from anterior to posterior (p<0.001). MFCd and MFCr had equivalent thickness at all the three sites (2.04±0.41mm vs. 2.27±0.49mm at site 0; 1.99±0.33mm vs. 2.13±0.34mm at site 1; and 1.87±0.20mm vs. 2.02±0.25mm at site 2, **Figure 3.3.C**). LFCd were thicker than the MFCd or MFCr at all sites (2.49±0.40mm at site 0, p<0.05, 2.96±0.29mm at site 1, p<0.001, and 2.92±0.31 at site 2, p<0.001, **Figure 3.3.C**).

All sites fit fairly well to a sphere (**Figure 3.2.A**). The average radius of the best-fit spheres was 22.1±0.8mm for all sites (**Figure 3.3.A**). Posterior sites tended to fit better than anterior, as determined by the vertical deviation from the sphere between MFCd, MFCr, and LFCd (p<0.001, **Figure 3.3.B**). There was no difference between MFCd and MFCr at any individual site, and LFCd was only different from MFCd and MFCr at site 1 (p<0.001, **Figure 3.3.B**).

Characterization of OCA. Computational placement of OCA, by rotating by α and β, and translating in z, to minimize s_{RMS} between 20mm edge annuli of graft and host, was accomplished with s_{RMS}<~0.5mm for all virtual repairs. As can be seen in a representative virtual OCA placement, the edges of the graft and host in the sagittal and coronal planes match at roughly the same height. As such, the deviation and step-off are low (**Figure 3.4**).

Overall, the fit of MFCd and LFCd OCA was good, with nearly 100% acceptability. There was no significant difference between s_{RMS}, A_{acc}, or A_{proud} for any combination of MFCd or LFCd site and MFCr site, although variations in the deviation patterns did exist (**Figure 3.5.A**). Typically, the lower s_{RMS} values were found with orthotopically-paired donor and recipient sites, and these maps display a lower variation in the deviation. MFCd OCA repaired MFCr defects with A_{acc}≥99%, whereas LFCd OCA repaired MFCr defects with A_{acc}≥98% (**Figure 3.6.A**).

The step-off results differed between donor and recipient sites, however there was no clear pattern for this. Although $h_{step,RMS}$ was depended on site (p<0.001), C_{acc}, and C_{proud} did not for any combination of MFCd or LFCd site and MFCr site. Variations in the step-off patterns did exist (**Figure 3.5.B**). All OCA repaired MFCr defects with C_{acc}=100%, except MFCd and LFCd site 0 had C_{acc}≥99% and ≥95%, respectively (**Figure 3.6.B**).

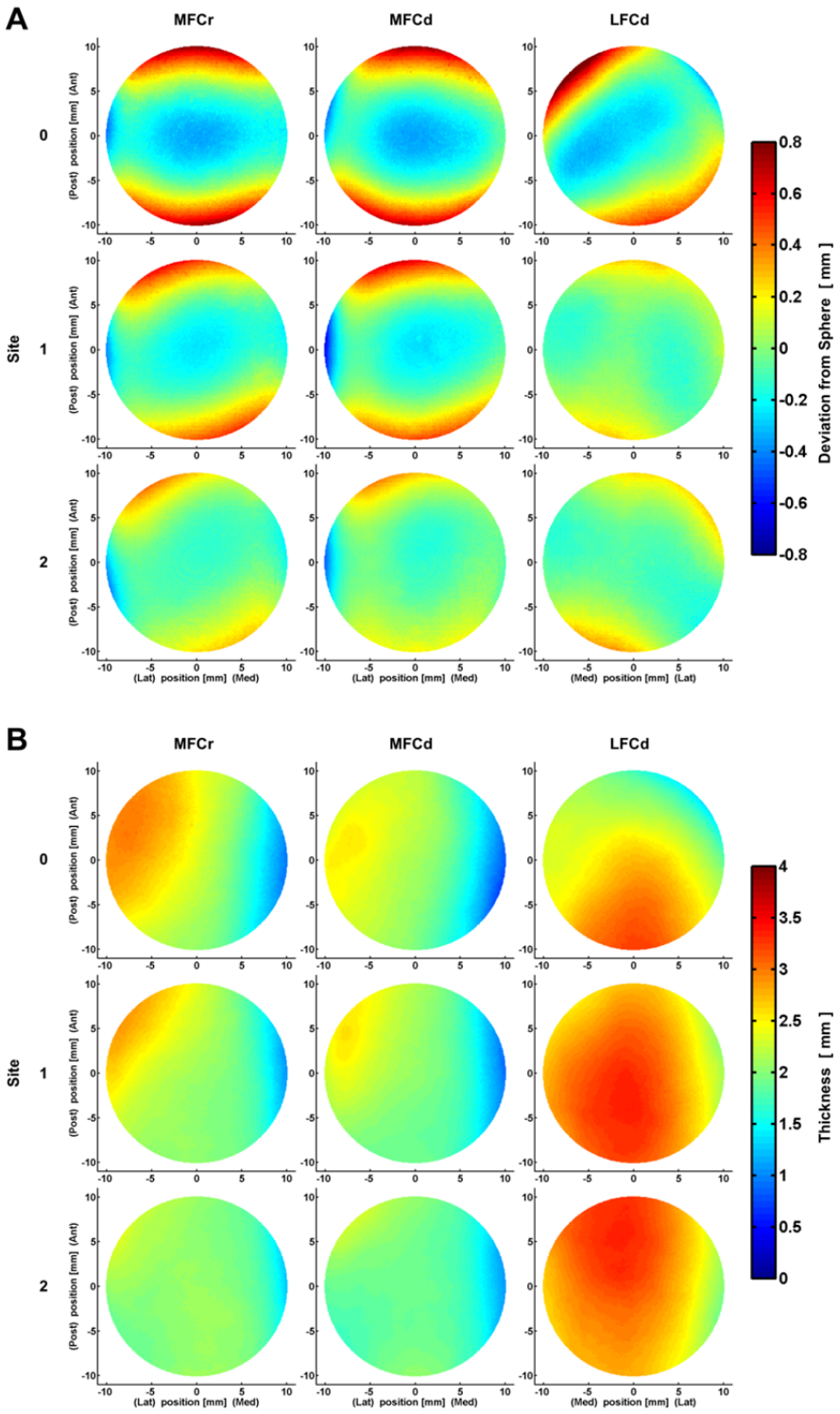

Figure 3.2: Sphere-Fit and Thickness of Donor and Recipient Sites. Maps of average (**A**) vertical deviation from a best-fit sphere and (**B**) articular cartilage thickness for MFCr, MFCd, and LFCd sites.

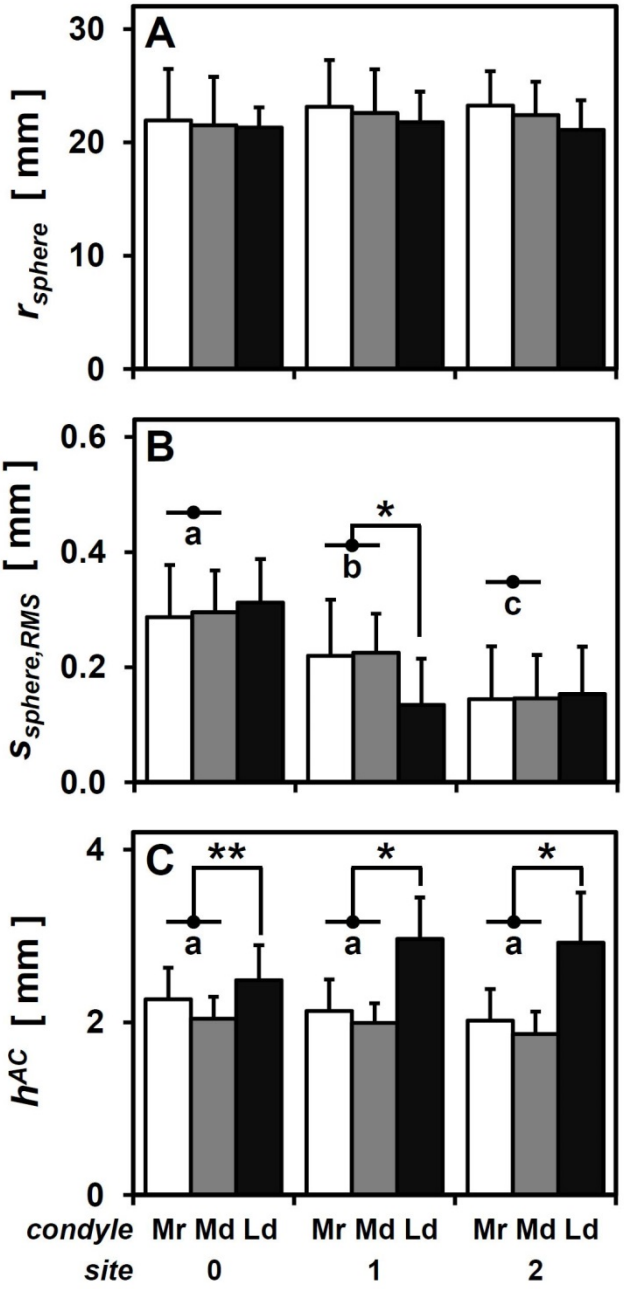

Figure 3.3: Sphere Fit Radius and Vertical Deviation from the Sphere Fit, and Tissue Thickness of Donor and Recipient Sites. (**A**) Average radius of the best-fit spheres, (**B**) RMS average values of deviation from the best-fit spheres, and (**C**) thickness of articular cartilage for MFCr, MFCd, and LFCd. Values shown are mean±SD, N=8. Letters (a, b, c) indicate significantly different groups (p<0.001), with shared letters indicating no difference. *=p<0.001 and **=p<0.05 for LFC vs. MFC.

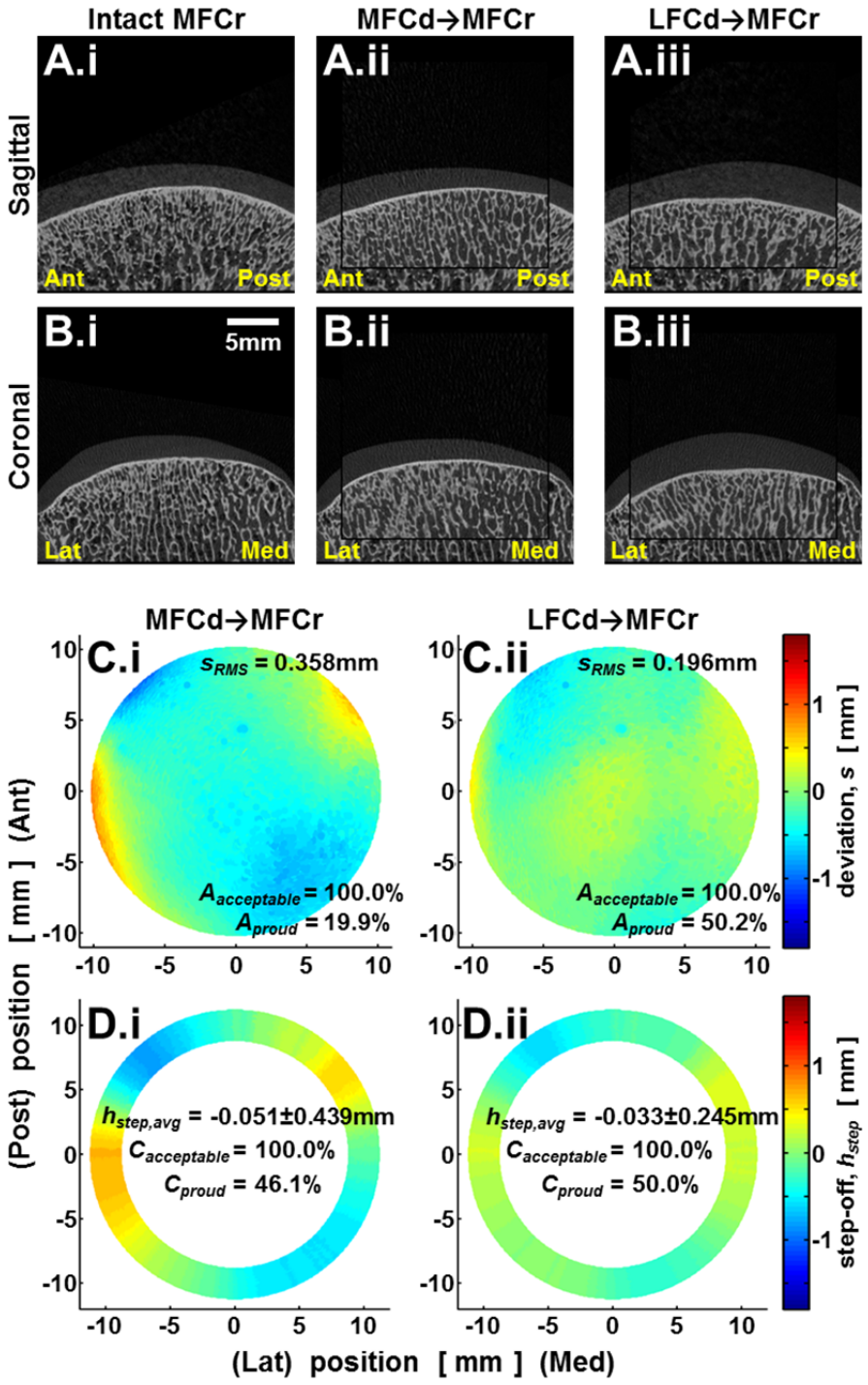

Figure 3.4: Representative Computational OCA Transfer. (**A**&**B**) µCT images of representative OCA placement, showing the (**A.i** & **B.i**) intact MFCr repaired computationally with (**A.ii** & **B.ii**) an orthotopic MFCd OCA and (**A.iii** & **B.iii**) a non-orthotopic LFCd OCA, and the associated (**C**) vertical deviation maps and (**D**) step-off maps.

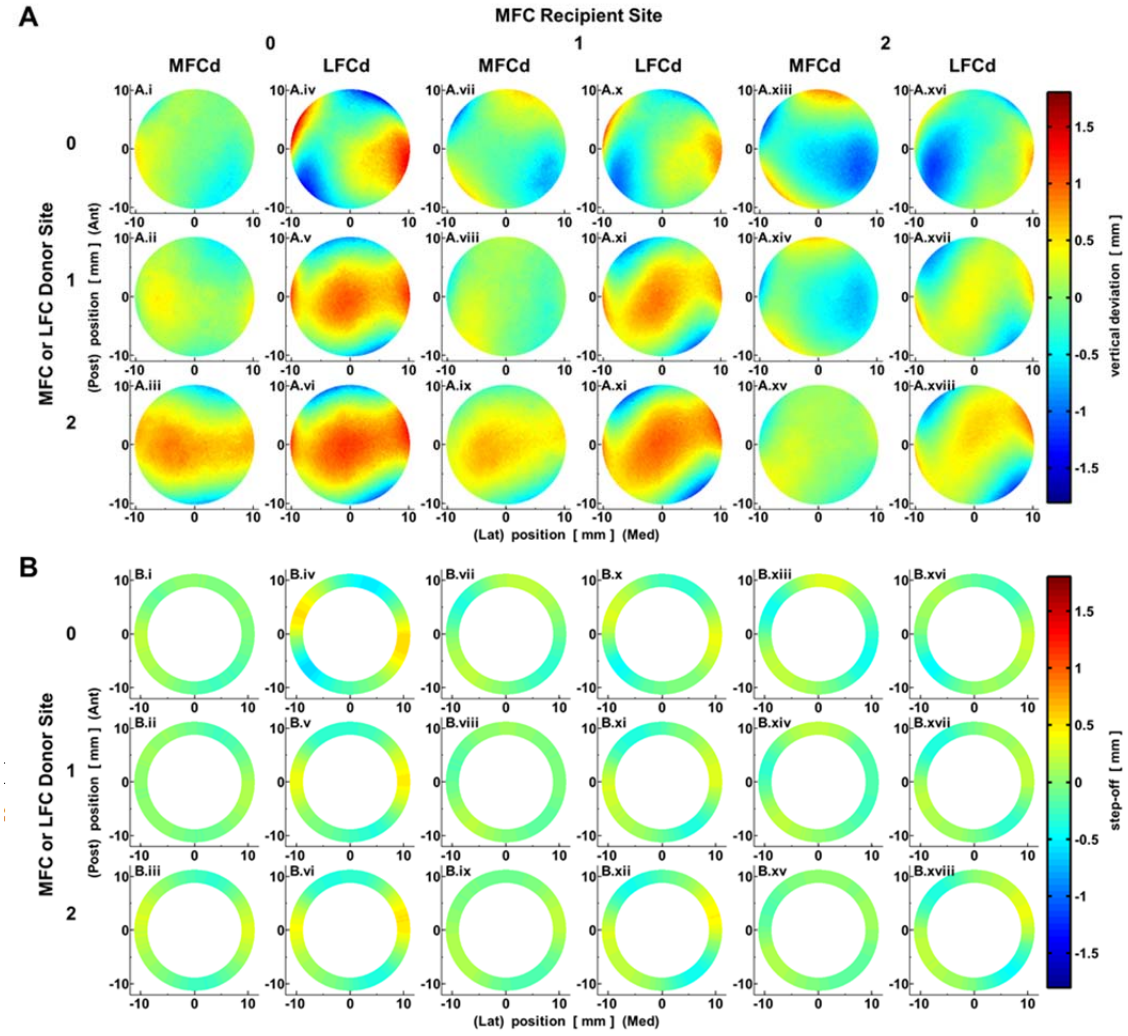

Figure 3.5: Average Vertical Deviation and Step-off for Computational OCA. Maps of average (**A**) vertical deviation and (**B**) radial step-off for computational OCA.

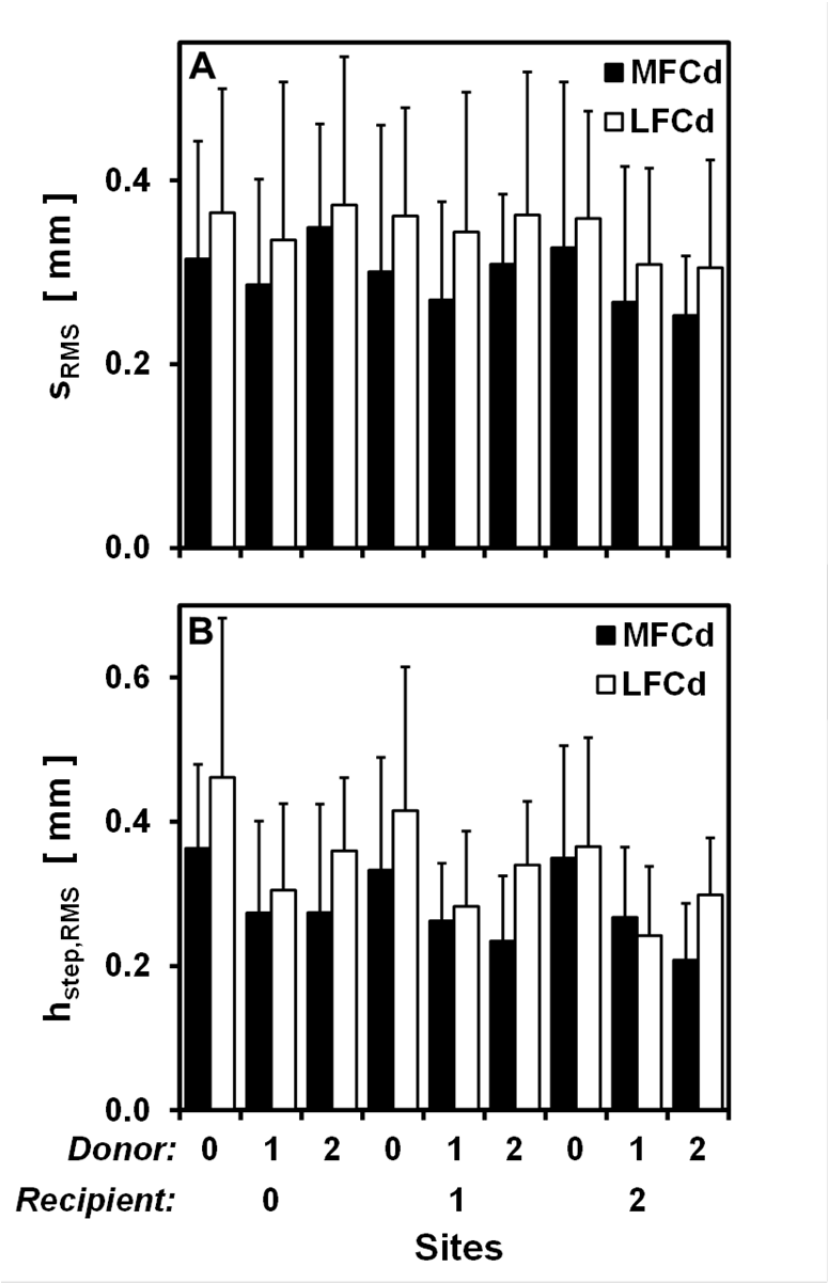

Figure 3.6: Vertical Deviation and Step-off of Computational OCA. (**A**) Vertical deviation between donor and recipient and (**B**) step-off at the edges of computational OCA. Values shown are mean±SD, N=8.

3.5 Discussion

These results indicate that OCA harvested from multiple sites on donor LFCs and placed in multiple recipient sites on MFCs provides a match to the original surface topology that is at least as good as OCA harvested from multiple sites on donor MFCs. The LFC was a good choice for a non-orthotopic donor because the curvature, quantified here as the fit to a sphere, was shown to be equivalent to the MFC, and the thickness of the cartilage was greater than the MFC. There were no significant differences between the donors, whether they were MFCd or LFCd, in any of the computed measures of fit. From the computational placement of OCA performed in this study, non-orthotopic OCA, from LFCd or MFCd, can be utilized for repairing defects in the MFC.

The computational placement of OCA was achieved with a topographical match between the edges of the graft and host. This was done to mimic the osteochondral allograft techniques utilized clinically, where the surgeon places the OCA at a depth that makes the edges flush.[7, 21, 34] Based on the results, some deviation may allowable at the edges to make the central region of the graft match the repaired site topographically. Others have suggested countersinking the OCA slightly to avoid increased pressures associated with proud OCA.[18, 24] Additionally, rotation was only performed about the medial-lateral and anterior-posterior axes of the OCA; based on the deviation and step-off maps, some rotation of OCA about their vertical axis may improve the match.

The acceptability in the match of non-orthotopic and orthotopic OCA was assessed from the vertical deviation and step-off of the entire 20mm OCA, however, regional variations in these measures exist. For example, common pattern for LFCd OCA was to have sunk anterior and posterior boundaries, and a proud central region. Despite these regional variations, nearly 100% of the area was within the ±1mm criteria for deviation and step-off, and thus deemed acceptable. However, the regional variations have implications for the contact mechanics, leading to focal contact pressure[18] and strain increases,[4, 36] which may affect the repair outcome.

The computational OCA transfer software developed in this study is a powerful tool for assessing the fit of OCA *a priori*, however certain limitations must be considered when applying it to the surgical situation. The software creates an ideal repair scenario, where the 1mm-wide edges of the 20mm-diameter repair sites are matched topographically. There are several aspects of the OCA transfer that the computational OCA transfer does not address, in the current version. These aspects include site-specific differences in cartilage thickness[1, 2, 12] and mechanical properties[3], observed in humans and other mammals. Stiffer OCA have correlated favorably with repair assessments,[30] although the relationship between stiffness, thickness and the contact mechanics of the joint, and the ultimate success of OCA repair, are not clearly understood.[8, 20] The thickness will also affect how well the subchondral bone surfaces are aligned, depending on the flush placement of the articular surfaces. Large deviations in subchondral bone alignment has been associated with sub-optimal cartilage mechanical properties, and may adversely affect the repair.[8] An additional consideration for the subchondral bone are cysts and channels

that develop, possibly from synovial fluid invasion or bone contusion,[10, 19, 26, 27] which are associated with failure of the OCA due to insufficient osseous support or integration.[13, 17, 25, 35] When an OCA is placed surgically, it undergoes several procedures not modeled here. The bottom bone surface of the OCA is trimmed based on the depth of the cylindrical socket reamed at the recipient site, then the OCA is gently tamped flush into place.[7] The impulse of tamping induces apoptosis of the chondrocytes, especially in the superficial layer.[6] A geometric mismatch in the bottom bone surface of the OCA and the bottom of the recipient socket, up to 0.5 to 1mm, is thought to increase chondrocyte apoptosis from tamping.[6] This geometric mismatch between the OCA and socket may also affect osseous integration.

Ultimately, *in vivo* studies are needed to assess the efficacy of donor OCA not site-matched to the MFC recipient sites, whether from adjacent locations on the MFC, or from locations on the LFC. While acceptable topological matches were achieved in this study, the mechanobiological aspects of OCA repair were not addressed. The software tools developed in this study can be directly applied to animal species commonly utilized in OCA repair models, such as the goat. Using the software, one or more acceptable donor sites can readily be identified for potential testing.

3.6 Glossary

LFC – Lateral Femoral Condyle

MFC – Medial Femoral Condyle

OCA – osteochondral allograft

MFCd – medial femoral condyle donor

LFCd – lateral femoral condyle donor

MFCr – medial femoral condyle recipient

FTA – Femoral transverse axis, formed by joining the centroids of spheres fit to the femoral condyles

h^{AC} – thickness of the articular cartilage

α – rotation about medial-lateral axis of OCA, computed during placement

β – rotation about anterior-posterior axis of OCA, computed during placement

z – translation along the vertical axis of OCA, computed during placement

s – vertical deviation of the OCA cartilage surface from the recipient cartilage surface, mapped for all points on the OCA surfaces

s_{RMS} – RMS vertical deviation of the OCA from the recipient

h_{step} – step-off between the edge of OCA and the recipient, mapped about the circumference of the OCA

$h_{step,RMS}$ – RMS average of step-off for all segments of the circumference

A_{acc} – percent of the OCA area that is acceptable by vertical deviation, where -1mm < s < 1mm

A_{proud} – percent of the OCA area that is proud, i.e. s>0

C_{acc} – percent of the OCA circumference that is acceptable by step-off, where -1mm < h_{step} < 1mm

C_{proud} – percent of the OCA circumference that is proud, i.e. h_{step}>0

3.7 Acknowledgments

This chapter, in full, will be submitted for publication. The dissertation author is the primary investigator and thanks co-authors, Esther Cory, M.S., William D. Bugbee, M.D., and Robert L. Sah, M.D., Sc.D.

This work was supported by research grants from the Joint Restoration Foundation, the National Institutes of Health (R01 AR051565, P01 AG007996) and an award to the University of California–San Diego under the Howard Hughes Medical Institute Professors Program (RLS).

3.8 References

1. Ahmad CS, Cohen ZA, Levine WN, Ateshian GA, Mow VC: Biomechanical and topographic considerations for autologous osteochondral grafting in the knee. *Am J Sports Med* 29:201-6, 2001.

2. Ateshian G, Soslowsky L, Mow V: Quantitation of articular surface topography and cartilage thickness in knee joints using stereophotogrammetry. *J Biomech* 24:761-76, 1991.

3. Athanasiou KA, Rosenwasser MP, Buckwalter JA, Malinin TI, Mow VC: Interspecies comparisons of in situ intrinsic mechanical properties of distal femoral cartilage. *J Orthop Res* 9:330-40, 1991.

4. Bae WC, Law AW, Amiel D, Sah RL: Sensitivity of indentation testing to step-off edges and interface integrity in cartilage repair. *Ann Biomed Eng* 32:360-9, 2004.

5. Bae WC, Payanal MM, Chen AC, Hsieh-Bonassera ND, Ballard BL, Lotz MK, Coutts RD, Bugbee WD, Sah RL: Topographic patterns of cartilage lesions in knee osteoarthritis. *Cartilage* 1:10-9, 2010.

6. Borazjani BH, Chen AC, Bae WC, Patil S, Sah RL, Firestein GS, Bugbee WD: Effect of impact on chondrocyte viability during insertion of human osteochondral grafts. *J Bone Joint Surg Am* 88:1934-43, 2006.

7. Bugbee W, Cavallo M, Giannini S: Osteochondral allograft transplantation in the knee. *J Knee Surg* 25:109, 2012.

8. Chan EF, Liu I-L, Semler EJ, Aberman HM, Simon TM, Chen AC, Truncale KG, Sah RL: Association of 3-dimensional cartilage and bone structure with articular cartilage properties in and adjacent to autologous osteochondral grafts after 6 and 12 months in a goat model. *Cartilage* 3:255-66, 2012.

9. Convery FR, Meyers MH, Akeson WH: Fresh osteochondral allografting of the femoral condyle. *Clin Orthop Rel Res* 273:139-45, 1991.

10. Cox L, Lagemaat M, Van Donkelaar C, Van Rietbergen B, Reilingh M, Blankevoort L, Van Dijk C, Ito K: The role of pressurized fluid in subchondral bone cyst growth. *Bone* 49:762-8, 2011.

11. Curl WW, Krome J, Gordon ES, Rushing J, Smith BP, Poehling GG: Cartilage injuries: a review of 31,516 knee arthroscopies. *Arthroscopy* 13:456-60, 1997.

12. Frisbie D, Cross M, McIlwraith C: A comparative study of articular cartilage thickness in the stifle of animal species used in human pre-clinical studies compared to articular cartilage thickness in the human knee. *Vet Comp Orthop Traumatol* 19:142, 2006.

13. Görtz S, Bugbee WD: Fresh osteochondral allografts: graft processing and clinical applications. *J Knee Surg* 19:231-40, 2006.

14. Hjelle K, Solheim E, Strand T, Muri R, Brittberg M: Articular cartilage defects in 1,000 knee arthroscopies. *Arthroscopy* 18:730-4, 2002.

15. Huang FS, Simonian PT, Norman AG, Clark JM: Effects of small incongruities in a sheep model of osteochondral autografting. *Am J Sports Med* 32:1842-8, 2004.

16. Hurtig MB, Novak K, McPherson R, McFadden S, McGann LE, Muldrew K, Schachar NS: Osteochondral dowel transplantation for repair of focal defects in the knee: an outcome study using an ovine model. *Vet Surg* 27:5-16, 1998.

17. Kandel R, Gross A, Ganel A, McDermott A, Langer F, Pritzker K: Histopathology of failed osteoarticular shell allografts. *Clin Orthop Rel Res* 197:103-10, 1985.

18. Koh JL, Wirsing K, Lautenschlager E, Zhang L-Q: The effect of graft height mismatch on contact pressure following osteochondral grafting a biomechanical study. *Am J Sports Med* 32:317-20, 2004.

19. Landells J: The bone cysts of osteoarthritis. *J Bone Joint Surg Br* 35:643-9, 1953.

20. Lane JG, Massie JB, Ball ST, Amiel ME, Chen AC, Bae WC, Sah RL, Amiel D: Follow-up of Osteochondral Plug Transfers in a Goat Model A 6-Month Study. *Am J Sports Med* 32:1440-50, 2004.

21. McCulloch PC, Kang RW, Sobhy MH, Hayden JK, Cole BJ: Prospective Evaluation of Prolonged Fresh Osteochondral Allograft Transplantation of the Femoral Condyle Minimum 2-Year Follow-Up. *Am J Sports Med* 35:411-20, 2007.

22. Meyers MH, Akeson WH, Convery FR: Resurfacing of the knee with fresh osteochondral allograft. *J Bone Joint Surg Am* 71-A:704-13, 1989.

23. Mologne TS, Cory E, Hansen BC, Naso AN, Chang N, Murphy MM, Provencher MT, Bugbee WD, Sah RL: Osteochondral Allograft Transplant to the Medial Femoral Condyle Using a Medial or Lateral Femoral Condyle Allograft Is There a Difference in Graft Sources? *Am J Sports Med* 42:2205-13, 2014.

24. Nakagawa Y, Suzuki T, Kuroki H, Kobayashi M, Okamoto Y, Nakamura T: The effect of surface incongruity of grafted plugs in osteochondral grafting: a report of five cases. *Knee Surg Sports Traumatol Arthrosc* 15:591-6, 2007.

25. Oakeshott R, Farine I, Pritzker K, Langer F, Gross A: A clinical and histologic analysis of failed fresh osteochondral allografts. *Clin Orthop Rel Res* 233:283-94, 1988.

26. Ondrouch A: Cyst formation in osteoarthritis. *J Bone Joint Surg Br* 45:755-60, 1963.

27. Pallante-Kichura AL, Cory E, Bugbee WD, Sah RL: Bone cysts after osteochondral allograft repair of cartilage defects in goats suggest abnormal interaction between subchondral bone and overlying synovial joint tissues. *Bone* 57:259-68, 2013.

28. Pallante AL, Bae WC, Chen AC, Gortz S, Bugbee WD, Sah RL: Chondrocyte viability is higher after prolonged storage at 37 degrees C than at 4 degrees C for osteochondral grafts. *Am J Sports Med* 37 Suppl 1:24S-32S, 2009.

29. Pallante AL, Gortz S, Bae WC, Chen AC, Bydder GM, Chung CB, Amiel D, Sah RL, Bugbee WD: In vivo analysis of cartilage defect repair with frozen and fresh osteochondral allografts in the goat. *Am Ortho Soc Sports Med,* San Diego, CA, Submitted, 2011.

30. Pallante AL, Gortz S, Chen AC, Healey RM, Chase DC, Ball ST, Amiel D, Sah RL, Bugbee WD: Treatment of articular cartilage defects in the goat with frozen versus fresh osteochondral allografts: effects on cartilage stiffness, zonal composition, and structure at six months. *J Bone Joint Surg Am* 94:1984-95, 2012.

31. Rios D, Jansson KS, Martetschlager F, Boykin RE, Millett PJ, Wijdicks CA. Normal curvature of glenoid surface can be restored when performing an inlay osteochondral allograft: an anatomic computed tomographic comparison. In: Knee Surg Sports Traumatol Arthrosc. 2013/01/25 ed; 2014:442-7.

32. Victor J, Van Doninck D, Labey L, Van Glabbeek F, Parizel P, Bellemans J: A common reference frame for describing rotation of the distal femur: a ct-based kinematic study using cadavers. *J Bone Joint Surg Br* 91:683-90, 2009.

33. Widuchowski W, Widuchowski J, Trzaska T: Articular cartilage defects: study of 25,124 knee arthroscopies. *Knee* 14:177-82, 2007.

34. Williams RJ, 3rd, Ranawat AS, Potter HG, Carter T, Warren RF: Fresh stored allografts for the treatment of osteochondral defects of the knee. *J Bone Joint Surg Am* 89:718-26, 2007.

35. Williams SK, Amiel D, Ball ST, Allen RT, Tontz WL, Emmerson BC, Badlani NM, Emery SC, Haghighi P, Bugbee WD: Analysis of cartilage tissue on a cellular level in fresh osteochondral allograft retrievals. *Am J Sports Med* 35:2022-32, 2007.

36. Wong BL, Bae WC, Gratz KR, Sah RL: Shear deformation kinematics during cartilage articulation: effect of lubrication, degeneration, and stress relaxation. *Mol Cell Biomech* 5:197-206, 2008.

CHAPTER 4

COMPUTATIONAL TOPOGRAPHIC MATCH OF LATERAL FEMORAL CONDYLE DONOR OSTEOCHONDRAL ALLOGRAFTS TO MEDIAL FEMORAL CONDYLE RECIPIENT SITES IN THE BOER GOAT

4.1 Abstract

INTRODUCTION: Fresh osteochondral allograft (OCA) transplantation is a successful method for the repair of large articular lesions on the medial femoral condyle (MFC). Recent studies show that non-orthotopic OCA from the lateral femoral condyle (LFC) provide geometric surface match equivalent to orthotopic OCA from the MFC for treating MFC defects. In order to validate treatment of MFC defects with non-orthotopic LFC OCA, the topographical match of LFC OCA to MFC defects was investigated in a Boer Goat OCA model. HYPOTHESIS: Certain regions of the Boer Goat LFC can provide osteochondral allografts that can restore the topographical properties of the MFC. OBJECTIVE: The objective of this study was to

investigate the potential fit of OCA, recovered from LFCs, after placement into a MFC defect, to determine the best site for performing an *in vivo* study. METHODS: 8 Boer goat femora were scanned by μCT, and the images were registered to an anatomic coordinate system. An 8mm-diameter MFC recipient site, based on surgical accessibility, and five 8mm-diameter LFC donor sites were then identified. OCAs from the five LFC donor sites were virtually implanted in the MFC recipient site. Vertical deviation, step-off height, differences in thickness, and an estimate for the *in vivo* compressive strain were calculated for the 8mm-diameter OCA, and used to evaluate the match. For one site with a good match, the diameter of the OCA was adjusted to determine the effect of diameter on surface match. RESULTS: The vertical deviation between the LFC OCA and the MFC recipient, and step-off at the OCA edges were typically low (8mm OCA: LFC site P2 s_{RMS}=0.159±0.049mm & h_{step}=0.024±0.010 vs. MFC site 0 s_{RMS}=0.087±0.014mm & h_{step}=0.000±0.012mm), with 100% acceptability. The tissue thickness was much less in the LFC donor sites than the MFC recipient site, which contributed to high estimates of strain (8mm grafts: LFC site P2 ε_z=0.234±0.040mm/mm vs. MFC site 0 ε_z=0.150±0.031mm/mm), which was only 85.9% acceptable by strains less than 0.30mm/mm. A smaller diameter did increase the percentages for acceptability by strain (98.3% at 6mm to 100% at 4mm). CONCLUSION: 6mm OCA from LFC site P2 was determined to have an acceptable topographical match to the MFC recipient site, indicating this can be utilized in an *in vivo* OCA study.

4.2 Introduction

The osteochondral allograft (OCA) repair technique is effective clinically in treating large articular defects on the medial femoral condyle (MFC).[5, 23, 39] However, the strategy of repairing defects with orthotopically-matched OCA from a donor MFC creates a paucity of available donor tissue. The incidence of defects is greater on the MFC compared to the lateral femoral condyle (LFC).[8, 13, 38] Thus, more MFC donor grafts are requested,[11] yet much less MFC grafts than LFC grafts are available.[24] A recent ex vivo study demonstrated that LFC OCA can provide a topographic match to MFC defects equivalent to MFC OCA.[24] However, it is unclear how the LFC grafts would behave *in vivo*. Therefore, the long-term efficacy of LFC OCA placed in MFC defects should be tested in an animal model.

Cartilage repair by OCA has been modeled in the goat to characterize the natural history of the repair and to test strategies to improve the success of OCA.[6, 14, 21, 29, 30, 35] The caprine OCA model is preferred in these studies because of the ability to investigate the long-term effects of OCA repair, from 3 months to 6 or even 12 months.[1, 6, 21] This is due in part to the lack of spontaneous healing of cartilage of large defects in the goat, like in humans.[15, 34] Additionally, the goat femoral condylar cartilage thickness relative to body weight is similar to that in humans.[10, 16, 32]

In the osteochondral allografting technique, the depth at which the osteochondral allograft (OCA) is placed influences the success of the repair. Depressed grafts in mosaicplasty provide better repair than protuberant grafts, which have caused a catching sensation during activity.[25] Flush OCA can restore the

contact pressure of the intact surface, whereas sunk or proud OCA increase the contact pressure.[19] In the goat OCA model, deviations in the cartilage surface and bone-cartilage interface influenced the mechanical properties of the repair at 6 and 12 months after OCA implantation.[6, 21] Although the effect of cartilage thickness on repair success is not well understood, it is thought to affect the contact mechanics. Therefore, considerations of the *in vivo* compressive strain must be considered when evaluating OCA placement *ex vivo*.

In this study, we investigated the topographic match, computationally in 3-D, in the non-orthotopic repair of the Boer goat MFC defects with OCA from LFC donors. We hypothesized that one or more sites, with a preferred diameter, on the Boer goat LFC would be identified as a topographic match to a MFC recipient site, preparatory to an *in vivo* study. The objective was to determine whether any in a series of defined sites on the LFC, and at which diameter, would achieve a topographic match, by surface deviation and step-off, as well as estimated *in vivo* compressive strain, to a recipient site on the MFC, by implanting OCA computationally using μCT images.

4.3 Methods

Study Design. Implantation of OCA, taken from the LFC, placed in the MFC, was performed computationally in 3-D using μCT images of Boer goat femora to identify both a recommended site and a recommended diameter preparatory to performing the LFC OCA repair of MFC defects *in vivo*. This study was performed in three steps. (1) A recipient site on the MFC was determined from MR images of N=7 Boer goat femora from previous *in vivo* OCA studies.[28, 30] This same MFC site (MFCr), in addition to 5 sites on the LFC, were defined, within a standard coordinate system, on N=8 normal, skeletally mature left Boer goat femora. (2) The 8 femora were paired randomly as donors and recipients, and OCA from the MFC site and LFC sites of the donor, 8mm in diameter, were implanted, computationally with the custom MATLAB (Mathworks, Natick, MA) software, in the MFC site of the recipient. The fit of the OCA was characterized by the vertical deviation, step-off at the edges, and an estimate of the *in vivo* compressive strain. (3) The implantation and fit calculations were then repeated for a particularly well-matched LFC site using 6mm and 4mm diameter OCA for determining the effects of diameter on the match.

MFC Recipient Site. MR images of OCA placed surgically in Boer goat femora [28, 30] were utilized to define a recipient site on the MFC that would be accessible with the established surgical methods.[6, 29, 30] The MR images were roughly aligned with the femur diaphysis vertical, and the condyles horizontal. The angle from the

diaphysis to the OCA repair site, measured from the center of the condyles, was estimated. The average angle was then computed for the N=7 repaired femora.

Imaging and Registration of Femora to an Anatomic Coordinate System. The distal end of N=8 normal, skeletally mature Boer goat femora were scanned at $(36\mu m)^3$ resolution by μCT (Skyscan 1076, Skyscan, Kontich, BE) to provide the 3-D image sets for performing the virtual OCA implantation. In order to locate the recipient site in the μCT images, the scans were aligned to an anatomic coordinate system by means of an atlas, a template onto which the femora could be registered.

The atlas was created from a μCT scan of a normal Boer goat femur and was aligned to a coordinate system defined from anatomic structures. The entire femur was scanned at $(36\mu m)^3$ resolution by μCT (Skyscan 1172, Skyscan, Kontich, BE) and the bone surfaces of the MFC, LFC, and diaphysis were determined by thresholding in Mimics (Materialise, Leuven, BE). The anatomic coordinate system was based on sphere fits to the condyles and a cylinder fit to the diaphysis.[37] In this formulation, the diaphysis was fit to a cylinder, creating an anatomic axis, denoted as the z^{FEM} axis. Next, the bone surfaces of the MFC and LFC were each fit to a sphere, and the centroids of these spheres were connected to create the femoral transverse axis (FTA).[37] Then, the cross product of the z^{FEM} axis and the FTA was computed to produce the y^{FEM} axis. The final step was to perform the cross product of the y^{FEM} axis and z^{FEM} axis, to give the x^{FEM} axis, which was almost parallel with the FTA (**Figure 1.A**).

The μCT images of the distal end of Boer goat femora were registered to the atlas, aligning them to the anatomic coordinate system (**Figure 4.1.A**). The subchondral bone surface of the femora was determined by thresholding. The medial or lateral sulci, as well as the posterior boundary of the LFC and MFC, were identified on the subchondral bone of the atlas and the samples. These anatomic markers guided the registration of each distal femur to the anatomic coordinate system.

Donor and Recipient Sites. With the femora aligned to the anatomic coordinate system, the OCA repair site on the MFC and the donor sites were located. The first site (MFC site 0), used as both a recipient site and a donor site, was defined from the repair site angle found above, and placed at the center of the medial-lateral width of the MFC. A contralateral site was defined on the LFC (LFC site 0), at the same angle, and placed at the center of the LFC. Two sites anterior (LFC sites A1 and A2) and two sites posterior (LFC sites P1 and P2) were defined from LFC site 0, spaced at 4mm by arc-length in the anterior-posterior direction, and in the center of the condyles by medial-lateral width (**Figure 1.A**). The images were aligned with the normal vectors, based on an 8mm-diameter area surrounding the defined site, of these six sites (1 on the MFC, 5 on the LFC), maintaining the medial-lateral alignment, for characterization and virtual OCA placement. The images of MFC site 0 were inverted across the medial-lateral direction such that lateral OCA from left femora would be placed in medial recipient sites on the right femur.

The 8mm regions surrounding the MFC site and five LFC sites were characterized by nearest-neighbor thickness, h^{AC}. At these sites, the articular cartilage

surface was determined by thresholding, creating a $(72\mu m)^2$ grid in the medial-lateral and anterior-posterior directions. The nearest-neighbor distance from each point in this grid to the subchondral bone surface was then computed.

Computational Placement of OCA. The extent to which grafts from the MFC donor site and LFC donor sites fit the MFC recipient site was analyzed (**Figure 4.1.B**). The N=8 femora were randomly paired as donors and recipients, creating 8 unique donor-recipient pairings. Grafts from the five LFC sites and the one MFC site, as a positive control, of the donors were placed computationally in the MFC site of the recipients, creating (5+1)*8=48 unique repairs. First, the OCA surface was rotated about the medial-lateral and anterior-posterior axes, by α and β, respectively (each, -5° to 5°). At each α-β combination, the translation along the vertical axis of the OCA, z, was found by minimizing the s_{RMS} between 1mm-wide edges of the OCA and recipient. The α-β-z combination with the lowest s_{RMS} was selected as the optimal graft placement position, and the μCT image of the OCA was rotated, translated, and cropped in 3-D to place it in the μCT image of the recipient.

Effect of OCA Diameter. For the site LFC P2, which was identified to have the closest thickness match to MFC site 0, the computational implantation was repeated with OCA of smaller diameter. This was done with OCA diameters of 6mm and 4mm, to determine the relationship between graft diameter and acceptability. Once these smaller-diameter OCA were placed, the measures of fit were computed.

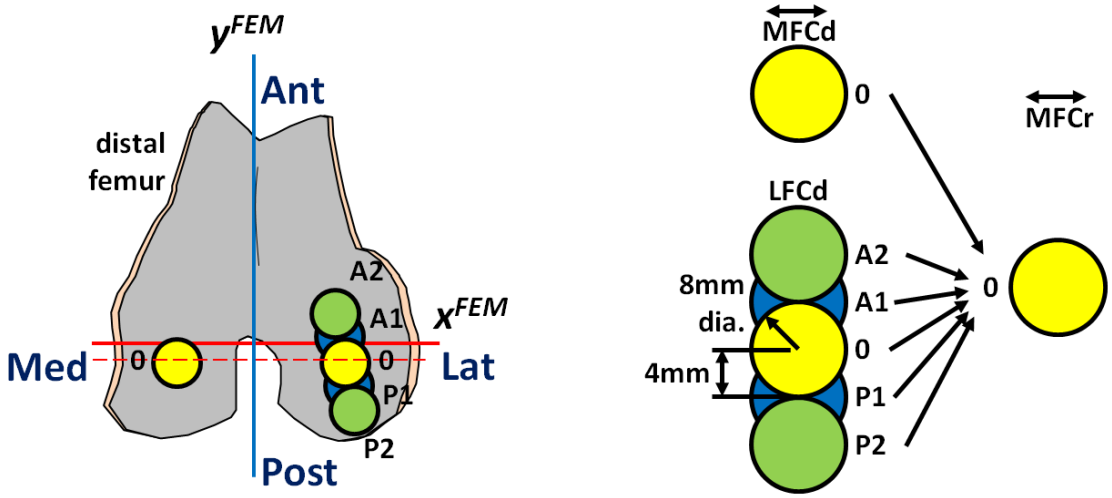

Figure 4.1: Goat Computational OCA Overview. (A) Images of goat femora were aligned to a standard coordinate system, and the MFC repair site, MFC site 0, was identified in the center of the condyle. A contralateral site on the LFC, LFC site 0, was identified, at the same angular location (dashed red line). Two sites anteriorally (A1, A2) and two sites posteriorally (P1, P2) were defined at 4mm arclengths from LFC site 0. (B) Goat femora were paired as donors and recipients. OCA from MFC site 0 of the donor was computationally implanted in the MFC site 0 of the recipient as a positive, orthotopic match. OCA from LFC sites were then implanted in MFC site 0 of the recipient to identify an appropriate matching site.

Quantification of Repairs. To describe the fit of each donor site to each recipient site, the vertical deviation, s, and step-off height, h_{step}, were mapped, and RMS values of these measures, s_{RMS} and $h_{step,RMS}$, respectively, were computed for each case. Additionally, the percent of the graft surface area that was acceptable (within ±0.5mm, $A_{acceptable}$) or proud (>0mm, A_{proud}) in deviation, and the percent of the graft circumference that was acceptable (within ±0.5mm, $C_{acceptable}$) or proud (>0mm, C_{proud}) in step-off height, were computed. The criteria was chosen as 0.5mm because the thickness of Boer goat condylar cartilage measured here was roughly half that reported for humans,[3] in which allowable deviations for OCA is 1mm.[25]

Since the cartilage thickness on the Boer goat LFC was noted to be much less than that of the MFC, another criterion was applied to the virtual repairs, using the thickness difference and vertical deviation to estimate the compressive strain that would be applied *in vivo* to these grafts. The estimate of strain was a first-order estimate, assuming uniform linear elasticity for cartilage. It was also assumed that the proximity of the subchondral bone surfaces of the host femur and tibia would be constant, with or without the OCA, when in contact. Considering a cartilage compressive strain of 15% for the tibia and femur, such that would be experienced in humans during standing,[12] an estimate of compressive strain, ε_z^{AC}, can be made based on the proximity of the femur and tibia subchondral bone, the host femur AC thickness, $h^{AC,host}$, tibia AC thickness, $h^{AC,tib}$, OCA AC thickness, $h^{AC,OCA}$, and the vertical deviation of the OCA surface from the host femur surface, $s^{AC,OCA}$, for each point i in the $(72\mu m)^2$ grid (**Figure 4.2**):

$$\varepsilon_{z,i}^{AC,OCA} = \frac{0.15h_i^{AC,host} + 0.15h_i^{AC,tib} + s_i^{AC,OCA}}{h_i^{AC,tib} + h_i^{AC,OCA}}$$

A constant ratio of femur to tibia cartilage thickness was also assumed. For humans and animals, there is a ratio between the femur and tibia cartilage thickness of ~1.2.[3, 9, 18, 31-33, 36] Applying this ratio to the equation, the strain estimate became:

$$\varepsilon_{z,i}^{AC,OCA} = \frac{0.33h_i^{AC,host} + s_i^{AC,OCA}}{1.2h_i^{AC,host} + h_i^{AC,OCA}}$$

In order for the compressive strain to have been considered acceptable, it must have been less than 0.30mm/mm. At strains greater than 0.35mm/mm in bovine articular cartilage explants, apoptosis, GAG release, swelling, and loss in mechanical stiffness has been observed.[22] Estimated compressive strain was mapped for the virtual OCA repairs, and an average value was computed. Also, the percent of the OCA area with strain less than 0.30mm/mm strain, $A_{\varepsilon<0.3}$, was computed to assess acceptability.

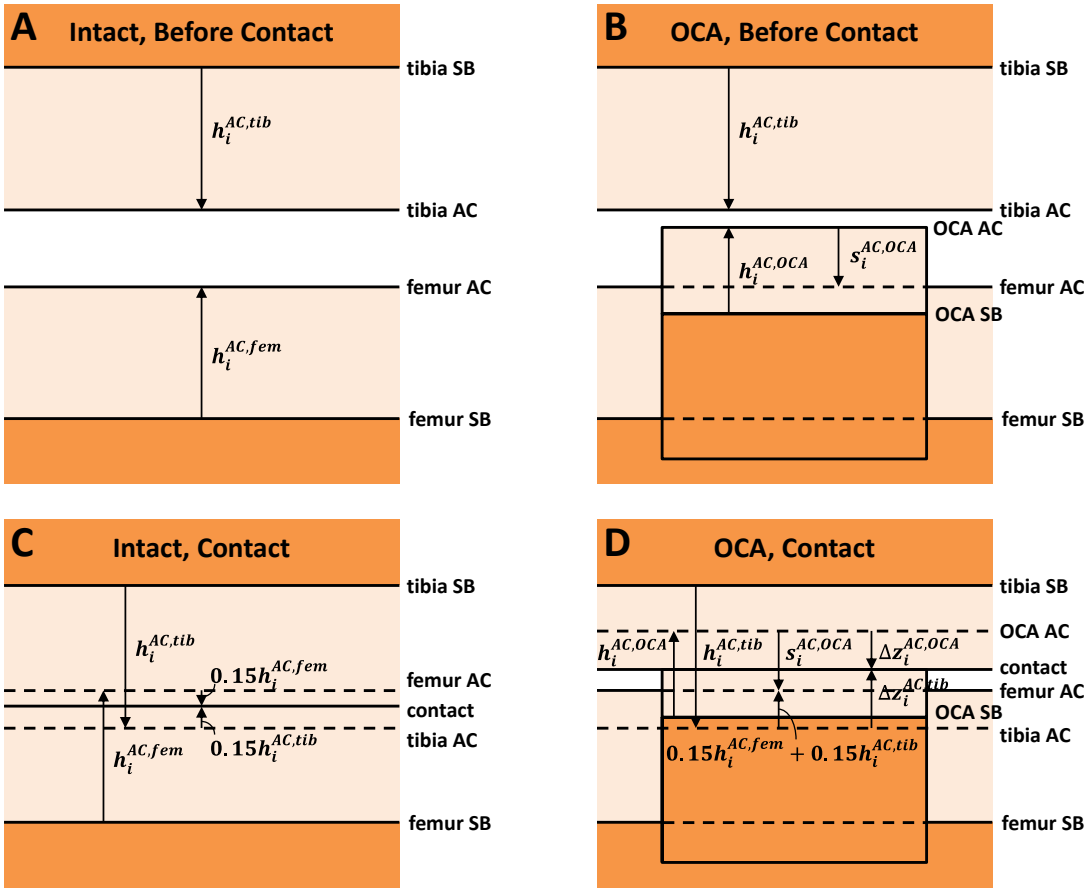

Figure 4.2: Schematic of Contact between OCA and Opposing Tibial Surface. Representation of the thickness and vertical deviation relationships at a location between femoral and OCA cartilage when in contact with the tibia.

Statistics. The effect of OCA donor location on the computed measures of fit, and the thickness, was tested by ANOVA. The effect of OCA diameter on the computed measures of fit was also tested by ANOVA for LFC site P2. The percent acceptable area and circumference data were arcsine transformed prior to statistical analysis.

4.4 Results

Donor and Recipient Sites. The repair site on the MFC from a previous study[28, 30] was determined from MR images to be at a sagittal plane angle of 19°, in roughly the center of the condyle. The remaining sites were defined, repeatably, based on this angle. The thickness was fairly uniform for the 8mm area of all sites, and was significantly greater at the MFC site than the LFC sites (p<0.001, **Figure 4**). Thickness at MFC site 0 was 1.54±0.35mm, 2x as thick as the LFC sites, which had an average thickness of 0.74±0.24mm. Thickness of cartilage on the LFC tended to increase posteriorally, from 0.66±0.15mm at LFC site A2 to 0.82±0.30mm at LFC site P2, but this variation was not significant.

Computational OCA. Placement of 8mm OCA in MFC site 0 virtually was achieved for donor MFC site 0 and all LFC sites with low surface deviation, s_{RMS}, and step-off, $h_{step,RMS}$. For example, a representative MFC site 0 to MFC site 0 graft shows very little surface deviation and step-off, and very low estimates for compressive strain (**Figure 4.5.A**,**C**,**E**,**G**). A representative LFC site P2 graft, placed in MFC site 0, also had very little surface deviation and step-off, however the compressive strain estimate is slightly higher, due to the thin, proud region at the center of the graft (**Figure 4.5.B**,**D**,**F**,**H**).

The vertical deviation, s_{RMS}, between the LFC OCA and the MFC recipient, and step-off, $h_{step,RMS}$, at the OCA edges were typically low. For example, MFC site 0 repaired MFC site 0 with s_{RMS}=0.087±0.014mm and $h_{step,RMS}$=0.083±0.023mm, and

LFC site P2, the LFC site with the best thickness match, repaired MFC site 0 with s_{RMS}=0.159±0.049mm and h_{step}=0.115±0.050. There was no statistical difference between donor sites in terms of vertical deviation, s_{RMS}, or step-off, $h_{step,RMS}$ at this site (**Figure 4.6.A&B**). On average, the MFC donor maps have roughly zero vertical deviation and step-off. However, there were distinct patterns in the LFC repairs, with a proud (s_i>0) region extending in the anterolateral to posteromedial direction. Step-off, $h_{step,i}$, followed this same trend (**Figure 4.7.A&B**). All grafts had 100% acceptability by vertical deviation and step-off.

Estimates of compressive strain were low for OCA from MFC site 0, but slightly high for OCA from LFC sites, however this was not statistically significant (p=0.056, **Figure 4.6.C**). The strain estimate for OCA from MFC site 0 was 0.15±0.03mm/mm, whereas the estimate at LFC site A2 was 0.242±0.03mm/mm. The maps of estimated strain show the same trends as the vertical deviation, with high strain estimates extending from the anterolateral to posteromedial regions (**Figure 4.7.C**). There was less area with strain values less than 0.30 for the LFC grafts, however this trend was not significant (**Figure 4.6.D**).

Effect of Diameter on Acceptability. Decreasing the diameter of OCA at LFC site P2 increased the acceptability of the virtual repairs. Vertical deviation, s_{RMS}, was 0.104±0.035mm for 6mm OCA, and 0.063±0.014mm for 4mm OCA, which were significant decreases (p<0.001, **Figure 4.8.A**). Step-off, h_{step}, also decreased, to 0.017±0.008mm for 6mm OCA, and to 0.013±0.010mm for 4mm OCA, although this

was not significant (**Figure 4.8.B**). Compressive strain estimates decreased with diameter, from 0.234±0.040mm/mm for 8mm, to 0.203±0.033mm/mm for 4mm, although this, too, was not significant (**Figure 4.8.C**); however, the area with strain less than 0.30mm/mm did increase significantly, from 85.9% for 8mm OCA, to 98.3% for 6mm OCA, and 100% for 4mm OCA ($p<0.001$, **Figure 4.8.B**).

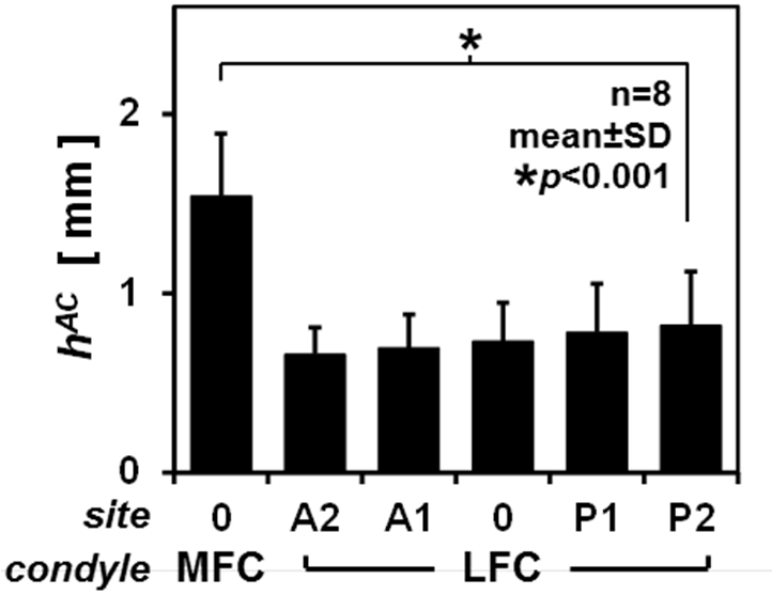

Figure 4.4: Site-specific Articular Cartilage Thickness of Boer Goat Femoral Condyles. Mean±SD, N=8.

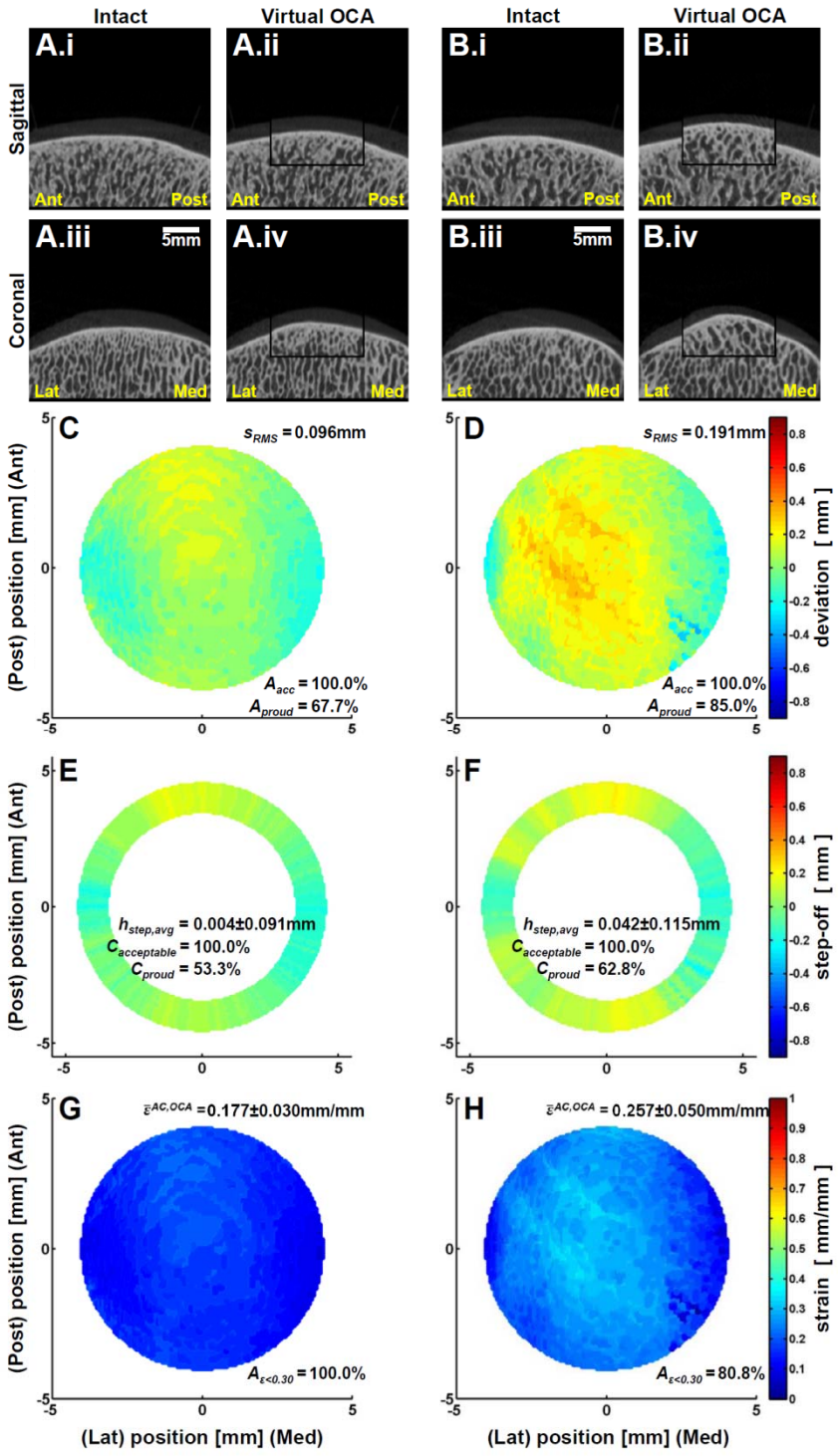

Figure 4.5: Representative Computational OCA Repairs. MFC recipient site 0 with (**A**,**C**,**E**,**G**) MFC site 0 OCA and (**B**,**D**,**F**,**H**) LFC site P2 OCA. (**A-B**) Computational μCT of the repair and the measures of (**C-D**) vertical deviation, (**E-F**) step-off, and (**G-H**) estimated compressive strain.

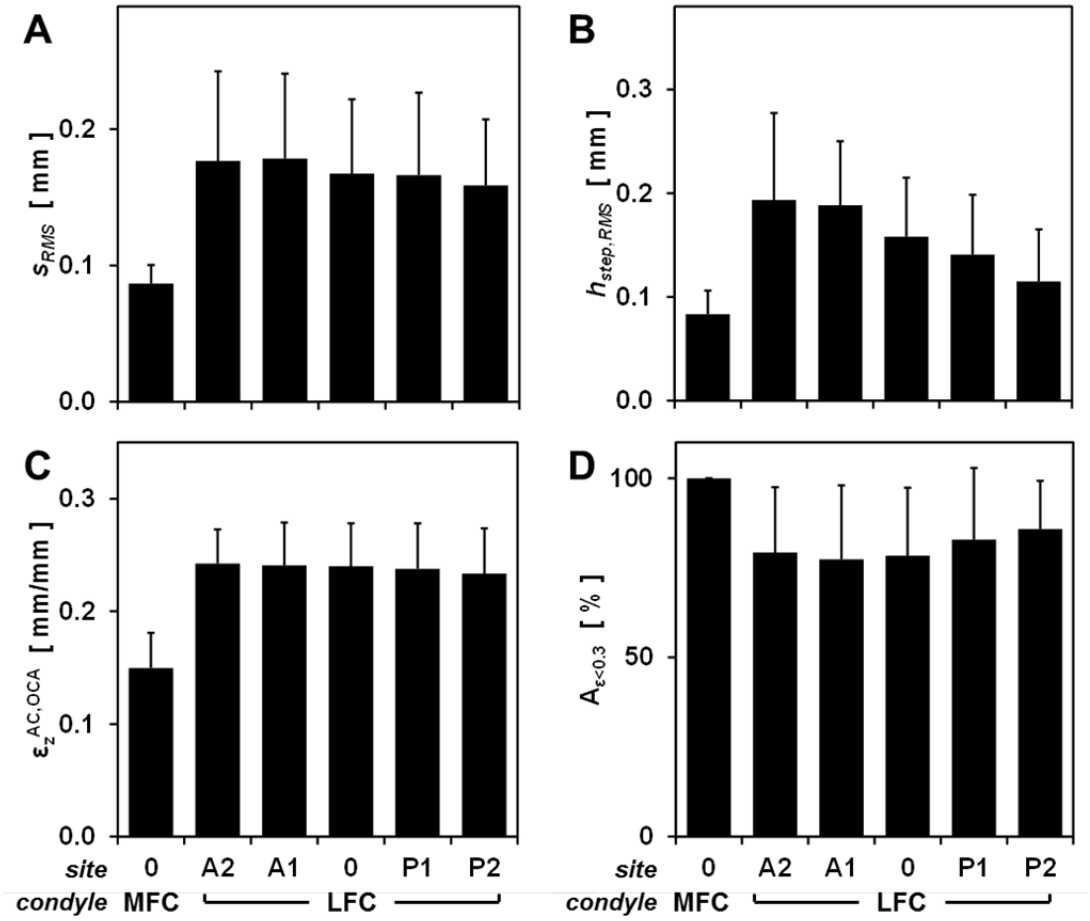

Figure 4.6: Average Measures of Fit for Goat OCA. Average (**A**) vertical deviation, s_{RMS}, (**B**) step-off, $h_{step,RMS}$, (**C**) estimated compressive strain, $\varepsilon^{AC,OCA}$, and (**D**) OCA area with strain <0.3mm/mm, $A_{\varepsilon<0.30}$. Mean±SD, N=8.

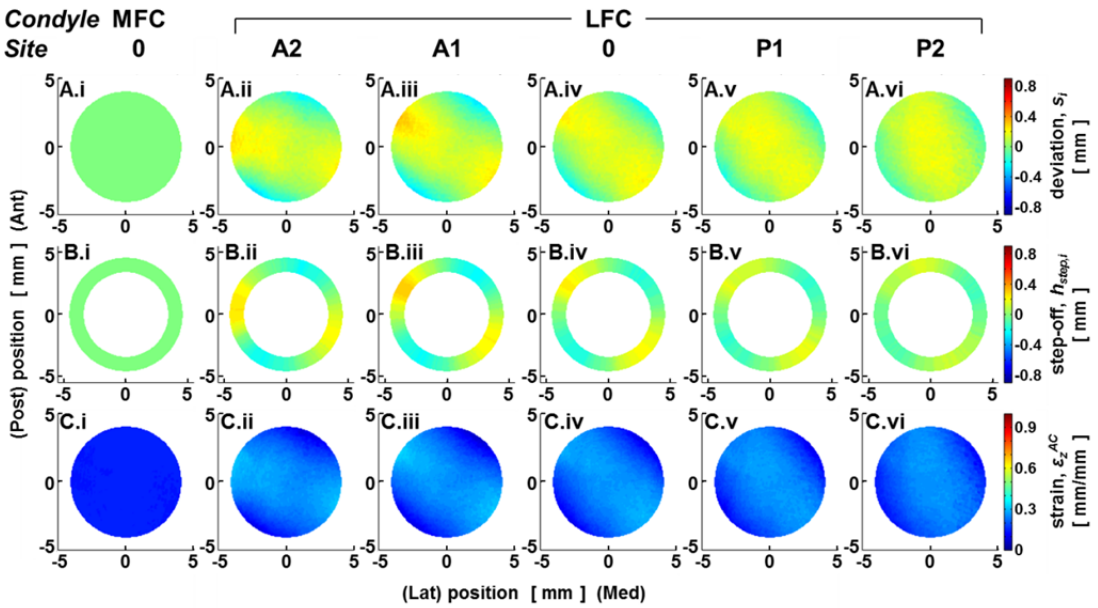

Figure 4.7: Goat OCA Deviation, Step-off, and Strain Maps. For the MFC donor site (**i**) and LFC donor sites (**ii-vi**), maps of average (**A**) deviation, s_i, (**B**) step-off, $h_{step,i}$, and (**C**) compressive strain, $\varepsilon_{z,i}^{AC}$.

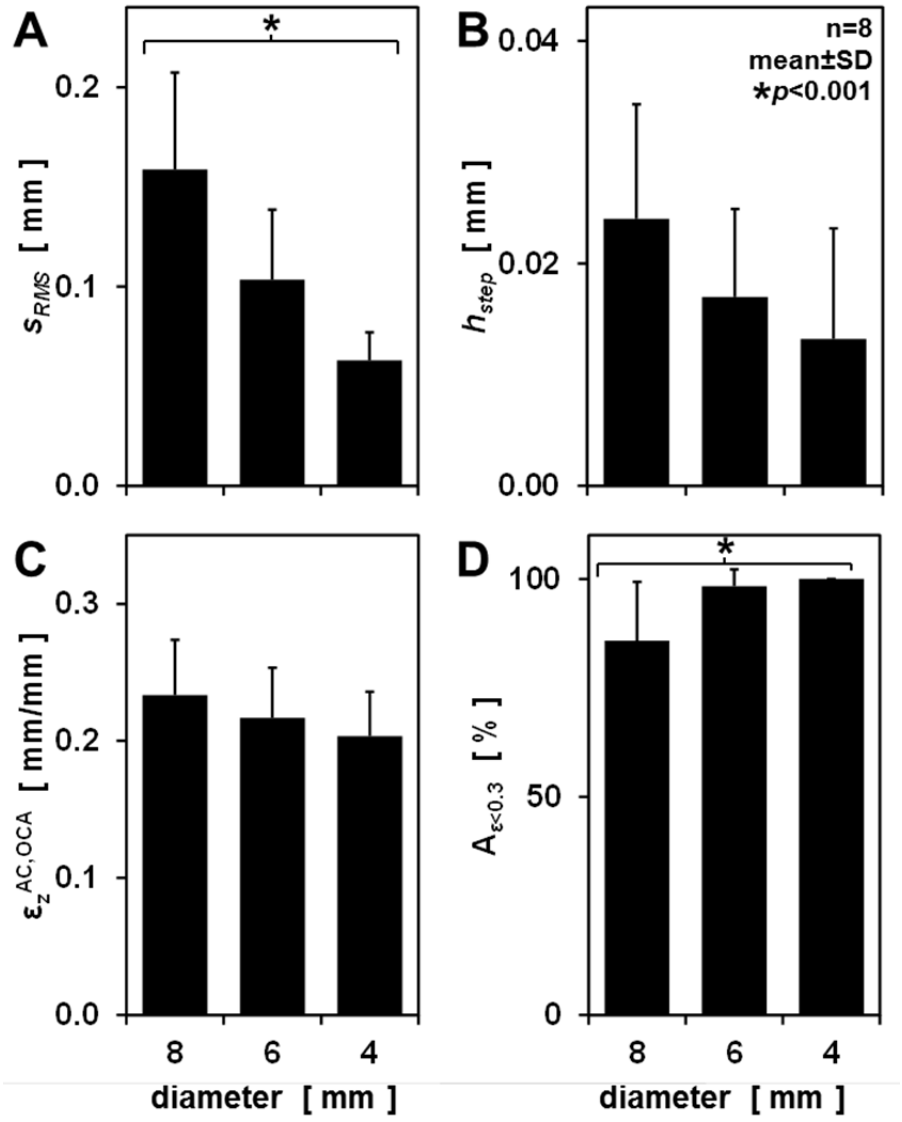

Figure 4.8: Average measures of fit for goat OCA of different diameter. Average (**A**) vertical deviation, s_{RMS}, (**B**) step-off, h_{step}, (**C**) estimated compressive strain, $\varepsilon^{AC,OCA}$, and (**D**) OCA area with strain <0.3mm/mm, $A_{\varepsilon<0.30}$ for 8mm, 6mm, and 4mm diameter grafts.

4.5 Discussion

This study has shown that OCA harvested from sites on donor Boer goat LFCs and placed in a surgically-accessible recipient site on MFC provides a match to the original surface topology that is as acceptable as OCA harvested from an orthotopic donor MFC. Five donor sites on the LFC, and one donor site on the MFC as a positive control, were defined within a standard coordinate system. The site on the MFC, used as both a donor and the recipient site, was identified from previous studies,[28, 30] so that it would be accessible surgically in an *in vivo* model of non-orthotopic OCA repair. Computational OCA repair was performed in 3-D, randomly pairing the N=8 Boer goat femora as donors and recipients, where OCA were taken from the donor MFC site and LFC sites and implanted, by rotating the surface about the medial-lateral and anterior-posterior axes, to match the edges. Quantification of grafts was performed as done previously in a human *ex vivo* OCA study, with calculation of vertical deviation between OCA and recipient cartilage surfaces and step-off at the interface of the OCA and recipient cartilage.[24] An additional parameter, a first-order estimate of *in vivo* compressive strains, was derived for evaluating the match. Finally, it was determined that decreasing the diameter to 6mm and 4mm further improved the match.

The goat is a standard model for cartilage defect repair by OCA and other cartilage repair methods.[1, 6, 21, 29, 30] One consideration in selecting the animal model is the thickness of the cartilage in comparison to humans.[1, 10, 16, 32] In this study, the LFC was investigated as a tissue source for MFC defect repair in the Boer goat model. The thickness of the LFC cartilage was determined to be between

0.66±0.15mm and 0.82±0.30mm, roughly half that of the MFC cartilage, measured here as 1.54±0.35mm. This is a significant consideration, given that previous goat OCA studies have identified thickness, in conjunction with vertical surface deviation, as a major indicator of the success of the repair.[6, 21] The thickness will also affect how well the subchondral bone surfaces are aligned, depending on the flush placement of the articular surfaces. Large deviations in subchondral bone alignment has been associated with sub-optimal cartilage mechanical properties, and may adversely affect the repair.[6] An additional consideration for the subchondral bone are cysts and channels that develop, possibly from synovial fluid invasion or bone contusion,[7, 20, 27, 28] which are associated with failure of the OCA due to insufficient osseous support or integration.[11, 17, 26, 40]

In this study, the acceptability criteria for vertical deviation and step-off were set at 0.5mm, half the value suggested for human treatments.[2, 25] The reason for using this value was that the thickness of articular cartilage on the femoral condyles of the goat was determined to be roughly half that of the human MFC, roughly 2mm.[3, 10, 32] Assessment of the computational OCA acceptability with these criteria indicated that 100% of the LFC OCA area and circumference provide an acceptable match to the MFC recipient site area and circumference. The criteria could be modified to consider the contour of the goat MFC, relative the human MFC, or the mechanics of the cartilage. In a goat autograft study, it was noted that stiffness of the repair was within 15% of nonoperated joints when deviation was close to 0mm, but

that stiffness for the repair was 60% less than nonoperated joints when grafts were recessed >-0.15mm.[6]

In this study, a new criterion, estimated *in vivo* compressive strain, for evaluating potential graft sites is presented, addressing the thickness difference and vertical surface deviation between the OCA and recipient femoral cartilage. Of particular concern is the case where an OCA with a thin cartilage surface, relative to the recipient site, is elevated, with respect to the surrounding tissue. The mismatch in the cartilage surfaces and the subchondral bone surfaces create a less than ideal situation for repair.[6] The formulation presented here addresses this issue, however it is a first-order approximation, making assumptions of equal elastic properties for tibial, femoral, and OCA cartilage, the proximity of the bones under loading, the amount of compressive strain cartilage experiences under normal compressive loading, and the thickness of the opposing tibial cartilage. This criterion could be rederived with implementation of nonlinear and site-varying mechanical properties. The loading conditions could be altered to include variations in the contact areas based on normal loading [2] and the depth of placed grafts,[19] and the thickness of the tibia could be measured directly. Another factor that is ignored in this criterion is that the surrounding host tissue will experience greater strains if the OCA is depressed. Furthermore, the grafts will experience shear deformations during normal ambulation, and this equation does not address this. Considerations of these strains can also improve the determination of an acceptable match.

Reducing the diameter from 8mm to 6mm improves the acceptability of OCA based on *in vivo* strain estimates from 85.9% to 98.3%. Due to this improvement, the

6mm graft is recommended. 6mm has been identified as a common defect diameter single-site goat femoral condyle repair studies.[1] Importantly, defects of this size do not spontaneously repair in the goat.[15] Reducing the OCA diameter further to 4mm improves acceptability to 100%; however, this diameter may be problematic in an *in vivo* study, as slightly smaller defects of 3mm-diameter have been noted to spontaneously repair.[15]

The computational OCA transfer software used in this study is a powerful tool for assessing the fit of OCA *a priori*, however certain limitations must be considered when applying it to the surgical situation. When an OCA is placed surgically, it undergoes several procedures not modeled here. The bottom bone surface of the OCA is trimmed based on the depth of the cylindrical socket reamed at the recipient site, then the OCA is gently tamped flush into place.[5] The impulse of tamping induces apoptosis of the chondrocytes, especially in the superficial layer.[4] A geometric mismatch in the bottom bone surface of the OCA and the bottom of the recipient socket, up to 0.5 to 1mm, is thought to increase chondrocyte apoptosis from tamping.[4] This geometric mismatch between the OCA and socket may also affect osseous integration.

In conclusion, 6mm OCA from the LFC site P2, defined in this study, are recommended for an *in vivo* Boer goat study to assess the efficacy of donor OCAs that are not site-matched to the MFC recipient sites. While acceptable topological matches were achieved in this study, there are biomechanical and biological aspects of OCA repair which were not addressed using the current version of the software, but may be answered in the *in vivo* study.

4.6 Glossary

LFC – Lateral Femoral Condyle

MFC – Medial Femoral Condyle

OCA – osteochondral allograft

MFCd – medial femoral condyle donor

LFCd – lateral femoral condyle donor

MFCr – medial femoral condyle recipient

FTA – Femoral transverse axis, formed by joining the centroids of spheres fit to the femoral condyles

h^{AC} – thickness of the articular cartilage

α – rotation about medial-lateral axis of OCA, computed during placement

β – rotation about anterior-posterior axis of OCA, computed during placement

z – translation along the vertical axis of OCA, computed during placement

s – vertical deviation of the OCA cartilage surface from the recipient cartilage surface, mapped for all points on the OCA surfaces

s_{RMS} – RMS vertical deviation of the OCA from the recipient

h_{step} – step-off between the edge of OCA and the recipient, mapped about the circumference of the OCA

$h_{step,RMS}$ – RMS average of step-off for all segments of the circumference

A_{acc} – percent of the OCA area that is acceptable by vertical deviation, where -1mm < s < 1mm

A_{proud} – percent of the OCA area that is proud, i.e. s>0

C_{acc} – percent of the OCA circumference that is acceptable by step-off, where -1mm < h_{step} < 1mm

C_{proud} – percent of the OCA circumference that is proud, i.e. h_{step}>0

ε_z^{AC} – estimated *in vivo* compressive strain, mapped for all points on the OCA surfaces

$A_{\varepsilon<0.3}$ – percent of the OCA area with estimated compressive strain less than 0.3

4.7 Acknowledgments

This chapter, in full, will be submitted for publication. The dissertation author is the primary investigator and thanks co-authors, Esther Cory, M.S., Karen E. Samy, B.S., Andrea L. Pallante-Kichura, Ph.D., Albert C. Chen, Ph.D., William D. Bugbee, M.D., and Robert L. Sah, M.D., Sc.D.

This work was supported by research grants from the National Institutes of Health (R01 AR051565, P01 AG007996) and an award to the University of California–San Diego under the Howard Hughes Medical Institute Professors Program (RLS).

4.8 References

1. Ahern B, Parvizi J, Boston R, Schaer T: Preclinical animal models in single site cartilage defect testing: a systematic review. *Osteoarthritis Cartilage* 17:705-13, 2009.

2. Ahmad CS, Cohen ZA, Levine WN, Ateshian GA, Mow VC: Biomechanical and topographic considerations for autologous osteochondral grafting in the knee. *Am J Sports Med* 29:201-6, 2001.

3. Ateshian G, Soslowsky L, Mow V: Quantitation of articular surface topography and cartilage thickness in knee joints using stereophotogrammetry. *J Biomech* 24:761-76, 1991.

4. Borazjani BH, Chen AC, Bae WC, Patil S, Sah RL, Firestein GS, Bugbee WD: Effect of impact on chondrocyte viability during insertion of human osteochondral grafts. *J Bone Joint Surg Am* 88:1934-43, 2006.

5. Bugbee W, Cavallo M, Giannini S: Osteochondral allograft transplantation in the knee. *J Knee Surg* 25:109, 2012.

6. Chan EF, Liu I-L, Semler EJ, Aberman HM, Simon TM, Chen AC, Truncale KG, Sah RL: Association of 3-dimensional cartilage and bone structure with articular cartilage properties in and adjacent to autologous osteochondral grafts after 6 and 12 months in a goat model. *Cartilage* 3:255-66, 2012.

7. Cox L, Lagemaat M, Van Donkelaar C, Van Rietbergen B, Reilingh M, Blankevoort L, Van Dijk C, Ito K: The role of pressurized fluid in subchondral bone cyst growth. *Bone* 49:762-8, 2011.

8. Curl WW, Krome J, Gordon ES, Rushing J, Smith BP, Poehling GG: Cartilage injuries: a review of 31,516 knee arthroscopies. *Arthroscopy* 13:456-60, 1997.

9. Faber S, Eckstein F, Lukasz S, Mühlbauer R, Hohe J, Englmeier K-H, Reiser M: Gender differences in knee joint cartilage thickness, volume and articular surface areas: assessment with quantitative three-dimensional MR imaging. *Skeletal Radiol* 30:144-50, 2001.

10. Frisbie D, Cross M, McIlwraith C: A comparative study of articular cartilage thickness in the stifle of animal species used in human pre-clinical studies compared to articular cartilage thickness in the human knee. *Vet Comp Orthop Traumatol* 19:142, 2006.

11. Görtz S, Bugbee WD: Fresh osteochondral allografts: graft processing and clinical applications. *J Knee Surg* 19:231-40, 2006.

12. Halonen K, Mononen M, Jurvelin J, Töyräs J, Salo J, Korhonen R: Deformation of articular cartilage during static loading of a knee joint–Experimental and finite element analysis. *J Biomech*, 2014.

13. Hjelle K, Solheim E, Strand T, Muri R, Brittberg M: Articular cartilage defects in 1,000 knee arthroscopies. *Arthroscopy* 18:730-4, 2002.

14. Jackson DW, Halbrecht J, Proctor C, Van Sickle D, Simon TM: Assessment of donor cell and matrix survival in fresh articular cartilage allografts in a goat model. *J Orthop Res* 14:255-64, 1996.

15. Jackson DW, Lalor PA, Aberman HM, Simon TM: Spontaneous Repair of Full-Thickness Defects of Articular Cartilage in a Goat Model A Preliminary Study. *J Bone Joint Surg Am* 83:53-, 2001.

16. Kääb M, Ap Gwynn I, Nötzli H: Collagen fibre arrangement in the tibial plateau articular cartilage of man and other mammalian species. *J Anat* 193:23-34, 1998.

17. Kandel R, Gross A, Ganel A, McDermott A, Langer F, Pritzker K: Histopathology of failed osteoarticular shell allografts. *Clin Orthop Rel Res* 197:103-10, 1985.

18. Karvonen R, Negendank W, Teitge R, Reed A, Miller P, Fernandez-Madrid F: Factors affecting articular cartilage thickness in osteoarthritis and aging. *J Rheumatol* 21:1310-8, 1994.

19. Koh JL, Wirsing K, Lautenschlager E, Zhang L-Q: The effect of graft height mismatch on contact pressure following osteochondral grafting a biomechanical study. *Am J Sports Med* 32:317-20, 2004.

20. Landells J: The bone cysts of osteoarthritis. *J Bone Joint Surg Br* 35:643-9, 1953.

21. Lane JG, Massie JB, Ball ST, Amiel ME, Chen AC, Bae WC, Sah RL, Amiel D: Follow-up of Osteochondral Plug Transfers in a Goat Model A 6-Month Study. *Am J Sports Med* 32:1440-50, 2004.

22. Loening AM, James IE, Levenston ME, Badger AM, Frank EH, Kurz B, Nuttall ME, Hung HH, Blake SM, Grodzinsky AJ, Lark MW: Injurious mechanical compression of bovine articular cartilage induces chondrocyte apoptosis. *Arch Biochem Biophys* 381:205-12, 2000.

23. McCulloch PC, Kang RW, Sobhy MH, Hayden JK, Cole BJ: Prospective Evaluation of Prolonged Fresh Osteochondral Allograft Transplantation of the Femoral Condyle Minimum 2-Year Follow-Up. *Am J Sports Med* 35:411-20, 2007.

24. Mologne TS, Cory E, Hansen BC, Naso AN, Chang N, Murphy MM, Provencher MT, Bugbee WD, Sah RL: Osteochondral Allograft Transplant to the Medial Femoral Condyle Using a Medial or Lateral Femoral Condyle Allograft Is There a Difference in Graft Sources? *Am J Sports Med* 42:2205-13, 2014.

25. Nakagawa Y, Suzuki T, Kuroki H, Kobayashi M, Okamoto Y, Nakamura T: The effect of surface incongruity of grafted plugs in osteochondral grafting: a report of five cases. *Knee Surg Sports Traumatol Arthrosc* 15:591-6, 2007.

26. Oakeshott R, Farine I, Pritzker K, Langer F, Gross A: A clinical and histologic analysis of failed fresh osteochondral allografts. *Clin Orthop Rel Res* 233:283-94, 1988.

27. Ondrouch A: Cyst formation in osteoarthritis. *J Bone Joint Surg Br* 45:755-60, 1963.

28. Pallante-Kichura AL, Cory E, Bugbee WD, Sah RL: Bone cysts after osteochondral allograft repair of cartilage defects in goats suggest abnormal interaction between subchondral bone and overlying synovial joint tissues. *Bone* 57:259-68, 2013.

29. Pallante AL, Chen AC, Ball ST, Amiel D, Masuda K, Sah RL, Bugbee WD: The in vivo performance of osteochondral allografts in the goat is diminished with extended storage and decreased cartilage cellularity. *Am J Sports Med* 40:1814-23, 2012.

30. Pallante AL, Gortz S, Chen AC, Healey RM, Chase DC, Ball ST, Amiel D, Sah RL, Bugbee WD: Treatment of articular cartilage defects in the goat with frozen versus fresh osteochondral allografts: effects on cartilage stiffness, zonal composition, and structure at six months. *J Bone Joint Surg Am* 94:1984-95, 2012.

31. Panula HE, Hyttinen MM, Arokoski JP, Långsjö TK, Pelttari A, Kiviranta I, Helminen HJ: Articular cartilage superficial zone collagen birefringence reduced and cartilage thickness increased before surface fibrillation in experimental osteoarthritis. *Ann Rheum Dis* 57:237-45, 1998.

32. Pedersen DR, Goetz JE, Kurriger GL, Martin JA: Comparative digital cartilage histology for human and common osteoarthritis models. *Ortho Res Rev* 2013:13, 2013.

33. Räsänen T, Messner K: Regional variations of indentation stiffness and thickness of normal rabbit knee articular cartilage. *J Biomed Mater Res* 31:519-24, 1996.

34. Shahgaldi B: Repair of large osteochondral defects: load-bearing and structural properties of osteochondral repair tissue. *Knee* 5:111-7, 1998.

35. Shahgaldi B, Amis A, Heatley F, McDowell J, Bentley G: Repair of cartilage lesions using biological implants. A comparative histological and biomechanical study in goats. *J Bone Joint Surg Br* 73:57-64, 1991.

36. Shepherd D, Seedhom B: Thickness of human articular cartilage in joints of the lower limb. *Ann Rheum Dis* 58:27-34, 1999.

37. Victor J, Van Doninck D, Labey L, Van Glabbeek F, Parizel P, Bellemans J: A common reference frame for describing rotation of the distal femur: a ct-based kinematic study using cadavers. *J Bone Joint Surg Br* 91:683-90, 2009.

38. Widuchowski W, Widuchowski J, Trzaska T: Articular cartilage defects: study of 25,124 knee arthroscopies. *Knee* 14:177-82, 2007.

39. Williams RJ, 3rd, Ranawat AS, Potter HG, Carter T, Warren RF: Fresh stored allografts for the treatment of osteochondral defects of the knee. *J Bone Joint Surg Am* 89:718-26, 2007.

40. Williams SK, Amiel D, Ball ST, Allen RT, Tontz WL, Emmerson BC, Badlani NM, Emery SC, Haghighi P, Bugbee WD: Analysis of cartilage tissue on a cellular level in fresh osteochondral allograft retrievals. *Am J Sports Med* 35:2022-32, 2007.

CHAPTER 5

CONCLUSIONS

The general motivation for this dissertation was to characterize how the structural and functional properties vary across the surface of the joint in health, injury, and in repair. Specifically, the dissertation aimed to 1) determine early, site-specific changes to the articular cartilage following transection of the anterior cruciate ligament (ACLT) in the rabbit; 2) investigate the fit computationally of orthotopic and non-orthotopic OCA, from both LFC and MFC donors, in MFC recipient sites; and 3) determine the variation in the fit of non-orthotopic grafts from multiple sites on the Boer goat femoral condyles, thereby guiding future *in vivo* studies. This chapter will summarize and discuss the findings of these studies, as well as provide general direction for future studies.

5.1 Summary of Findings

The major findings of this dissertation are:

- Chapter 2: Indentation stiffness was lower in the weight-bearing region of the MFC of NZW rabbits 28 days following ACLT.
- Chapter 3: Considering multiple non-orthotopic graft sites, LFC grafts provide as acceptable repair as MFC grafts in human MFC.
- Chapter 4: A preferred donor site on the LFC of the Boer goat was identified for *in vivo* studies to test the use of non-site-matched OCA for cartilage repair.

5.2 Discussion

This dissertation has made major contributions to the understanding of the site-specific structure and function of articular cartilage. Specifically, in Chapter 2, 3, and 4, the thickness of cartilage was determined at defined locations on rabbit, human, and Boer goat femora. In addition, the inherent site-specific mechanical properties of the rabbit femoral condyles were determined in Chapter 2. Also, in Chapter 3, the spherical fit of defined sites was determined, giving insight to the variations in contour on the human femoral condyles.

A significant contribution in Chapter 2 was the determination of the effects of joint injury on articular cartilage structure and function. Lower stiffness and collagen matrix disruption were correlated for the distal, weight-bearing region of the MFC. This location corresponds to the location of full-thickness erosion observed at later time points in the rabbit ACLT model.[4, 6]

The results of Chapters 3 and 4 have important clinical implications for cartilage repair by OCA technique. In Chapter 3, it was determined that non-orthotopic grafts could be utilized to create a topographic match equivalent to orthotopic grafts for repair of the MFC. In Chapter 4, a site and diameter of an OCA from the Boer goat LFC was identified preparatory to an *in vivo* assessment of non-orthotopic repair of MFC defects. This will help address the current paucity of MFC donor tissue by providing an alternate source of tissue for repair of large defects on the MFC.[8]

This dissertation work also presents several important technical achievements. Methodologies were established in Chapters 2, 3, and 4 to define anatomic coordinate systems for the distal femur for the rabbit, human, and goat. Chapter 2 presented a novel robotic indentation test system, which can address the limitations of current

bench-top mechanical testing by automating the alignment of the mechanical tester to the articular surface. The software developed in Chapters 3 and 4 can simulate graft placement to evaluate the topographical match of OCA.

5.3 Future Directions

The work presented herein can be expanded by investigating the site-specific cartilage properties in human knee joints and in animal models of osteoarthritis. For instance, the time course of post-traumatic osteoarthritis could be determined in the rabbit ACLT model. The robotic indentation test can be applied to different time points in the ACLT model to determine the site-specific progression of the damage, correlating the stiffness at known locations of defects at later time points.[4, 6] In Chapter 4, a site and diameter were defined on the LFC that would provide an OCA that matches the topographic properties of the site MFC, commonly used in goat single-site osteochondral defect models.[1, 9] Using Boer goat OCA model, the *in vivo* viability of LFC OCA placed in the MFC can be determined.

The technological advancements presented in this dissertation offer opportunities for further applications and advancements. The robotic indentation system can be adapted for determining the site-specific mechanical properties of cartilage in larger animal models and humans.[2] Adaptation of the system to accommodate larger joints would require only slight adjustments to the hardware and no additional programming, as any number of sites on any size of surface can be located within 100μm, as determined in Chapter 2.

An additional application of the robotic indentation system would be to replace the indenter with different end-effectors. The site-specific properties of the cartilage

surface could be investigated with imaging techniques, by replacing the indenter with a digital camera or dissecting microscope. By defining the focal length and direction of the optics, specific locations could be targeted for India ink analysis,[4] for example. The indenter could also be replaced with a computer numerical control drill, which could be used to harvest osteochondral dowels for mechanical testing of cartilage[7] or synovial fluid[10], tissue culture, or even for allografting. Robotic technology is rapidly being integrated into orthopaedic research and clinical applications.

Several advancements were identified in Chapters 3 and 4 that would improve the computational OCA software. These include higher-order considerations of compressive strain and shear strains, modeling the mechanics of the joint by finite element methods, or modeling of the tissue homeostasis.

A significant advancement could be achieved by combining the robotic indentation system and the computational OCA software to perform screening of donor tissue mechanically and topographically. The stiffness of the tissue may influence the repair,[3, 5] and selecting a location based not only on topographic match but also biomechanical match has important implications for clinical repair.

5.3 References

1. Ahern B, Parvizi J, Boston R, Schaer T: Preclinical animal models in single site cartilage defect testing: a systematic review. *Osteoarthritis Cartilage* 17:705-13, 2009.

2. Athanasiou KA, Rosenwasser MP, Buckwalter JA, Malinin TI, Mow VC: Interspecies comparisons of in situ intrinsic mechanical properties of distal femoral cartilage. *J Orthop Res* 9:330-40, 1991.

3. Chan EF, Liu I-L, Semler EJ, Aberman HM, Simon TM, Chen AC, Truncale KG, Sah RL: Association of 3-dimensional cartilage and bone structure with articular cartilage properties in and adjacent to autologous osteochondral grafts after 6 and 12 months in a goat model. *Cartilage* 3:255-66, 2012.

4. Chang DG, Iverson EP, Schinagl RM, Sonoda M, Amiel D, Coutts RD, Sah RL: Quantitation and localization of cartilage degeneration following the induction of osteoarthritis in the rabbit knee. *Osteoarthritis Cartilage* 5:357-72, 1997.

5. Lane JG, Massie JB, Ball ST, Amiel ME, Chen AC, Bae WC, Sah RL, Amiel D: Follow-up of Osteochondral Plug Transfers in a Goat Model A 6-Month Study. *Am J Sports Med* 32:1440-50, 2004.

6. Laverty S, Girard CA, Williams JM, Hunziker EB, Pritzker KP: The OARSI histopathology initiative - recommendations for histological assessments of osteoarthritis in the rabbit. *Osteoarthritis Cartilage* 18 Suppl 3:S53-65, 2010.

7. Loening AM, James IE, Levenston ME, Badger AM, Frank EH, Kurz B, Nuttall ME, Hung HH, Blake SM, Grodzinsky AJ, Lark MW: Injurious mechanical compression of bovine articular cartilage induces chondrocyte apoptosis. *Arch Biochem Biophys* 381:205-12, 2000.

8. Mologne TS, Cory E, Hansen BC, Naso AN, Chang N, Murphy MM, Provencher MT, Bugbee WD, Sah RL: Osteochondral Allograft Transplant to the Medial Femoral Condyle Using a Medial or Lateral Femoral Condyle Allograft Is There a Difference in Graft Sources? *Am J Sports Med* 42:2205-13, 2014.

9. Pallante AL, Gortz S, Chen AC, Healey RM, Chase DC, Ball ST, Amiel D, Sah RL, Bugbee WD: Treatment of articular cartilage defects in the goat with frozen versus fresh osteochondral allografts: effects on cartilage stiffness, zonal composition, and structure at six months. *J Bone Joint Surg Am* 94:1984-95, 2012.

10. Schmidt TA, Sah RL: Effect of synovial fluid on boundary lubrication of articular cartilage. *Osteoarthritis Cartilage* 15:35-47, 2007.